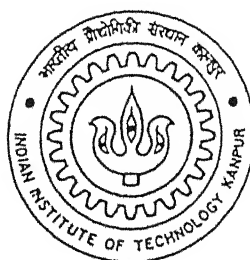# STUDIES OF METAL SUBSTITUTED BARIUM FERRITES SYNTHESIZED BY A NOVEL AUTOIGNITION METHOD FOR ULTRA HIGH DENSITY RECORDING APPLICATIONS

BY

P.Gayatri Prasad

MATERIALS SCIENCE PROGRAMME

INDIAN INSTITUTE OF TECHNOLOGY KANPUR
SEPTEMBER 1998

TUDIES OF METAL SUBSTITUTED BARIUM FERRITES SYNTHESIZED BY A NOVEL UTOIGNITION METHOD FOR ULTRA HIGH DENSITY RECORDING APPLICATIONS

A Thesis Submitted
in Partial Fulfillment of the Requirements
for the degree of

Master of Technology

BY
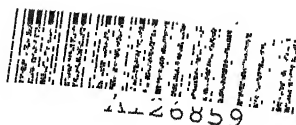**P.Gayatri Prasad**

to the

MATERIALS SCIENCE PROGRAMME

INDIAN INSTITUTE OF TECHNOLOGY KANPUR
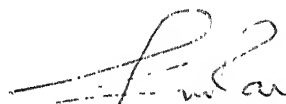**SEPTEMBER 1998**

MS-1998-M- Pla. STU

CERTIFICATE

It is certified that the work contained in the thesis entitled **Studies of metal substituted barium ferrites synthesized by a novel autoignition method for ultra high density recording applications** by P.Gayatri Prasad has been carried out under our supervision and has not been submitted elsewhere for a degree.

Jitendra Kumar

Jitendra Kumar
Professor
Materials Science Programme
Indian Institute of Technology
Kanpur - 208016

K.N.Rai
Professor
Materials Science Programme
and Department of Materials and
Metallurgical Engineering
Indian Institute of Technology
Kanpur - 208016

September 1998

ACKNOWLEDGEMENTS

ABSTRACT

Barium ferrite particulate media have generated immense interest in magnetic recording because of their ultra high densities potential at relatively low manufacturing cost. The media essentially consist of small (sub-tenth micron) particles of platelet morphology and having magnetic anisotropies of competing nature and comparable magnitude. Attempt has been made to synthesize high quality barium ferrite by a novel autoignition method for ultra high density recording applications. For this, barium and ferric nitrates in appropriate proportions have been mixed with an aqueous solution of citric acid and heated to form a gel. One gram mole of citric acid is used for each gram mole of metal ions present. Ethylene diamine which acts as a chelating agent is used to control the pH of the solution. Autoignition combustion of gel yields ash comprised of light flakes. The process is instantaneous and non-explosive. It makes use of the heat energy liberated by the exothermic anionic oxidation reduction reaction between the citrate and nitrate ions. Final product is obtained after calcination of the ash. Various parameters such as pH of the solution during gel formation and calcination temperature have been varied to find out the optimum conditions for synthesis of barium ferrite. Magnetic moment measurements, X-Ray diffraction (XRD) and differential thermal analysis (DTA) have been used for characterization of the products. Pure barium ferrite is shown to be formed at pH of 4.0 and calcination temperature of $900^{\circ}C$ (duration being five hours). Its coercivity being high (~5190 Oe) makes the product unsuitable for high density recording applications. To reduce the coercivity, partial substitution of Fe^{3+} ions with cobalt, bismuth or cobalt-

titanium together has been tried out. It is shown that while bismuth substitution maintains the hexagonal crystal structure of barium ferrite, without causing reduction in coercivity, cobalt substitution of 1.5 Fe^{3+} ions per $BaFe_{12}O_{19}$ molecule leads to significant reduction in the coercivity value to ~1945 Oe. Substitution of iron by both cobalt and titanium caused reduction in coercivity to as low as 300 and 89 Oe; composition presumably being $BaFe_{12-x}Co^{3+}_{x-2\delta} Co^{2+}_{2\delta} Ti_{\delta}O_{19}$ or $BaFe_{12-x-\delta} Co^{3+}_{x-\delta} Co^{2+}_{\delta}Ti_{\delta}O_{19}$ with x = 0.5 or 0.75 respectively and δ remaining unknown.

CONTENTS

LIST OF FIGURES

CHAPTER 1

INTRODUCTION

Magnetic recording involves an extremely important technology. It is principally responsible for the widespread, relatively inexpensive use of recorded sound and video images. Also, in conjunction with semiconducter technology, magnetic recording has contributed significantly to the growth of computer development. The progress has been so rapid that the capacity of floppy disks have increased from 360 Kbytes to one Gbytes in just a decade and attempts are underway to cross 10 Gbytes level soon. The development of high density floppies, (i.e., one Gb and beyond) involved two major technological innovations [1]: (i) highly sensitive magnetoresistive heads and (ii) advanced signal detection system.

Magnetic recording requires suitable recording media, disks and sensitive signal detection heads. The recording systems have undergone development along two different lines [2]: fixed heads involving linear recording and rotating head involving helical recording . While the first is useful for digital data and analog audio applications, the second is meant for video and digital audio applications. Linear recording has fast access and high throughput of data capability but the associated areal densities are rather low because of wide track widths. On the other hand, helical recording achieves very high areal densities but has slower access and poor transfer capacity. Head technology has also evolved in two different ways. There are either discrete structures of laminated metal and glass-bonded ferrite heads including metal-in-gap (MIG) ferrite heads or

batch fabricated thin film structures of inductive heads with the read function. The latter offers significant advantages in sensitivity and eliminates the need for a large number of turns in read head having importance in systems with relatively low head to tape velocities. It also offers the ability to fabricate arrays of integrated head structures which can be servo-controlled to write and read a large number of tracks simultaneously increasing thereby the throughput bandwidth of the system. Magnetic tapes have dominated the arena of large capacity mass storage, back-up of rigid disks, audio-video recording and archival data applications. This is mainly so because of their low cost and volumetric density advantages. Acicular particles of gamma-ferrite (γ-Fe_2O_3), cobalt modified γ-Fe_2O_3 and CrO_2 have been largely used during early years, but, recently high performance media incorporating acicular metal particles (MP) and platelet shaped barium hexaferrite have been developed .

The fundamental problem essentially lies in determining the optimum combination of tape, head and system parameters to meet the requirements of information super highway. As the future digital storage systems are to have tens of gigabytes capacity per module or cartridge, they must be of low cost and fast access capability with wide transfer bandwidth. It seems that most of these attributes can be provided by a linear system with servo-controlled multi-track arrays of integrated thin film write/MR-read heads. Currently, the concentration is primarily on advanced metal particles and barium ferrite particulate tapes which have shown excellent characteristics. While the former's usage is limited to the densities of 100 kfci due to the large size of metallic particles and their associated low coercivities [2], the latter offers superior recording performance, higher signal to noise ratio, corrosion stability and capacity of supporting densities

2

above 160 kfci [2]. After the invent of gaint magneto resistive (GMR) heads, plans are underway to produce commercial barium ferrite tapes [3]. In the present study, we have therefore synthesized barium ferrite by using a novel auto ignition method and tried to engineer its properties by different metal substitutions so as to meet the requirements of magnetic recording media.

CHAPTER 2   MAGNETIC RECORDING

AND MATERIALS CHARACTERISTICS

2.1 BASIC PRINCIPLE

In order to deal with the requirements imposed on materials for recording media, it is imperative to describe the basic principle of magnetic recording itself [4]. The information, be it sound, images, or numerical data is expressed as a time varying electrical current. The recording head consists of

(i) a small coil, through which the current passes, and

(ii) a gapped magnetic structure that intensifies and localizes the resulting magnetic field.

The recording medium is a magnetic material, coated on the surface of a tape or disc that moves relative to the head in close proximity by maintaining a gap. The head field magnetizes the coating species according to the current in the coil such that the time varying electrical signal gets converted into a spatially varying magnetic pattern along a track on the medium surface. Reversal of the current causes flip over and produces transitions between regions of opposite magnetization. The read back process involves movement of the tape surface once again over the head. Now, the field of the magnetized region gives rise to a magnetic flux in the coil. Thus, on relative motion between the head and the medium, voltage gets induced in the coil in accordance

with the changes in magnetization of the medium. Thus, a spatially varying pattern is converted back into a time varying electrical signal.

In magnetic recording, the encoding of information can be analog or digital type. In analog recording, the pattern of magnetization on the recording medium should be a precise representative of the incoming stream of information so that the signal obtained on reading back gives an exact reproduction of the original. Digital recording involves converting the information into a sequence of ones and zeroes which are then recorded to represent a sequence of regions of opposite magnetization. While the analog recording has been widely used to store audio and video information, the digital recording is confined to data storage. This picture is changing and digital recording is now being used increasingly in audio and video recording as well principally because of the possibility of making dynamic corrections to reconstruct and copy repeatedly the original information. Whether the recording method is analog or digital, similar (though not identical) properties are required of the recording materials.

2.2   CHARACTERISTIC REQUIREMENTS OF MEDIA

The primary characteristics required of the magnetic materials for use in recording media can be summarized as follows [5,6]: The retained magnetization intensity (or retentivity) must be sufficiently high as it determines the strength of the field sensed by the read back head. The retentivity depends on the intrinsic magnetization of the media material and the preferred directions thereof. The other property relates to the field strength needed to cause magnetic reversal of the material and is generally characterized by the coercivity (H_c), i.e., the field where

slope is maximum in the magnetization curve. The coercivity (H_c) value must not be so large as to prevent successful writing and possibly overwriting or erasure by available heads. It must, however, be large enough to resist unwanted changes or degradation of the signal caused by the internal or self-demagnetizing field during storage. This field being proportional to the magnetization intensity of the media itself, the coercivity needs to be high in strongly magnetizable coatings. The internal demagnetization field is important principally at high densities of magnetic transitions where opposite magnetic poles in the recorded pattern are in close proximity to each other. Higher coercivity therefore tends to be important with increasing recording density. Besides coercivity, the breadth of the dM/dH versus H curve is also crucial. This is commonly expressed by the switching field distribution (SFD) [6]. A narrow SFD clearly

Figure 1. The coercivity H_c is an average property and must be supplemented with switching field distribution, $\Delta H/H_c$ which can be measured by dM/dH versus H curve using the hysterisis loop.

facilitates the writing of sharp and well-defined magnetic transitions and hence contributes to the ability to record information at high densities (Fig 1). A broad SFD not only corresponds to diffuse transitions but also indicates a variety of adverse effects, e.g., problems in erasure, overwriting, etc. The appropriate SFD is important in systems requiring thorough erasure using special heads (e.g., analog) and in others where some residual overwritten signal can be tolerated but no erase head is used (e.g., digital).

The above magnetic properties of the recording medium must be stable under the conditions that prevail during its usage and storage. Temperature, relative humidity and atmospheric pollutants provide significant threat in this regard. Although irreversible transitions resulting due to exposure of recording media to elevated temperatures are simply unacceptable, reversible changes can also be troublesome sometimes. The strong temperature dependence of coercivity can endanger signal stability and also create problems during adjustment of writing and erasing head fields. The overwriting capability can be critically affected in situations where data is originally recorded at a different temperature. Digital equipment such as disk drives can face temperature related difficulties because of internally generated heat by motors and other components. Finally, the temperature at which the spontaneous magnetization disappears (i.e., Curie temperature) of the recording media must be safely (~50 degrees centigrade) higher than any temperature likely to be encountered during use, transportation, or storage of the recording medium.

The characteristics discussed so far relate to the bulk or macroscopic magnetic properties of a desired medium. However, the microstructure is equally important. Recording media must contain rigidly held small discrete magnetic units that are at least partially, if not fully, independent of each

other so that the transitions between different directions of magnetization in the recorded pattern are stable. Each magnetized segment in the written record must contain enough sub units to make the signal to noise ratio adequate. Also, if the number of particles present per cubic centimetre is n, the dependence of signal to noise ratio is of $\sqrt{n}$ type [6]. So, a good recording media should contain a large number of very small particles.

If the magnetic units correspond to particles or grains, a further reason exists for making them as small as possible, i.e., for ensuring a smooth (tape or disk) surface. The effectiveness of recording and reading processes depends critically on the gap between the head and the medium. The spacing between the two is the most important parameter in magnetic recording. The loss encountered is exponential function of separation to the recorded wavelength (d/λ) ratio. This amounts to 44 (d/λ) dB and 55 (d/λ) dB during writing and reading, respectively [6]. The enormous loss involved in increasing the recording density (by decreasing the wavelength) without being able to reduce the separation between head and medium are without doubt the critical limiting factors in magnetic recording today, e.g., at a density of mere 50,000 bits per inch corresponding to the wavelength of 1 μm, a separation of 0.125 μm between head and tape during writing and reading is sufficient to cause a loss of 75 percent of the available signal. Such a close separation is difficult to achieve repeatedly. This is particularly so when recording material is removable i.e., in case with tapes, flexible disks, and some rigid disks. Recording performance is always improved by reducing the head-medium spacing. But, there is a serious negative aspect of a small spacing, e.g., there is increased likelihood of a "head-crash" or, in general, some mutually destructive contacts between head and medium. So, a balance must exist

recording performance on one hand and ease of media interchange, durability and longevity on the other. Reducing the head-medium separation requires not only a right aerodynamic design of the head but also an appropriate finish of the surface of the medium. The best surface is not necessarily the smoothest, since the important functional factors of durability, friction, and stiction are usually optimal when the surface of the medium is not mirror like. The commercial processes involved produce invariably a distribution of particle sizes for recording media. As the average size is reduced to improve signal to noise ratio, there is an increasing possibility that a growing fraction of particles in the distribution will be superparamagnetic and thus quite useless for recording purposes. We need particles that are small enough so that 10^{14} -10^{15} of them can be packed in each cubic centimetre of the magnetic coating, but, they must not be so small that their magnetization states become unstable.

2.3   MATERIALS FOR MAGNETIC RECORDING

2.3.1   Iron oxide:

The commercial magnetic recording tape was first produced in late 1940's using iron oxide (i.e., γ-Fe_2O_3) particles. The γ-Fe_2O_3 is the most useful among various oxides, mainly because of its great chemical and physical stability. Particles size, shape and formation technique of γ-Fe_2O_3 have been greatly improved in last five decades. The particles in use are of acicular shape, contributing significantly to the anisotropy. Also, the magnetostatic energy becomes the least when the direction of magnetization is collinear with the particles longest dimension. A secondary

contribution to the magnetic anisotropy in γ-Fe_2O_3 arises from the interaction of electron spins with its crystal structure. The above two anisotropic effects determine the field needed to switch the magnetization from one energetically preferred direction to another and, in turn, determine the coercivity [7]. Further, both types of anisotropies exhibit a poor temperature dependence. γ-Fe_2O_3 particles have typical saturation magnetization density of about 340 emu/cm^3 and coercivity of 300-400 Oe. Their magnetic characteristics together with the high chemical and physical stability make them suitable for a number of applications not requiring high recording densities.

2.3.2 Chromium dioxide:

Low coercivity values (usually 300-400 Oe) of γ-Fe_2O_3 cause a serious limitation as the level of recording density increases. The requirement of high coercivity was first met in the mid-1960's with the introduction of chromium-dioxide CrO_2 particles. Like iron oxides, CrO_2 particles are magnetically uniaxial and derive their magnetic anisotropy both from their acicular shape and magneto crystallinity. Further, the particles have high perfection and uniformity of shape, qualities that lead to efficient packing and orientation build-up when coated on polymer tapes.

The latest development centres around the control of particle size and coercivity by addition of iron and antimony [8]. Rhodium and iridium are also used as dopants [9]. Iridium doped CrO_2 particles available commercially today, have coercivities of 500-600 Oe, magnetization intensities of 350-400 emu/cm^3 and low Curie temperature of 125°C but the price is three to four times more than that of γ-Fe_2O_3. Chromium dioxide was first introduced into computer and then in audio tapes and is currently used in some video cassettes and data recording cartridges. However, the

production process for CrO_2 requires high pressures. CrO_2 particles are quite abrasive and also somewhat reactive. Its chemical and physical stability are achieved through coatings of appropriate organic components. Nevertheless low Curie temperature ($125^{\circ}C$), of CrO_2 permits fabrication of tapes for use in thermomagnetic, duplication enabling there by copying of video information at high speeds.

2.3.3 Cobalt modified iron oxides :

Modern requirements in audio, video and data disks call for materials of high coercivity (1000-2500 Oe). As the wave length (or bit length) becomes shorter, demagnetizing field becomes larger, but the process can be resisted by high coercivity [10]. The magneto crystalline anisotropy constant is known to get tripled by substituting four percent (4%) of iron with cobalt in γ-Fe_2O_3 and, in turn, increases coercivity [11]. But, the particles in the process take almost spherical shape, i.e., the reduction of acicularity. Also, the coercivity then becomes very sensitive to temperature and pressure. Cobalt substituted γ-Fe_2O_3 particles are now widely used in magnetic recording media. The reason for this lies in exploiting both the high magneto crystalline anisotropy with stability (resulting due to cobalt) and high acicularity of γ-Fe_2O_3 particles by confining impregnation of small amount (~2-3wt%) of cobalt to their subsurface regions [12]. Also, the nature of particle surface is known to play an important role in determining the switching field [12].

2.3.4 Metallic particles (MP):

The principal attraction of using metals and alloys rather than oxides in recording materials is that they extend the range of choice of magnetization and coercivity [2]. Pure iron has a saturation magnetization of 1700 emu/cm^3 compared with 400 emu/cm^3 for γ-Fe$_2$O$_3$. When the anisotropy contribution is predominantly due the particle shape, the coercivity becomes directly proportional to magnetization. So, the coercivity of acicular particles of iron should be about 2.5 times higher than the coercivity of γ-Fe$_2$O$_3$ particles of the same shape. In fact, high coercivity (1100-1700 Oe) iron particles are commercially available. However, metal particles are usually susceptible and tend to *(i)* corrode in atmosphere and *(ii)* react with binders.

The particles having a coercivity of ~1000 Oe exhibit high signal to noise ratio and are therefore used in audio tape and 8-mm video tapes. Those having a coercivity of ~1500 Oe have potential use in high density flexible disks [13].

2.3.5 Barium hexaferrite :

Barium hexaferrite media have generated a lot of interest for advanced magnetic applications because of their potential for high density recording and relatively low cost. They consist of small (sub-tenth of a micron sized) platelets with competing orthogonal anisotropic (crystalline and shape) of comparable magnitude. These anisotropies, alongwith the quasi-perpendicular characteristics of barium ferrite coatings lead to many curious properties, requiring a careful and judicious choice of parameters for each application [15]. The choices of parameters include the

aspect ratio of the particles, coercivity, the binder loading, the degree and direction of magnetic orientation of particles, overwrite characteristics etc.

The key properties of different magnetic materials used for recording are summarized in Table 1. Of all the above materials, only metal particulate and barium ferrite are of current interest for ultra high density recording. Though metallic particles are popular, barium ferrite is replacing them at ultra high densities (5Gb/sq.in) following the development of Giant Magneto Resistance (GMR) heads. Many advanced applications are likely to have head sensitivity to system noise ratios such that the media signal to noise ratio (SNR) becomes the dominant figure of merit. Introduction of GMR heads will make this even more important, at narrower track widths [2]. Though barium ferrite has many

Table 1 Key properties of various magnetic materials.

Property \ Particle	$\gamma\text{-}Fe_2O_3$	$Co\cdot Fe_2O_3$	CrO_2	$Ba0.6\,Fe_2O_3 + Co, Ti$	Fe
saturation magnetization, σ_s emu/g	73-74	73-76.3	70-80	45-70	150-190
$\frac{\sigma_r}{\sigma_s}$	0.5	0.5-0.6	0.5	0.6-0.7	0.23-0.52
Curie Temperature, T_c, °C	[590]	[590]	115-126	320	768
magnetocrystalline anisotropy constant. K_1, ergs/cc	-4.64×10^4	-5 to $+100 \times 10^4$	$+2.5 \times 10^5$	$+3.3 \times 10^6$	$+4.4 \times 10^5$
saturation magnetostriction λ_s	-5×10^{-6}	-5 to -15×10^{-6}	$+1 \times 10^{-6}$		$+4 \times 10^{-6}$
coercivity, H_c, Oe	250-350	550-750	450-670	320-1970	375-1550
switching field distribution, $\frac{\Delta H}{H_c}$	0.78-0.61	0.30-0.6	0.35-0.6	0.16-0.8	0.5-0.75
temperature coeff. of coercivity, $H_c/H_c/°C$ (20-70°C)	-1×10^{-3}	impreg.^{d} -2.4×10^{-3} doped -10×10^{-3}	-5×10^{-3}	$+3.1 \times 10^{-3}$	-0.8×10^{-3}
specific surface area (BET), m^2/g	20-40	20-40	25-37	15-31	28
density, ρ, g/cc	4.68	4.80	4.88-4.95	5.34	5.3
crystal structure	cubic $a_0 = 25\,\text{Å}$, m3m	cubic	tetragonal $a = 4.4218\,\text{Å}$ $c = 2.9182\,\text{Å}$	hexagonal $c = 23.2\,\text{Å}$ $a = 5.88\,\text{Å}$	b.c.c. $a = 2.851\,\text{Å}$
ferro- or ferrimagnetic	ferri	ferri	ferro	ferri	ferro
particle size, μm	needles $l \approx 0.3$ $d \approx 0.05$	needles equi ax. $l \approx 0.3$ $l \approx 0.2$ $d \approx 0.06$	needles $l \approx 0.5$ $d \approx 0.05$	hex. platelets $d \approx 0.08-0.1$ thick $\approx 0.01-0.025$	needles $l \approx 0.3$ $d \approx 0.06$

13

advantages over metallic particles at ultra high densities[2,3], its greatest potential is exhibited in area of media-noise limited operation [2].

The major interest in barium ferrite particles comes mainly from their directions of magnetization. The platelets can be forced by means of a strong magnetic field to lie with their planes parallel to the substrate [14]. The direction of magnetization is then perpendicular to substrate and configuration becomes a potential media for perpendicular recording, (leading to revolution in the recording technology) with capacity to solve to a large extent the writing and demagnetization problems.

2.4   PERPENDICULAR MAGNETIC RECORDING:

According to Iwasaki and Nakamura [16], high density recording is inhibited by the nucleation of flux-cluster inside the recording media. This is termed as flux-closure phenomenon and named as the "circular magnetization mode". It is indeed another way of achieving demagnetization that led eventually to the invention of a practical method of perpendicular magnetic recording.

2.4.1   Magnetization transition regions:

When the current is increased in high density recording, the magnetization is arranged such that the magnetic flux tends to close by itself inside the medium and the flux available for reproduction is reduced. In order to attain high density recording, generation of the circular magnetization

14

should be avoided [18]. There are two ways to accomplish this. One involves magnetic recording with an enhanced longitudinal magnetization component, which occurs when the recording medium is made extremely thin so that the magnetization is forced to lie in plane. The use of thin magnetic films is equivalent to providing media with strong shape anisotropy so that magnetization easy axis is in-plane. The thinner the film is, the narrower becomes the magnetization transition becomes. The other involves magnetic recording with an enhanced perpendicular magnetization component. The recording media here has a high perpendicular anisotropy. In this case, the magnetization is forced to stand up, perpendicular to the medium plane, thus inhibiting generation of the circular magnetization. With this recording method, one obtains sharp magnetization transitions for high density recording.

Figure 2   Simple model for magnetization transitions in perpendicular and longitudinal recording

Figure 2 shows magnetization transitions for perpendicular and longitudinal recording. Assuming an ideal recording process, initial magnetization distributions for isolated transitions are given by stepwise changes M1 and M4 for perpendicular and longitudinal recording, respectively. At this stage, the demagnetizing fields Hd1 for M1 and Hd2 for M4 are induced. Regions, where the demagnetizing field exceeds the medium coercivity, for example, will be subject to demagnetization, reducing the shaded areas shown in the Figure 2. For perpendicular recording, the region around transition centre remains unchanged, resulting in a sharp transition M2. For longitudinal recording, the region around the transition centre is demagnetized, leading to a broad transition M5. The above explanation is based solely on the difference in magnetization direction. Therefore, the sharp magnetization transition in perpendicular recording and the broad transition in longitudinal recording are intrinsic properties originating from the difference in the nature of demagnetization.

2.4.2   Recording process effects:

In the preceding section an ideal magnetization distribution was assumed. In practice, however, the transition sharpness of a recorded magnetization distribution is affected by the medium magnetization-field (M-H) loop squareness and head field gradient such that,

$$\frac{dM}{dX} = \frac{\partial M}{\partial H} \bullet \frac{\partial H}{\partial X}$$

16

where dM/dX is the transition sharpness, $\partial M / \partial H$ is given by differential susceptibility or the slope of M-H loop at H_c of the medium and $\partial H / \partial X$ is head field gradient [19]. Therefore, media which have a high coercivity or a narrow switching field distribution (SFD) are best suited for high density recording. If the SFD is broad, the pulse width and peak shift increase with increase in recording current at high density and recording demagnetization occurs. Compared with longitudinal, perpendicular oriented films have a small SFD. Such a narrow SFD and a square hysteresis loop will be attributed to the sputtered films consisting of uniform size grains and are governed by a rotation mechanism for magnetization reversal.

2.4.3   Recording response:

There are two kinds of responses in high density recording. When recording current is increased beyond the saturation current, the amplitude and peak shift for reproduced pulses remain flat, indicating that no recording demagnetization takes place. The peak shift comes mostly from the reproducing process. This is often observed for perpendicular recording with thick or thin media, and for longitudinal recording only with very thin film.

In yet another kind of response, pulse amplitude decreases and peak shift increases as the recording current increases above the saturation current, i.e., severe recording demagnetization occurs and peak shift results from both recording and reproducing processes [18,19]. This is often found for particulate media and comparatively thick films. So, it can be said that although longitudinal recording is also applicable for high density recording but, it has to sacrifice the film thickness and signal amplitude.

17

2.4.4 Magnetostatic energy:

A high magnetostatic energy means that the magnetization state for the bit is unstable i.e., magnetization tends to rotate or demagnetization occurs. Therefore in order to maintain the magnetization in the desired direction, the magnetostatic energy must be reduced or the anisotropy energy must be increased, so as to counterbalance the magnetostatic energy. It is clearly shown that the extremely thin media are required for high density longitudinal recording [18]. When a 0.3-0.5μm thick perpendicular media is used at densities ranging from 50-100K FRPI, the corresponding longitudinal recording media which use the same magnetostatic energy should be less than 300-500A in thickness, i.e., about one order of magnitude thinner than the perpendicular medium [19].

The greatest difference between perpendicular and longitudinal recording is with regard to the medium thickness, is permissible at a given recording density level. In longitudinal recording the medium must be thin for high density. This fact causes, difficulties in (i) fabrication of uniform, corrosion-resistive films, (ii) increase in drop out and, (iii) decrease in reproduced signal amplitude due to reduced magnetic moment per bit [16-18].

From the above discussion, it can be concluded that, at high recording densities, practical limits will be reached for longitudinal magnetization and so, for ultra high densities (~5 Gb/sq.in), perpendicular magnetization is unavoidable.

2.5   BARIUM HEXA FERRITE

2.5.1   Crystal Structure:

The barium hexaferrite has a magnetoplumbite structure with hexagonal unit cell having parameters a = 5.892°A, c = 23.183 °A . Z = 2 and space group P6$_3$/mmc [20]. The unit cell contains two formula units of BaFe$_{12}$O$_{19}$. It consists of S and R blocks in the sequence of RSR*S*, where the asterisks indicate a 180 degree rotation with respect to the c-axis (Figure.3). The R block in this case is formed by the group $(BaFe_6O_{11})^{2-}$, whereas S block comprises of $(Fe_6O_8)^{2+}$ and has no barium cations. The close packing arrangement of oxygen has cubic configuration (i.e., ABCABC...) in the S unit and hexagonal layer sequence (i.e., ABABAB...) in the R block. The [111] cubic axis coincides with the [0001] hexagonal axis. Fe ions occupy five types of crystal sites. There are 12 octahedral 'k' sites, four octahedral f_{vi} (or f_1) sites, two octahedral 'a' sites, four tetrahedral f_{iv} (or f_2) sites and two 'b' five fold sites (Fig 3). The 12 iron sites in the k sublattice are shared by the R and the S units. The four f_{vi} are in the R block close to the Ba^{2+} and forming a (Fe_2O_9) group of two octahedra with a common face. The two 'a' sites are present in the S block. The two 'b' sites with five-fold symmetry are formed by two tetrahedra sharing a common face. A detailed XRD study showed that Fe ions lie in a double-well potential of the bypyramid centre.

Fig. 3 Unit cell of $BaFe_{12}O_{19}$, showing the polyhedra coordination for Fe in f_{iv} and f_{vi} sites. The common faces of two neighbouring f_{iv} and f_{vi} polyhedra are hatched

2.5.2 Magnetic properties:

The magnetic ions in barium ferrite are twenty four Fe^{3+} ions, each with a moment of $5\mu_B$ (bohr magneton). Their moments lie normal to the close-packed oxygen layers, i.e., parallel or antiparallel to the +c axis or [0001] of the hexagonal cell. By assuming the known spin directions of the Fe^{3+} ions in spinel configuration (or S block) and applying the principles governing the super exchange force, one can proceed from ion to ion throughout the cell and predict the direction of its net spin moment i.e., parallel or antiparallel to [0001]. This suggests spins of 16 ions in one direction and of 8 in the other. The net magnetic moment per cell should therefore be $(16-8) \times 5 \mu_B = 40 \mu_B$ per cell or $20 \mu_B$ per molecule of $BaFe_{12}O_{19}$. This matches well with the experimental value of 100emu/g [21].

Barium hexaferrite particles usually grow as platelets with their c-axis along the thickness, i.e., normal to the plane of the platelet. This growth habit leads to a moment arising due to shape and magneto crystalline anisotropies perpendicular to each other. The total anisotropy field is given by

$$H_K = \frac{2K}{M_s} - N_d M_s$$

where M_S is the saturation magnetization, N_d is the demagnetizing factor considered to be unity for thin platelets [20,21] and K is a magnetocrystalline constant. The second term on the right hand side stands for the reduction in the field caused by shape anisotropy.

2.5.3 Advantages and associated problems:

1. The major advantage of barium ferrite particles comes from their direction of magnetization. The strong magnetic fields can force platelets to lie parallel to the substrate. Consequently, they begin to respond to the perpendicular component of the field from the recording head, i.e., they have excellent potential for high recording density applications [15,22,23,24].

2. They can be synthesized with the existing low-cost mass production facilities.

3. The platelet shaped particles can be produced in small sizes, with a well defined size range with shape uniformity and morphological perfection.

4. They are chemically very stable and inert.

5. They capitalize on existing and well understood head/media interface.

There are some associated problems as well originating mainly from the competing orthogonal anisotropies (crystalline and shape) of the platelet-shaped particles [25]. The main areas of concern include i) temperature coefficients of the magnetic parameters and their dependence on particle aspect ratio, coercivity, particle-to-binder loading and orientation ii) particle aspect ratio selection iii) pigment loading effects on the ensuing magnetic properties [25,26], and iv) coercivity selection [27,28].

2.6   SYNTHESIS METHODS

Ferrites can be synthesized through solid state reaction route in a wide variety of forms: polycrystalline aggregates, thin and thick films, single crystals with specific microstructure, etc [20]. A few important methods are : Ceramic, Co-precipitation, sol-gel, glass-crystallization and autoignition.

2.6.1   Ceramic method:

This is the oldest of all existing methods . In this, the powder is usually prepared from the mixture of appropriate amounts of raw oxides or carbonates by crushing, grinding and milling. It is then calcined at about 1250°C for six hours to form barium hexaferrite [29]. The resulting product exhibits wide particle size distribution with a large average diameter of ~0.5μm. Also, due to extended milling, particles are generally strained and contaminated with worn out impurities of milled spheres.

2.6.2   Co-precipitation Method

It involves aqueous solutions of Fe^{3+} and Ba^{2+} in the appropriate concentrations and precipitation of their respective hydroxides by addition of NaOH and maintaining the pH in the range of 7.5-7.8. The precipitate is filtered, washed and then dried at 90°C for 12 hours . The final product is obtained by calcination at around 1050°C for six hours [30]. This method yields barium ferrite of high purity with a narrow particle size distribution and diameter in the range of 50-500 nm.

However, maintenance of pH is very critical as otherwise inhomogeneous precipitation may occur due to marked variation in solubilities of metal hydroxides in aqueous solutions.

2.6.3 Sol-gel Method:

The process is based on preparation of a sol by dispersing concentrated solution(s) of the cation(s) of interest in an organic solvent. For barium ferrite use is made of propoxides of iron and barium i.e., $Fe(OC_3H_7)_3$ and $Ba(OC_3H_7)_2$, respectively with C_3H_7OH as solvent. The sol is then destabilized by adding water. The presence of water modifies the pH of the sol and reduces the repulsion between particles. This results in a large increase in the viscosity of the system and forms a gel. The resulting alcogel is aged for 12-24 hours. The particles are seperated by centrifugation and put in an oven at $100^{\circ}C$ to form an amorphous powder on drying.The barium hexaferrite is then obtained by calcining the powder at $700^{\circ}C$ for 2 hours [31]. The method is capable of having control over the shape of the product. Fibers, films and monoliths of different materials have been obtained by this method.

2.6.4 Glass Crystallization Method:

In glass crystallization method, a homogeneous $BaO-B_2O_3-Fe_2O_3$ flux melt is produced at temperatures of about $1300^{\circ}C$ and quenched at velocities of 10^4-10^5 kelvin/second between two rotating rollers to form amorphous flakes or tapes of 30-100μm thickness. Annealing the glass flakes/tapes at temperatures above $550^{\circ}C$ leads to the nucleation and growth of borate and ferrite. The ferrite particles are extracted by dissolving the borate with (20%) acetic acid. The remaining

slurry is carefully rinsed and dried. This method yields particles having a narrow size distribution and of very small dimensions and, so, is widely used for preparation of barium ferrite for recording applications [32].

2.6.5 Autoignition Method:

The common feature in almost all the above methods involves mixing of components at the molecular level. Also, the impurities (e.g., chlorine in co-precipitation and borates in glass crystallization method) need to be removed to get a pure precursor. One way to get around this difficulty is to select the salts and a method of processing such that the yield is either free of impurities or contain such impurities which can be removed during calcination step. For this reason, we have extended the autoignition method used for synthesizing Bi-Pb-Sr-Ca-Cu-O superconductor [34] successfully to the barium hexaferrite system.

This process involves initiation of combustion at a low temperature and makes use of the heat energy liberated by the exothermic anionic oxidation reduction reaction between the citrate and nitrate ions. The combustion reaction undergoes a self propagating and non-explosive reaction, which is safe and instantaneous compared to other combustion processes [33,35]. The method is named as "Autoignition method" and produces precursor containing small amount of carbon impurities that get expelled by forming CO_2 on calcination. Thus, it cuts down to an extra step of purifying the precursor.

2.7 OBJECTIVE OF THE PRESENT WORK

The objective of the present work has been to synthesize barium hexaferrite by using an autoignition method and engineer its properties for magnetic recording applications. Attempt has therefore, been made to find out the synthesis conditions for pure barium hexaferrite by varying pH (2.0-8.0) of liquid reactants and calcining temperatures (800-1000°C). Further, for controlling the coercivity and other properties, partial substitution of iron with bismuth, cobalt and cobalt-titanium has been tried out . The products have been characterized at various stages by X-ray diffraction (XRD), differential thermal analysis (DTA), vibrating sample magnetometer (VSM) to obtain information about the phase(s) present, magnetization, coercivity, Curie temperature etc., and to determine the possible correlation(s).

CHAPTER 3

EXPERIMENTAL

In this chapter, the experimental procedures adopted for synthesis of barium ferrite with and without substitutions of iron with different metal ions (Bi,Co and Co-Ti) and characterization of products by X-ray diffraction (XRD), differential thermal analysis (DTA) and magnetic measurements are described.

Table 2 :- List of raw materials used with make and grade

MATERIAL	MAKE	GRADE
$Ba(NO_3)_2$	THOMAS BAKER	L.R
$Fe(NO_3)_3 9H_2O$	NICE	L.R
Citric acid	INTERNATIONAL CHEMICAL INDUSTRIES	A.R
$Co(NO_3)_2 6H_2O$	NICE	L.R
$Bi(NO_3)_3 5H_2O$	NICE	L.R
Ethylene diamine	S.D.FINE CHEM LTD	L.R

3.1 SYNTHESIS OF BARIUM HEXAFERRITE :

The raw materials used for synthesis with their make and grade are listed in Table 3.1.The stoichiometric amounts (here 1:12) of the aqueous solutions of $Ba(NO_3)_2$ and $Fe(NO_3)_3 9H_2O$ are mixed to get a solution of metal nitrates. Required amount of citric acid is then added to the aqueous solution. Here one gram mole of citric acid is used for each gram mole of metal ions. The resultant solution is stirred magnetically with the temperature maintained at $90^{\circ}C$. After stirring for twenty minutes, a solution of light yellowish colour is formed. The pH of the solution at this stage is around 2.0. To ensure the homogeneous mixing of the components, ethylene diamine is added. This raises the pH of the solution ethylene diamine is a base as well. The addition is continued till the pH reaches the value 4.0. The beaker is then transferred onto a hot plate and the liquid begins to set into a gel with colour changing to dark green. On further heating, the gel starts to foam and swell. After sometime the dry gel catches fire on its own with appearance of glowing flints and evolution of large amounts of light reddish coloured gases which are suspected to be of NO_x type. This self sustaining spontaneous combustion process gets completed within a few minutes producing a brown ash. The ash consists of fine flakes. The ash is calcined at $900^{\circ}C$ for five hours to yield finally a pure phase of barium hexaferrite. It is interesting to note that, unlike other combustion processes [33,35], the auto catalytic combustion occurs here irrespective of the heating rate, stoichiometry and mass to volume ratio of the mixture. Moreover, since this process is non-explosive, no extra care is necessary to check the vigour of the reaction.

3.1.1 METAL SUBSTITUTIONS

To see the effect of partial substitution of iron with other metals on the magnetic and structural properties, different metal ions are selected to form $BaFe_{12-x}Me_xO_{19}$, where x is the number of iron atoms substituted per barium ferrite molecule and Me is the metal ion which is replacing iron.

a) Cobalt substitutions:

As has been pointed out in the chapter 2, partial replacement of iron with cobalt leads to the drastic decrease in coercivity of barium ferrite. So, we have tried to substitute iron with cobalt to see its effect on various properties of ferrite and to check the tolerance limit of substitution. We have prepared six samples with different amounts of substitution and characterized them. The samples prepared were of the form $BaFe_{12-x}Co_xO_{19}$ with different values of 'x' as 0.5, 1.0, 1.5, 2.0, 2.5 and 3.0. For the preparation of these samples, appropriate amounts of $Ba(NO_3)_2$, $Fe(NO_3)_3$ $9H_2O$ and $Co(NO_3)_26H_2O$ were added to the citric acid solution. The ethylene diamine was added till the pH of the solution reaches 4.0. The solution was then stirred properly and heated till it yielded ash. The ash was calcined at 900^oC for five hours to give the final products.

b) Bismuth substitutions:

The bismuth ion exists in 3+ state in the bismuth nitrate and so can possibly replace iron (being also in 3+ state) in barium ferrite, without causing charge imbalance and deviation in the crystal structure. With such a conjecture, three samples ($BaFe_{12-x}Bi_xO_{19}$) with x=0.5, 1.0 and 1.5 were prepared. For this appropriate amounts of iron, barium and bismuth nitrate solutions were added to

the citric acid and different ashes, in turn, produced by using autoignition method were each calcined at 900°C for five hours.

c) Cobalt-Titanium substitutions:

To compensate for the extra charge created due to the presence of some Co^{2+} (in place of Fe^{3+}) in the solution, Ti^{4+} is added. But as no aqueous solution of Ti^{4+} is known, the addition of titanium was carried out by mixing required amount of TiO_2 powder in barium, cobalt and iron nitrates and citric acid solution. Since TiO_2 is not soluble in water, the proper mixing can be ensured only by high level of powder dispersion in the solution. To achieve this, the pH of the solution was maintained at 4.0 being the iso-electric point of TiO_2 [40]. The ash formed from such a mixture was calcined at 1100°C for ten hours to get the final product. The two samples thus synthesized corresponded to the composition $BaFe_{12-x}Co_xO_{19}.xTiO_2$ with x = 0.5 and 0.75, respectively.

3.2   CHARACTERIZATION METHODS

The X-ray diffraction (XRD), magnetic measurements (VSM) and differential thermal analysis (DTA) were used for characterization of samples at various stages.

3.2.1 X-Ray Diffraction:

The X-Ray Diffraction (XRD) patterns of various samples have been recorded using a Rich-Seifert X-Ray diffractometer (model Iso debyeflux 2002) to ascertain the amorphous and crystalline nature of barium ferrite and to find out the phases present. The powder was packed into a 1cm diameter

circular cavity in perspex sample holder which was then mounted in a position for diffraction. Nickel filtered K_α radiation ($\lambda = 1.5408A$) from copper target was used. The diffracted beam was received by a scintillation counter detector, held at an angle of 2θ with the transmitted beam. The rotation of specimen and detector are synchronized to maintain the focusing condition and to scan the reflecting planes and record the 2θ versus intensity pattern. The X-ray tube was operated at 20mA and 30kV with XRD patterns recorded at a scanning rate of 3°/min and chart speed of 30mm/min. The time constant was 10 seconds and sensitivity was either 5K or 2K counts per minute.

3.2.2 Magnetic measurements:

The magnetic measurements were carried out with the help of a parallel field vibrating sample magnetometer VSM (Princeton Applied Research Model-150A) in conjunction with a varian electromagnet model V-7200 providing a magnetic field of upto 11.5kOe. It measures the magnetic moment of the sample in electromagnetic units (emu). The temperature was set using an Indotherm temperature controller (model 401) and an IC regulated power supply (Networks model NPS 30/5D). A chromel-alumel thermocouple held close to the sample was used to indicate the temperature. The sample chamber was evacuated using pumping module during the heating process. The magnetic moment versus temperature data obtained at a fixed magnetic field of 100Oe or 10kG were used to determine Curie temperature (T_c) of the product. To make a pellet for magnetic measurements, 1 ml of 1% polyvinyl alcohol (binder) was added to one gram of ferrite sample and the slurry formed was mixed properly in a mortar pestle for fifteen minutes. After mixing, the slurry was kept in an oven at 90°C for two hours. After the sample was cooled, a pellet of size 3mm x

31

3mm x 4mm was made by using a special die. All pellets were kept at 400°C for two hours, so as to expel the polyvinyl alcohol present.

The properties measured at room temperature are specific magnetization M_s, remanence magnetization M_r, and coercive field H_c. The Curie temperature was determined for pure and some cobalt substituted barium ferrites only.

3.2.3 Differential thermal analysis (DTA):

Any phase transformation or chemical reaction accompanied by absorption or evolution of heat can readily be detected by DTA. In this, the temperature difference ($\Delta T = T_S - T_R$) of the test (T_s) and reference (T_R) samples are measured and plotted as a function of time. Platinum crucible is generally used to hold the samples because of its high thermal conductivity. For exothermic reaction ΔT should be greater than zero, whereas, for an endothermic reaction ΔT must be less than zero. In the present case, Shimadsu model DTA-50 with platinum crucible, dumbell type detector (Pt-Pt%Rhodium), noise range of $0.1\mu V$ or small, $\alpha-Al_2O_3$ powder as reference sample and capacity to go upto 1500°C, was used. DTA plots of gel and various ashes (formed by autoignition method) were recorded at a heating rate of 10°C/min upto a temperature of 500°C and 1000°C respectively. For higher accuracy the weight of the sample was always kept below 200mg.

CHAPTER 4

RESULTS AND DICUSSIONS

4.1 SYNTHESIS OF PURE BARIUM HEXA FERRITE

The aqueous solutions of $Ba(NO_3)_2$ and $Fe(NO_3)_3 6H_2O$ in appropriate proportions were mixed with the aqueous solution of citric acid (taking one gram mole for each gram mole of metal ions present), continuously stirred and heated upto ~90°C. After a clear solution of light yellow colour was formed, it was transferred onto a hot plate. The pH of the clear solution was around 2.0. On further heating, the liquid began to set into a gel which in turn, started to foam and swell. As the temperature approached around 200°C, the gel caught fire on its own with the appearance of glowing flints. Also, evolution of large amounts of gases occurred at this stage. Such a self sustaining spontaneous combustion process was over within a few minutes and yielded a brownish ash, comprising of light flakes of small size. Unlike other combustion processes[33,35], the autocatalytic combustion always occurred here irrespective of the heating rate, stoichiometry and mass to volume ratio of the mixture. Moreover, as the process was non explosive in nature no precaution was necessary for checking the vigour of the reaction. In the above process the citric acid reacts with Ba^{2+} and Fe^{3+} ions present in the solution and forms $Ba_3(cit)_2$, $Fe(cit)$ and/or some complex in which different metal ions are bonded to citrate (cit) ions. At this stage, the exothermic anionic oxidation-reduction reaction takes place between the citrate and nitrate ions.

In contrast to the solid state reactions, where two different solids diffuse into one another, the autoignition process undertaken involves ions themselves (that too in solution) and therefore the reaction takes place rather easily. For this reason perhaps, little energy is needed for the reaction.

4.1.1 Ash characteristics:

The DTA plot of the ash obtained after combustion of gel formed with solution of citric acid and metal nitrates at pH of 2.0 is shown in Figure 4. It depicts an exothermic peak around 300-380°C with maxima at ~351°C, arising due to combustion of organic residues. This observation suggests that the temperature during gel/ash formation remains below 300°C. Needless to say, Sujatha Devi and Maiti [34] have measured temperature during the combustion process itself in a similar situation for Bi-Pb-Sr-Ca-Cu-O superconductor system as 275°C. The XRD pattern of the ash produced from the solution having pH of 2.0 and calcined at 900°C for five hours is shown in Figure 5. Its analysis suggests, that the calcined product is a mixture of barium ferrite and γ-Fe_2O_3. The presence of γ-Fe_2O_3 means that the mixing of ions in solution before combustion is not uniform and leads to the formation of an inhomogeneous on combustion and subsequent calcination. In order to get a pure barium ferrite phase, the inhomogeneous precipitation has to be somehow avoided. To ensure uniform mixing of ions in the solution and to prevent inhomogeneous precipitation of individual components prior to combustion, ethylene diamine is added to the solution. Its details and the resulting effects are presented in the next section.
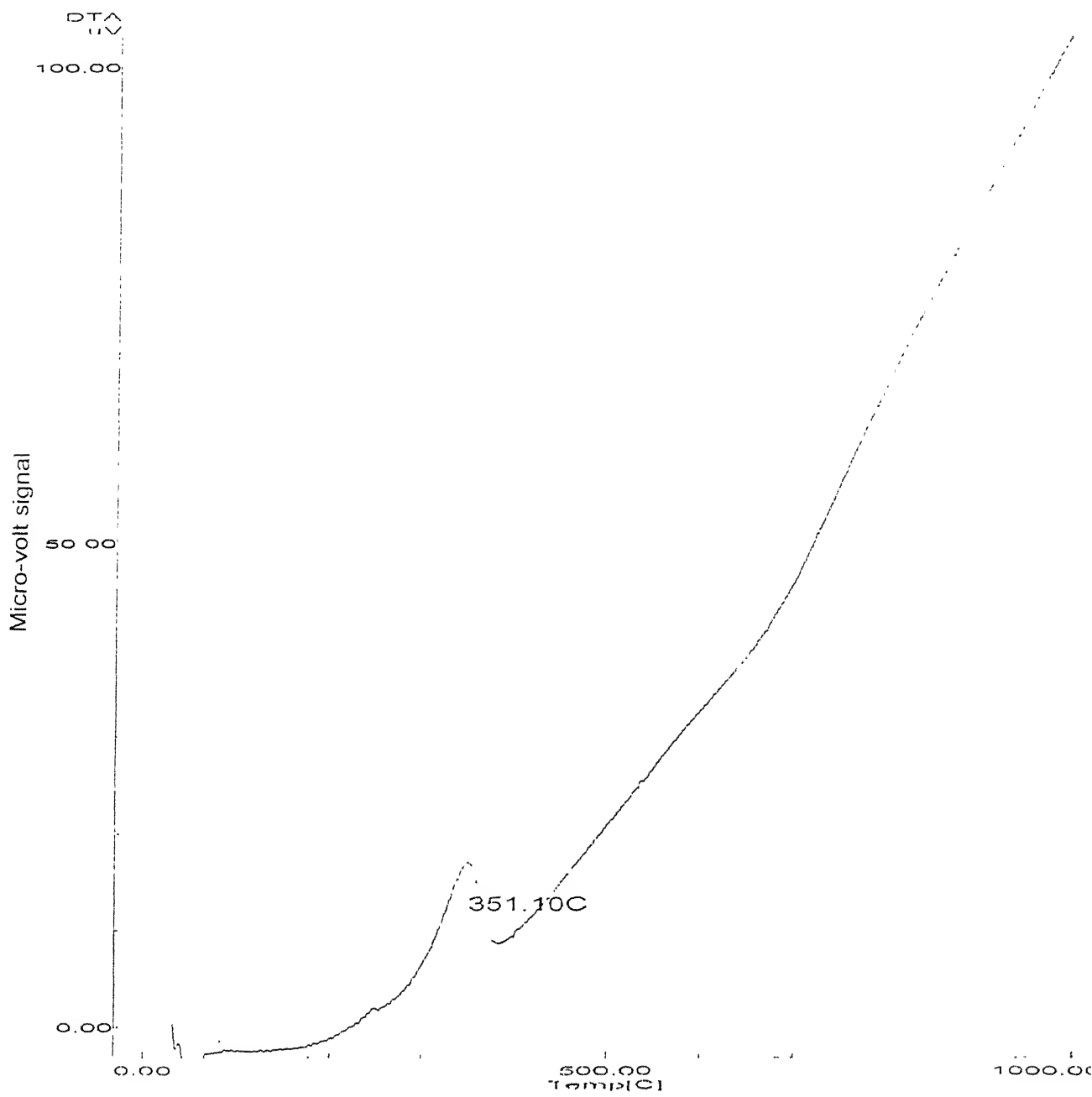
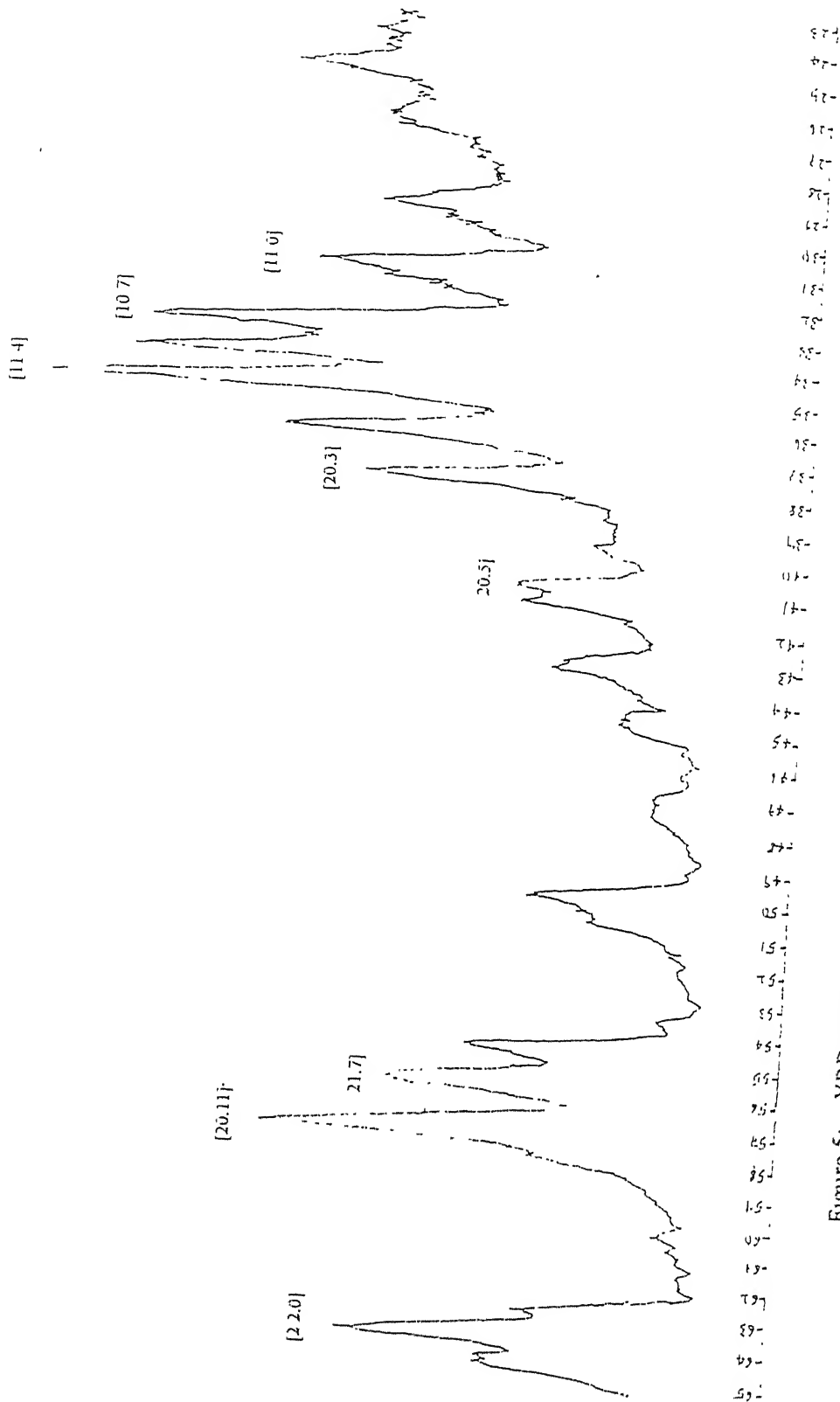Figure 4: DTA plot of ash obtained by autoignition of gel formed in the initial solution of pH 2.0.

Figure 5: XRD pattern of ash after calcination at 900°C for five hours. The ash was produced by autoignition of gel formed in the initial solution of pH 2.0.

4.1.2 Effect of ethylene diamine :

To get a pure phase of barium hexaferrite, ethylene diamine was added drop wise into the solution with constant stirring. Ethylene diamine being a base increases the pH of the solution and more importantly acts as a chelating agent [36], i.e., provides stability to the complex and prevents undesirable precipitation of the components prior to combustion[34]. Moreover, it aids and controls the combustion process by giving additional energy[34].

A complex by definition is a group formed by the association of two or more species, each capable of an independent existence. When one of the species is a metal ion, the resulting entity is known as a metal complex. Its characteristic feature is that the metal ion occupies a central position in the complex. The organic reactant which binds the metal ion and prevents latter to react further is known as a chelating agent. Also, the metal complex formed is called a chelate. Such a complex formation may carry a positive, negative or no charge. Almost all metal ions can serve as central ions, though some form chelate more readily than others. For example, transition metals are excellent species for forming chelates [36]. Thermodynamically, chelate effect is attributed to entropy. Also, ethylene diamine ($H_2NCH_2CH_2NH_2$) is an excellent chelating agent. The stability of its chelates with the transition metal follow the sequence Mn<Fe<Co<Ni [36]. In the present case, ethylene diamine on addition to the metal nitrates and citrate solution forms metal complexes with iron ions. The metal complex, in turn, binds itself with citrate ions along with barium ions in a subtle way. It will be shown below that the arrangement somehow provides the right composition during the combustion process and yields a pure barium hexaferrite on calcination.

In order to find out the optimum condition for the preparation of barium ferrite, the amount of ethylene diamine addition to the solution was varied. As pointed above, ethylene diamine being a base increases the pH of the solution. So, the pH of the solution was increased from ~2.0 (of solution without ethylene diamine) to 4,6 and 8 by adding appropriate amount of ethylene diamine. The ashes formed by all the three cases (i.e., for pH 4,6, and 8) were calcined at various temperatures.

The XRD patterns of ashes calcined at temperatures 800,900 and 1000^0C for 5 hours are shown in Figures 6, 7 and 8, respectively. The d-values corresponding to various diffraction peaks together with their intensities and data for pure barium ferrite are given in Tables 3, 4 and 5. These tables reveal that the crystallization of barium ferrite is not complete for ashes calcined at 800^oC and 900^oC for the case of the pH 6.0 and 8.0. However when the pH is 4.0 and the calcination carried out at temperature of 900^oC for five hours, the XRD pattern corresponds exactly to the known hexagonal phase of barium ferrite with excellent matching of intensities (see, e.g., Table 4). Similarly, ashes produced with solutions of pH of 6.0 and 8.0 on calcination at 1000^oC for five hours yield a pure barium hexa ferrite phase .

It is clear from the above observations that as the pH increases, the calcination temperature required for the formation of barium ferrite also increases. This is attributed to the increase in stability of the metal complex with the rise in pH caused by increased amount of ethylene diamine [36]. As the lowest calcination temperature required for ash to form barium ferrite was found to be 900^oC (and duration of 5 hours) for the case of pH = 4.0, all the subsequent synthesis were carried out under these very conditions.

Figure 6: XRD patterns of ashes after calcination at 800°C for five hours. The ashes were produced by autoignition of gels formed in the initial solutions of pH 4.0, 6.0 and 8.0.

Figure 7: XRD patterns of ashes after calcination at 900°C for five hours. The ashes were produced by autoignition of gels formed in the initial solutions of pH 4.0, 6.0 and 8.0.
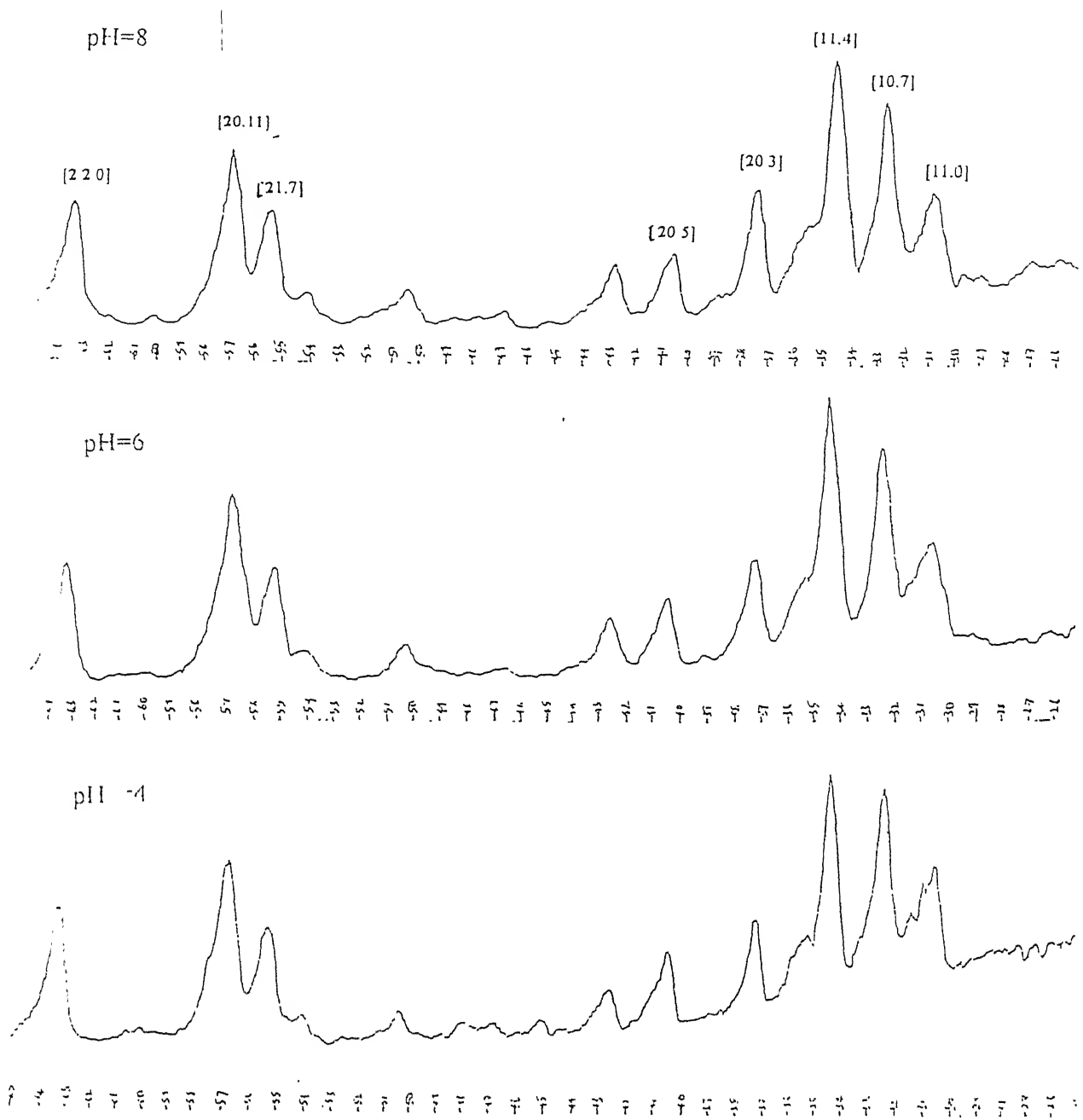
Figure 8: XRD pattern of ashes after calcination at 1000"C for five hours. The ashes were produced by autoignition of gels formed in the initial solutions of pH 6.0 and 8.0.

Table 3: Interplanar spacings and intensities of various peaks observed in XRDs of ashes after calcination at 800°C for five hours. The ashes were produced by autoignition of gels formed in initial solutions of pH 4.0, 6.0 and 8.0.

d-values for $BaFe_{12}O_{19}$ (A°)	pH =4 d (A°)	pH=6 d (A°)	pH=8 d (A°)	Intensities for $BaFe_{12}O_{19}$	pH=4	pH=6	pH=8	hk.l indices
2.94	2.97	2.97	2.98	55	59	43.8	41.2	1 1 .0
2.78	2.80	2.79	2.79	100	89	82.6	64	1 0 .7
2.62	2.64	2.63	2.63	98	100	100	100	1 1 .4
2.42	2.44	2.44	2.43	60	47	40.2	35.5	2 0 .3
2.23	2.26	2.25	2.25	29	26	29.3	37.4	2 0 .5
1.66	1.67	1.67	1.67	53	58.4	43.4	54	2 1 .7
1.63, 1.62, 1.61	1.63	1.63	1.63	30, 58, 10	86	73.9	92	2 0 .11
1.47	1.48	1.47	1.47	63	66.4	46.7	69.3	2 2 .0

The standard data for pure $BaFe_{12}O_{19}$ phase is given for comparison.

Table 4: Interplanar spacings and intensities of various peaks observed in XRDs of ashes after calcination at 900°C for five hours. The ashes were produced by autoignition of gels formed in initial solutions of pH 4.0, 6.0 and 8.0.
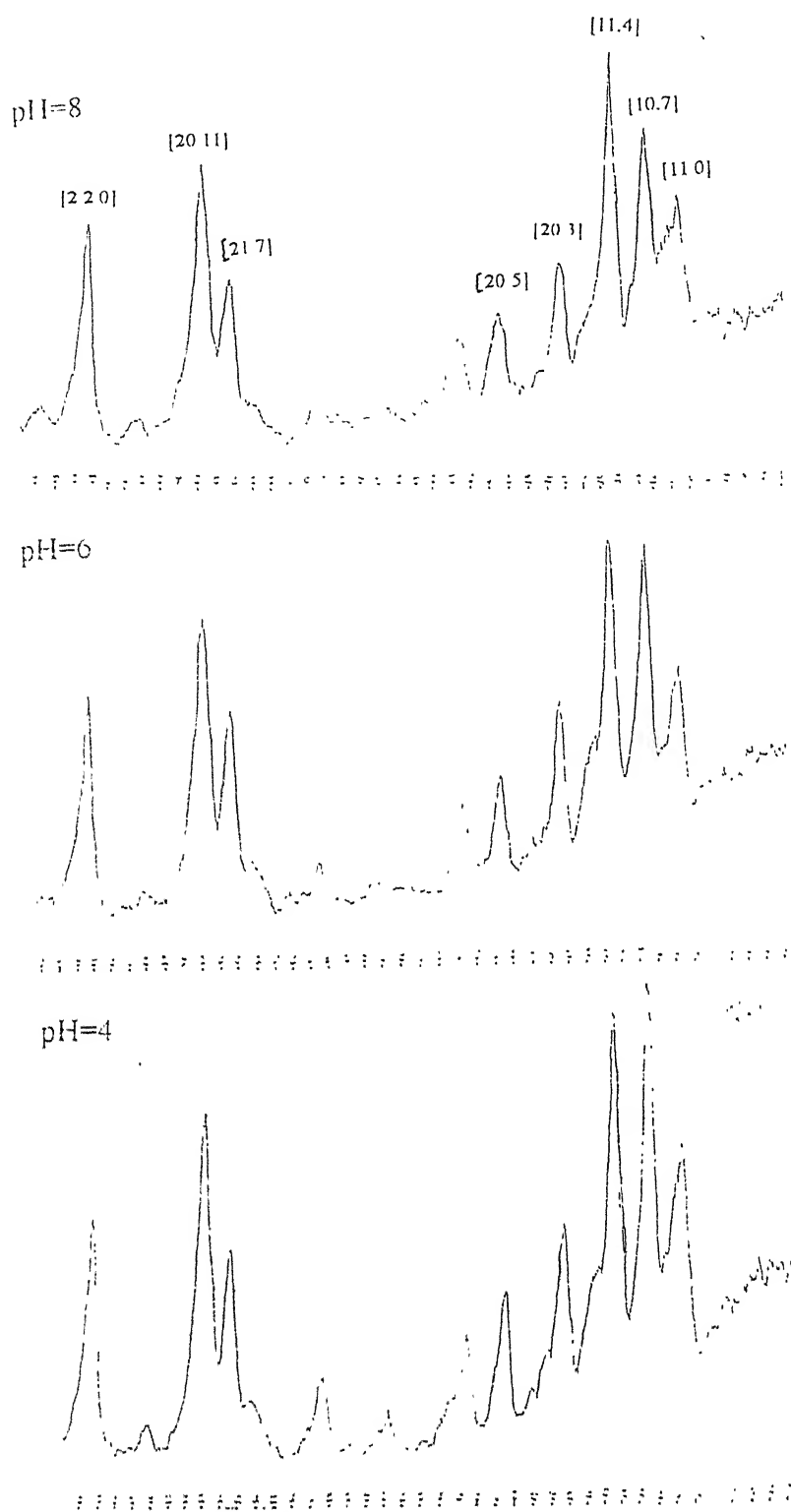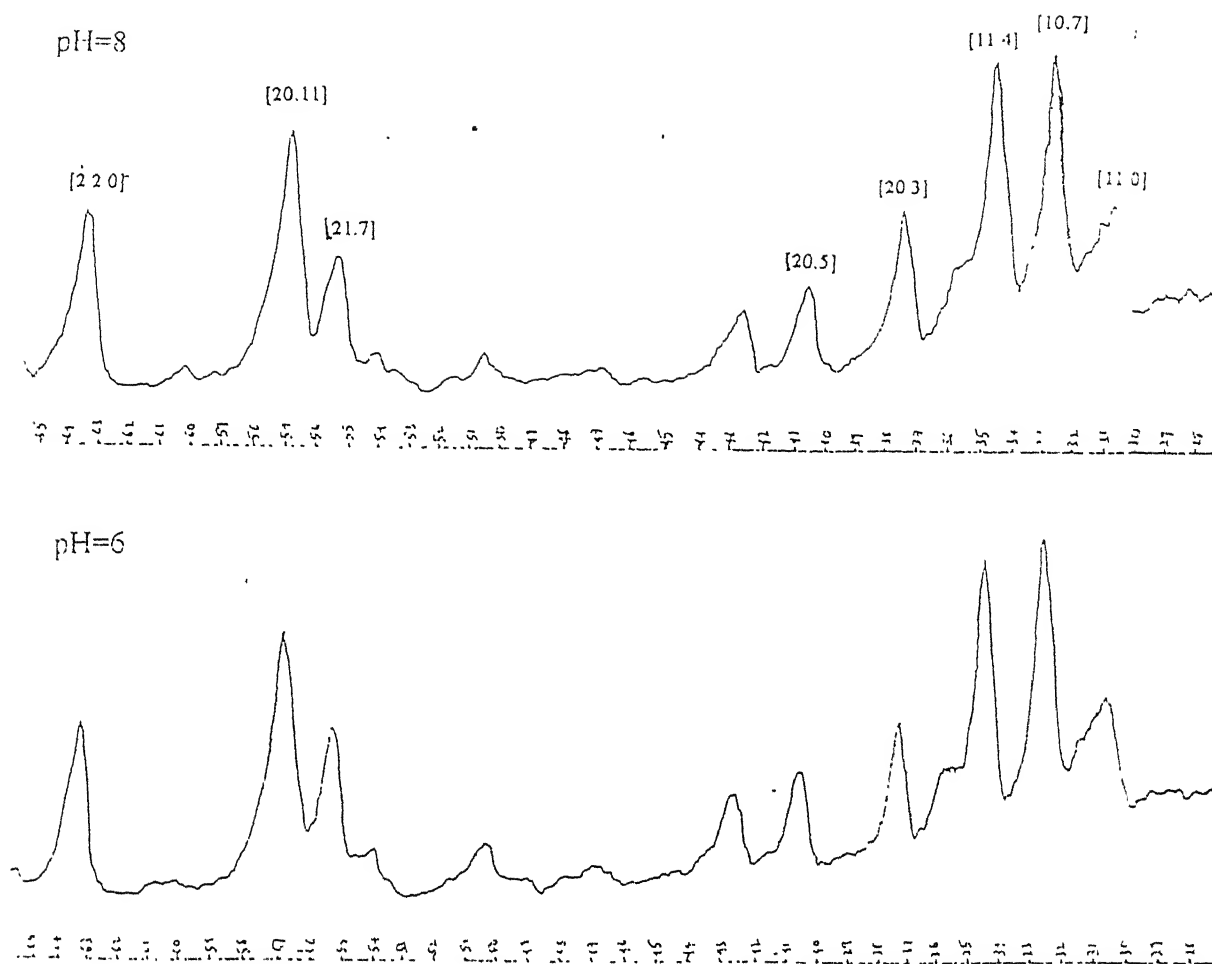
d-values for $BaFe_{12}O_{19}$ (A°)	pH =4 d (A°)	pH=6 d (A°)	pH=8 d (A°)	Intensities for $BaFe_{12}O_{19}$	pH=4	pH=6	pH=8	hk.l indices
2.94	2.94	2.95	2.94	55	58.1	50.3	47	1 1 .0
2.78	2.78	2.79	2.79	100	100	94.9	72	1 0 .7
2.62	2.63	2.63	2.63	98	98.6	100	100	1 1 .4
2.42	2.43	2.44	2.43	60	49.2	51.0	37.5	2 0 .3
2.23	2.24	2.24	2.24	29	28.8	34.3	27.3	2 0 .5
1.66	1.67	1.67	1.67	53	56.5	65.6	50	2 1 .7
1.63, 1.62, 1.61	1.62	1.63	1.62	30, 58, 10	94.7	97.4	87	2 0 .11
1.47	1.47	1.47	1.47	63	64.9	71.3	68.4	2 2 .0

The standard data for pure $BaFe_{12}O_{19}$ phase is given for comparison.

Table 5: Interplanar spacings and intensities of various peaks observed in XRDs of ashes after calcination at 1000°C for five hours. The ashes were produced by autoignition of gels formed in initial solutions of pH 6.0 and 8.0.

d-values for $BaFe_{12}O_{19}$ (A°)	pH = 6 d (A°)	pH = 8 d (A°)	Intensities for $BaFe_{12}O_{19}$	pH = 6	pH = 8	hk.l indices
2.94	2.94	2.94	55	43.8	49	1 1 .0
2.78	2.78	2.78	100	100	100	1 0 .7
2.62	2.63	2.64	98	99.5	99.6	1 1 .4
2.55	2.56	2.56	11	30.4	27	2 0 .0
2.42	2.43	2.43	60	49.5	47.3	2 0 .3
2.23	2.24	2.25	29	31.4	34	2 0 .5
1.81	1.82	1.82	10	20.9	18	2 0 .9
1.66	1.67	1.67	53	50.4	55	2 1 .7
1.63, 1.62, 1.61	1.63	1.62	30, 58, 10	72.3	86.4	2 0 .11
1.47	1.47	1.48	63	52.3	58	2 2 .0

The standard data for pure $BaFe_{12}O_{19}$ phase is given for comparison.

44

4.1.3 Differential thermal analysis (DTA) :

The DTA plot of the gel is shown in Figure 9. The pH of the solution in this case was 4.0. Notice that the gel exhibits a sharp exothermic peak around ~203°C, which can be associated with the autoignition combustion process itself. The reaction basically involves anionic oxidation-reduction between citrate and nitrate ions present in the gel.

Figures 10, 11 and 12 depict the DTA plots of various ashes, obtained by autoignition method using solutions of pH 4.0, 6.0 and 8.0, respectively. The exothermic peaks observed with central maxima around 373°C, 383°C and 397°C (Figures 10,11 and 12 respectively) corresponding to pH of the initial solution values of 4.0,6.0 and 8.0 respectively, are all due to the combustion of the organic residue. The increase in combustion temperature with increase in pH suggest the improved stability of metal complexes with rise in the ethylene diamine content. In other words, ethylene diamine somehow aids and controls the entire combustion process.

4.1.4 Magnetic measurements :

The magnetization versus applied field curve for barium ferrite is shown in Figure 13. Clearly, the magnetization increases with applied field and exhibits saturation. It shows the remanence (M_r) of 33.6 emu/g and coercivity (H_c) of 5190 Oe. The values of saturation magnetization (M_s) and coercivity (H_c) are listed in Table 6 along with the reported data for the sake of comparison. Clearly the saturation magnetization value obtained in the present work is somewhat higher.
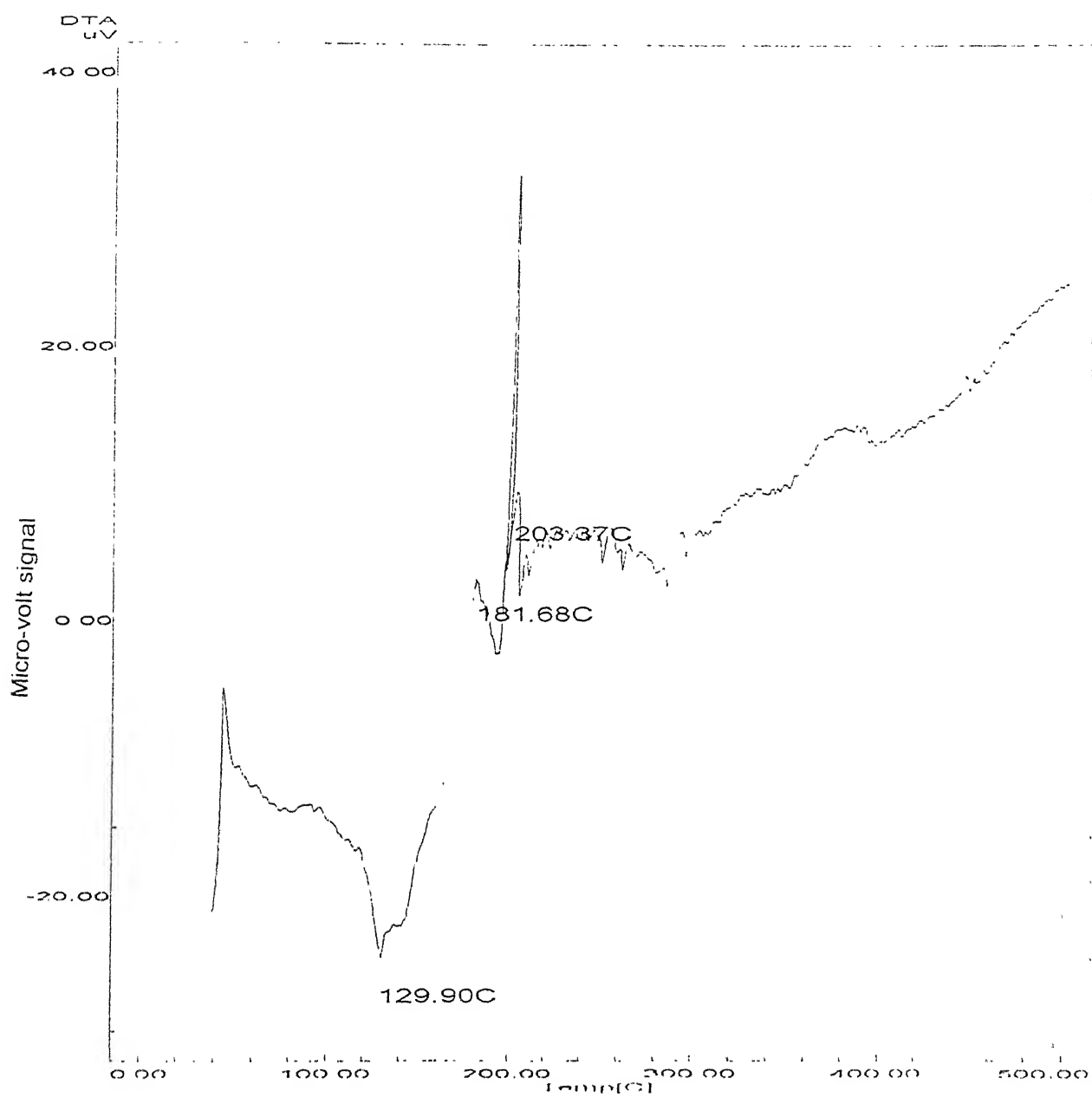
Figure 9: DTA plot of gel formed in the initial solution of pH 4.0.
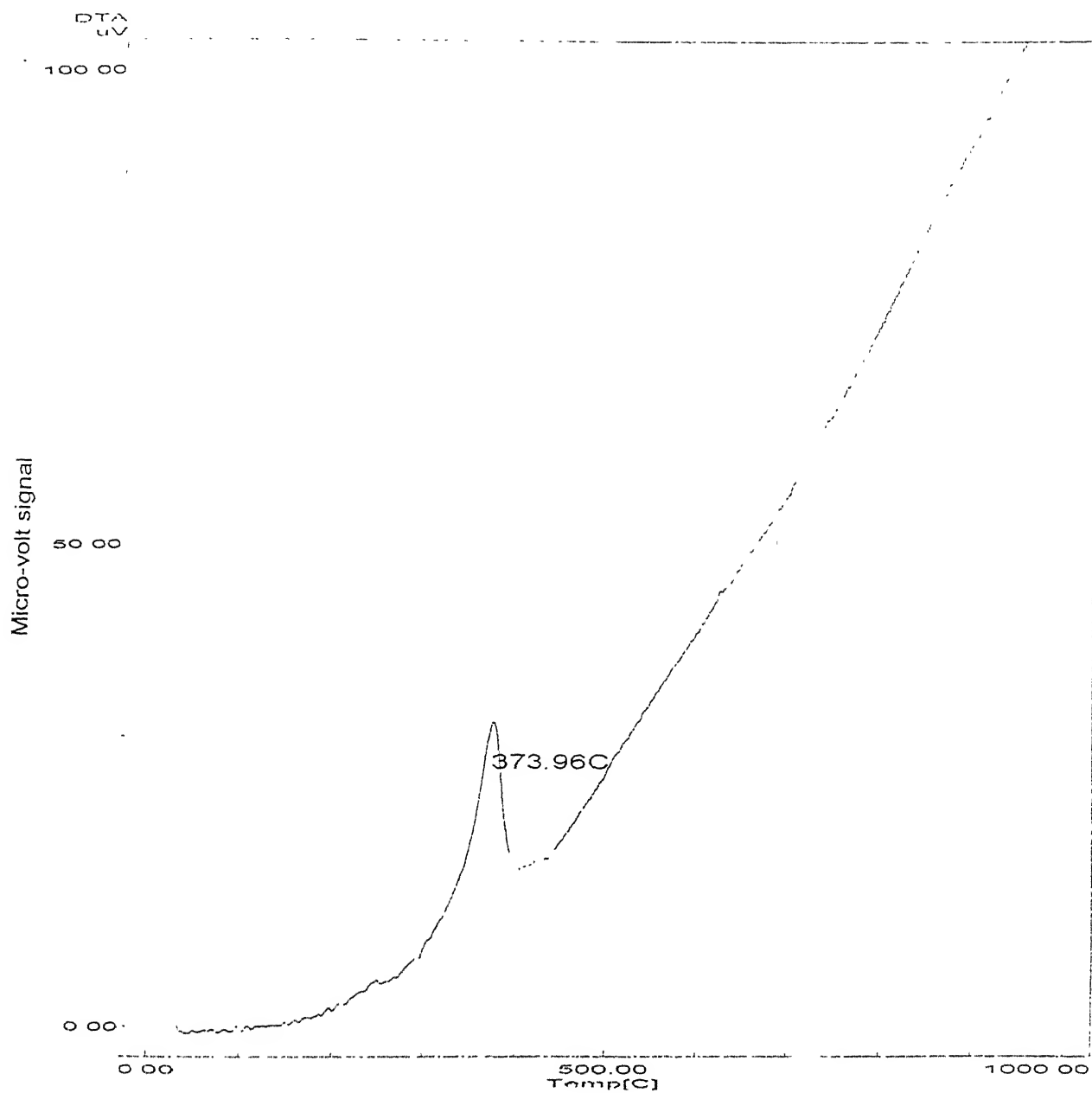
Figure 10: DTA plot of ash obtained by autoignition of gel formed in the initial solution of pH 4.0
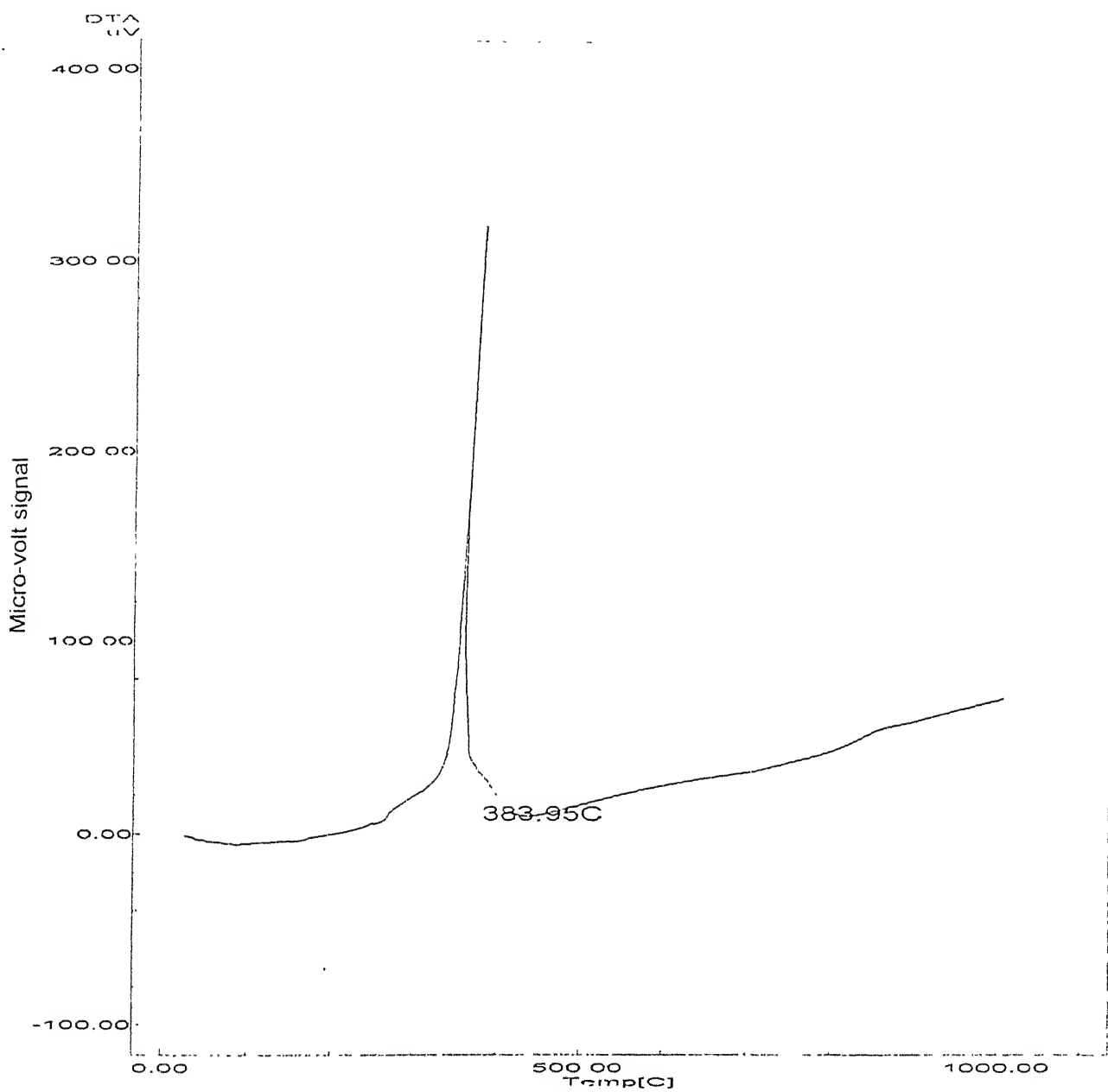
47

Figure 11: DTA plot of ash obtained by autoignition of gel formed in the initial solution of pH 6.0
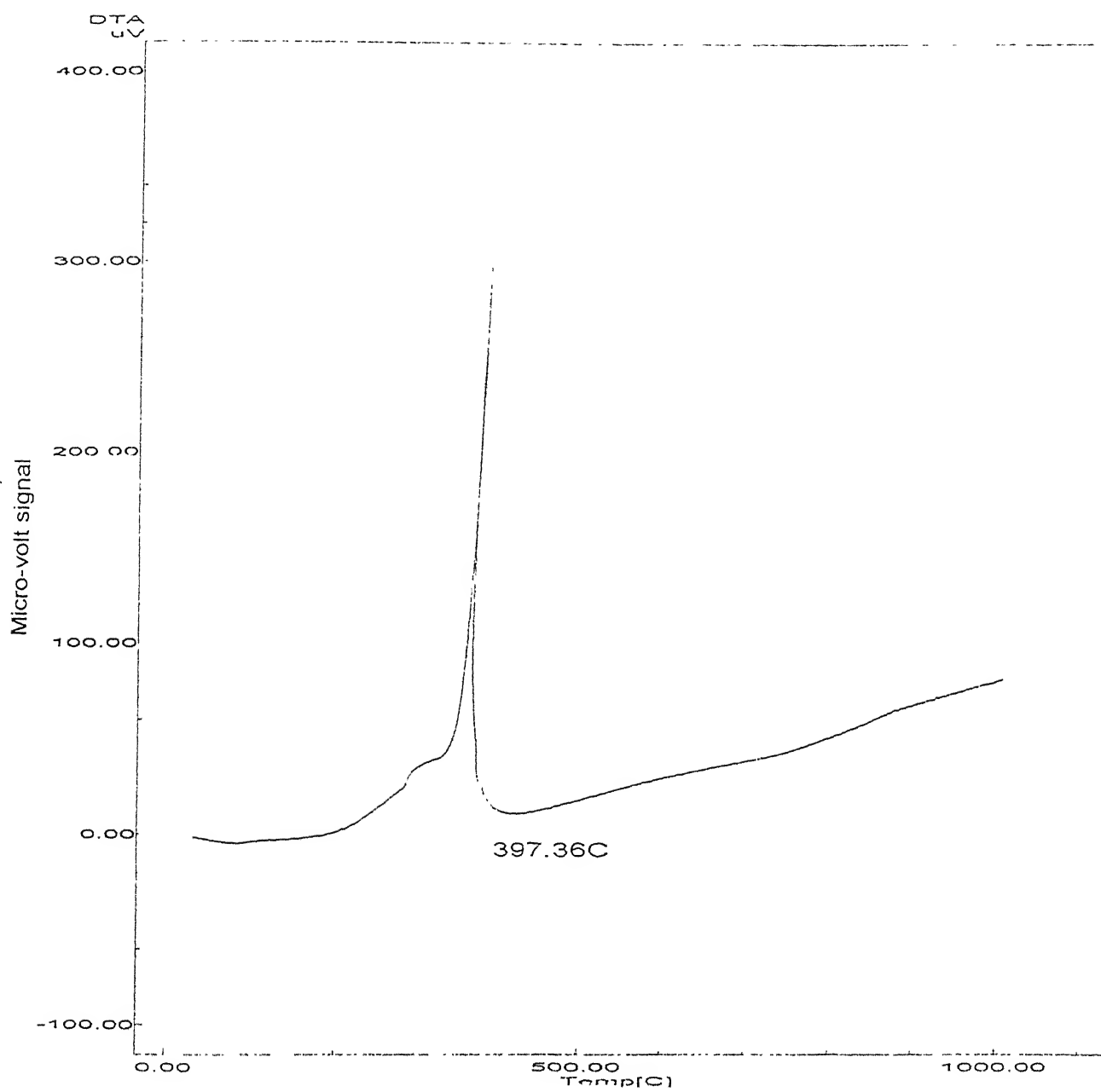
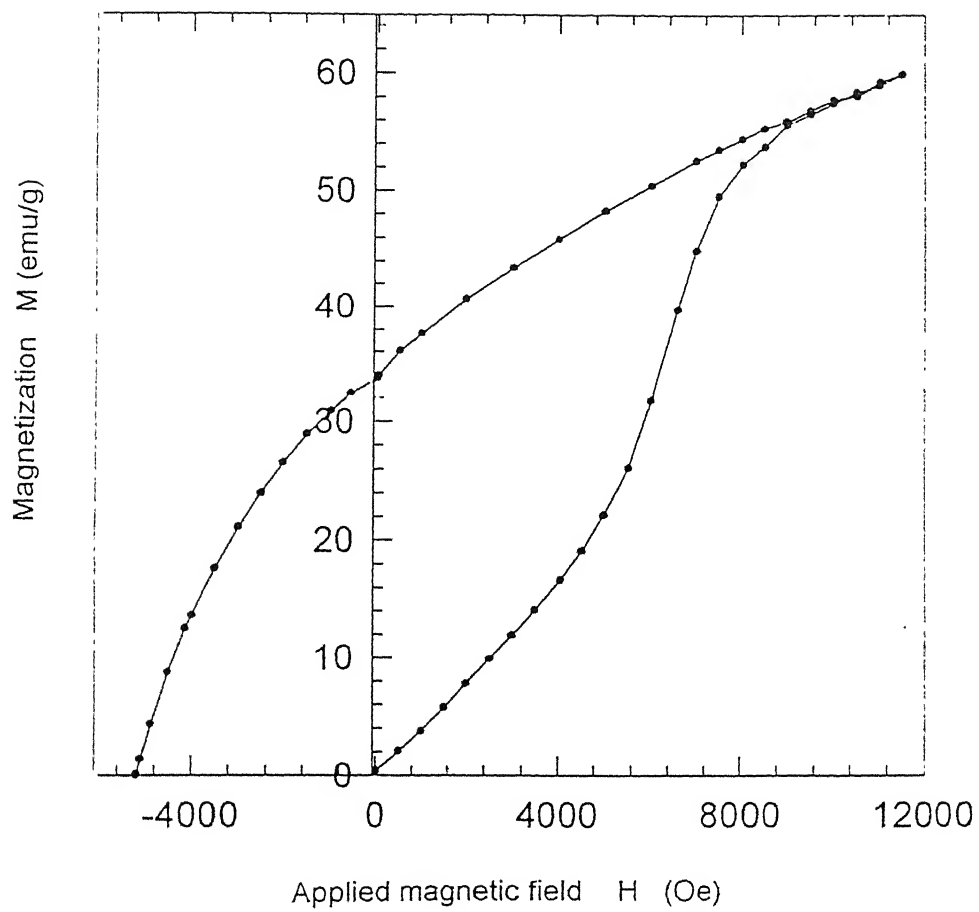Figure 12: DTA plot of ash obtained by autoignition of gel formed in the initial solution of pH 8.0

Figure 13:   Magnetization versus applied field curve of barium ferrite.

Table 6 Saturation magnetization (M_s) and coercivity (H_c) values of Barium ferrite:

Parameter	Present study	Reference [2]	Reference [37]
M_s emu/g	59	57	55
H_c Oe	5190	4000	3500

However, the coercivity value is significantly higher. For any magnetic material, with decrease in the particle size the coercivity increases, goes through a maxima and then tends to zero due to super para magnetism [21]. Therefore, the high value of coercivity here is indicative of the synthesized barium ferrite having a very small particle size.

The magnetization versus temperature curve at a fixed magnetic field of 10,000 Oe is depicted in Figure 14. This indicates the curie temperature as ~450°C, and is in excellent agreement with the known value of 450°C for barium ferrite [21]. Also, the nature of the curve indicates that there are no other magnetic phases present in the synthesized sample. It may be concluded that the autoignition method yields a pure phase of barium ferrite when the pH of the initial nitrate solution is adjusted to 4.0 and calcination carried out at 900°C for five hours.
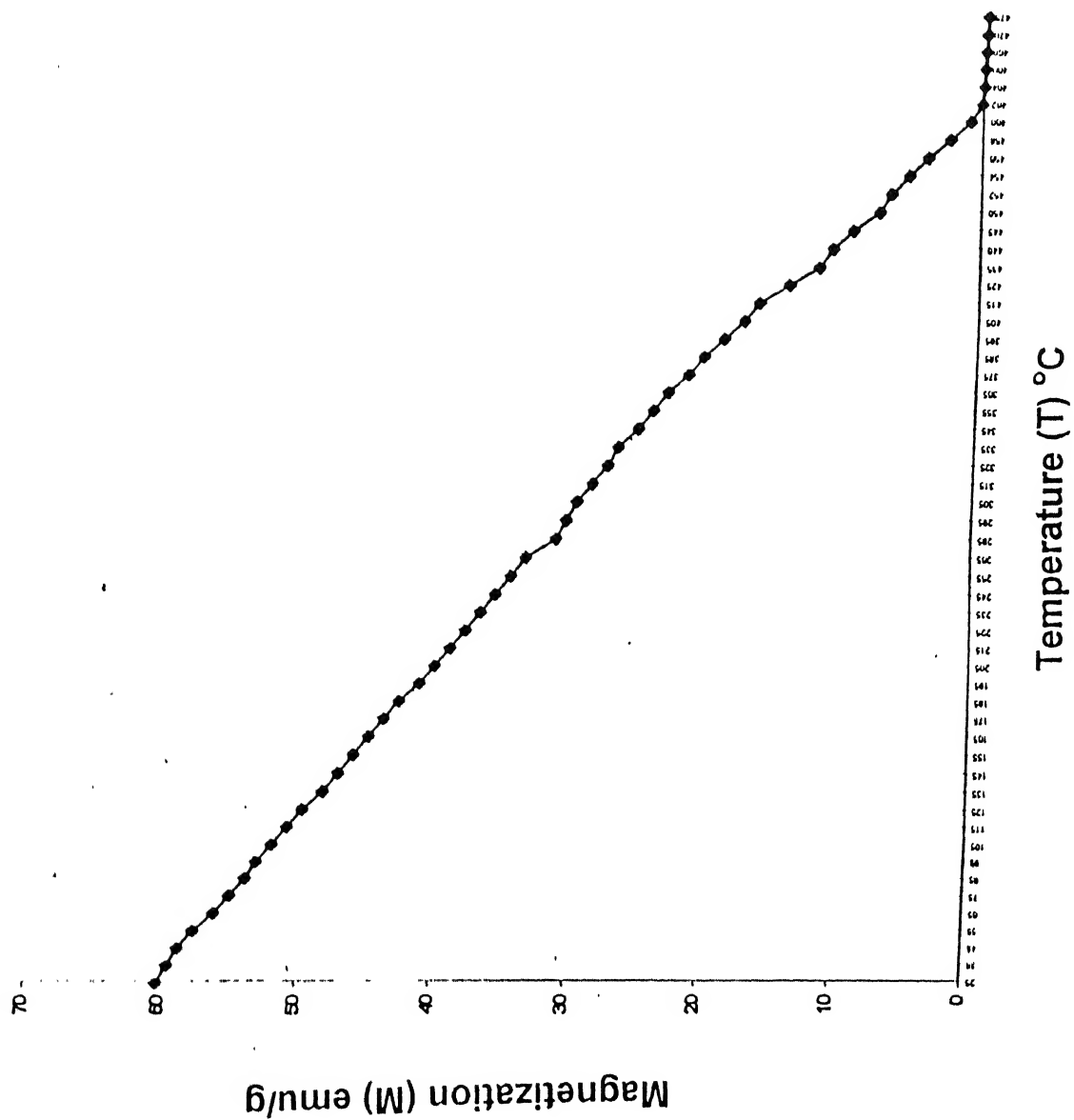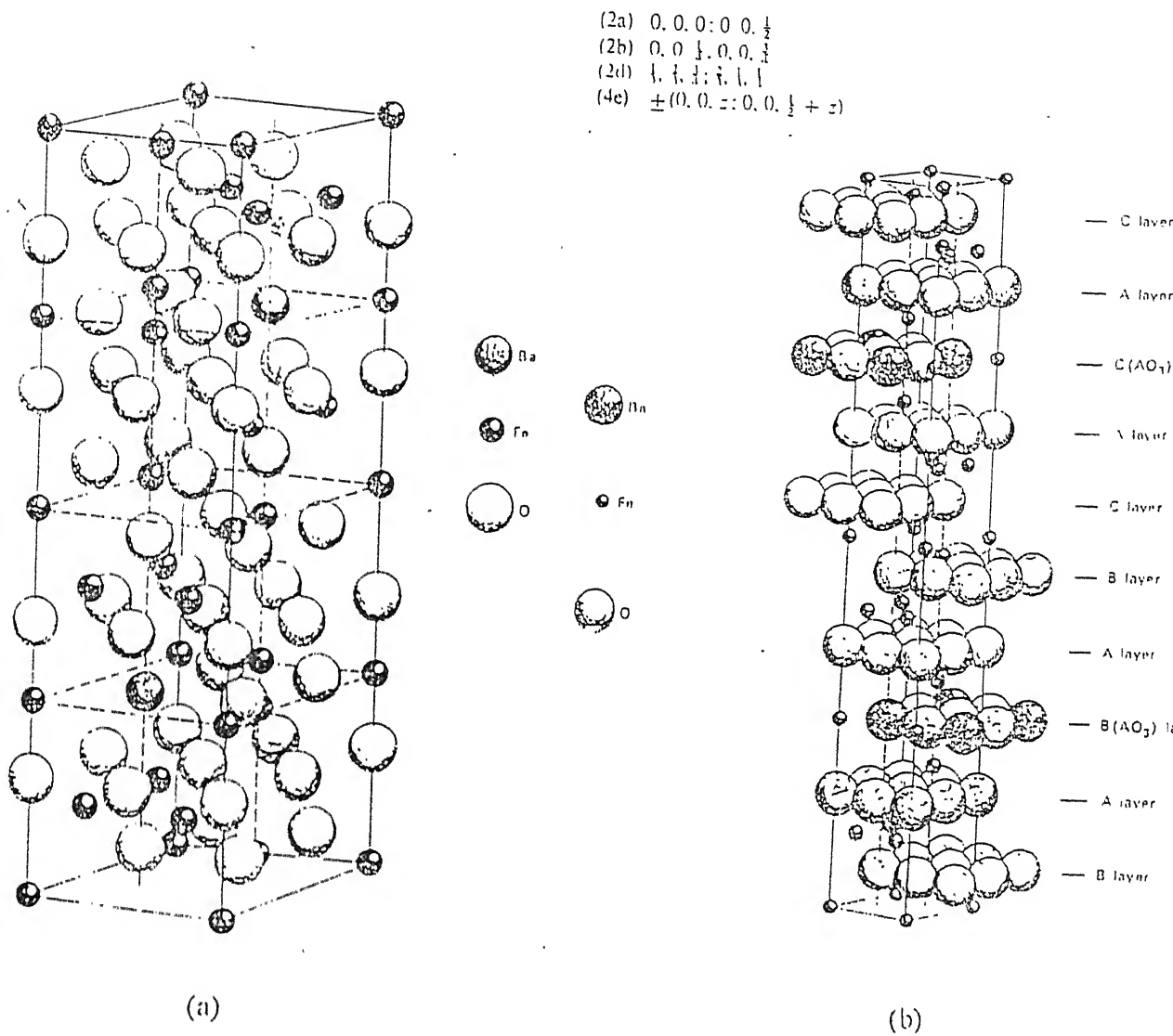
51

Figure 14: Magnetization versus temperature curve of barium ferrite at a fixed magnetic field of

4.2 SYNTHESIS OF METAL SUBSTITUTED BARIUM HEXA FERRITE

As has been pointed out in Chapter 2, current trends in the magnetic recording technology are strongly converging on the planar disposition of particles (i.e., shape anisotropy) which is known as perpendicular recording mode. The hexagonal ferrites are considered to be most promising in this regard due to their chemical, morphological and magnetic characteristics [25]. Though, of barium ferrite synthesized by auto ignition method satisfying most of the requirements, it displays high coercivity (e.g.,5190 Oe in the present case), as against the acceptable range of 1000-2500 Oe. One way to reduce the coercivity of barium ferrite ($BaFe_{12}O_{19}$) is to undertake partial substitution of iron with Co^{2+} and Ti^{4+} ions resulting in a phase of composition $BaFe_{12-2x}Co_xTi_xO_{19}$ with x upto 0.9 [27,28]. Such a substitution indeed reduces the coercivity(H_c) appreciably without affecting the specific magnetization [28]. Thus, the modified barium ferrite satisfies all the requirements of magnetic recording media [24,25].

Barium ferrite, $BaFe_{12}O_{19}$, has a magnetoplumbite structure with hexagonal unit cell having parameters a = 5.892°A, c = 23.183°A, Z = 2 and space group $P6_3/mmc$. It consists of spinel (S) blocks interposed by R blocks (containing oxygen-barium and O^{2-} closed packed layers in hexagonal sequence) and can be described as RSR^*S^*, where the R^* and S^* blocks are obtained from R and S, respectively, by a rotation of 180° about the c-axis [20]. Figure 15 shows the unitcell and layer sequence with distribution of various species. Twenty four Fe^{3+} ions present in barium ferrite unit cell occupy the positions as given in Table 7. The Fe^{3+} ions configuration number per formula unit, block location and spin direction are listed in Table 8.

The BaFe$_{12}$O$_{19}$ Structure (a) unit cell with distribution of species,

(b) close-packed layer sequence with location of iron ions.

Table 7   Positions of Fe^{3+} ions in hexagonal unit cell of barium ferrite

Site	Number of positions	Co-ordinates
2a	2	0,0,0; 0,0,1/2
2b	2	0,0,1/4; 0,0,3/4
4f	8	$\doteq$ (1/3,2/3,z; 2/3,1/3,1/2+z) z = 0.028,0.189
12k	12	$\pm$ (x,2x,z; 2x,x,z; x,x,z; x,2x,1/2-z; 2x,x,1/2+z; x,x,1/2+z) x = 0.167, z = -0.108

Table 8: Iron ions configuration: number per formula unit, block location and spin direction in barium ferrite $BaFe_{12}O_{19}$

Site	Configuration	Number	Block	Spin
$4f_{vi}$	Octahedral	2	R	down
2b	Bipyramidal	1	R	up
12k	Octahedral	6	R-S	up
$4f_{iv}$	Tetragonal	2	S	down
2a	Octahedral	1	S	up

These ions make different contributions to the magnetic properties, e.g.,

(1) The uniaxial magneto-crystalline anisotropy results largely from 2b and $4f_{vi}$ sites belonging to the R block, and

(2) Temperature dependence of the specific magnetization is attributed to the ions of 12k sites. According to Zhou, Morrish and Li [28], Co^{2+} and Ti^{4+} ions prefer to occupy the $4f_{vi}$ and 2b crystallographic sites. As a consequence, uniaxial anisotropy is significantly reduced causing the corresponding decrease in the coercivity. Also, an overall reduction in iron content could also give rise to slight reduction in the saturation magnetization of $BaFe_{12-2x}Co_xTi_xO_{19}$.

For a random particle assembly, the coercivity (H_c) can be described by [26]
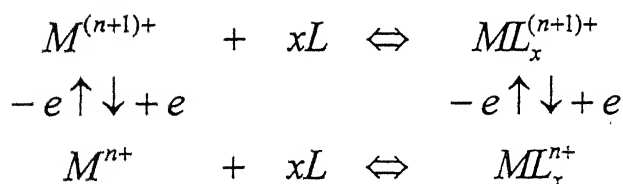
$$H_c = \left(\frac{2K}{M_s} - N_d M_s \right)$$

where K is the uniaxial magnetocrytalline anisotropy factor, M_s is the saturation magnetization and N_d is the shape demagnetization term (determined only by shape of the particles). Zhou, Morrish and Li [28] attributed dramatic decrease of coercivity (H_c) from 4425 to 445 Oe in $BaFe_{12-2x}Co_xTi_xO_{19}$ to the continuous decrease in the uniaxial magnetocrystalline anisotropy factor (K) with increase in the Co^{2+} and Ti^{4+} content, i.e., as x increases from zero to 0.9. However, their average particle planar dimension and height also show significant decrease with increase in x. Yet size contribution to the decrease in coercivity ignored by them altogether. With decrease in particle size, surface effects are expected to become important and cause reduction in coercivity through decrease in the value of anisotropic factor 'K' in a subtle way. Needless to say, Fujiwara

[24] also produced well seperated barium ferrite particles (platelet type with hexagonal shapes) with narrow size distribution (size as small as 50nm and specific surface area of $31m^2/g$) by employing glass crystallization method and substituting small amounts of Fe^{3+} by Co^{2+} and Ti^{4+}, their magnetization, coercivity and Curie temperature being 57 emu/g, 500 Oe and 320°C. These characteristics make the material ideal for high density perpendicular recording. The striking point to note is reduction in coercivity(H_c) and Curie temperature (the value for bulk being 452°C) without significant change in saturation magnetization.

4.2.1 Cobalt substitution :

When ethylene diamine is added to a solution containing metal ions, complexes known as chelates are formed. Also, complexes like ML^{n+} and $ML^{(n+1)+}$ where M is the metal ion and L is the ligand of same chemical composition but with different charge may exist in the solution and reach equilibrium following the scheme:

$$
\begin{array}{ccccc}
M^{(n+1)+} & + & xL & \Leftrightarrow & ML_x^{(n+1)+} \\
-e\uparrow\downarrow+e & & & & -e\uparrow\downarrow+e \\
M^{n+} & + & xL & \Leftrightarrow & ML_x^{n+}
\end{array}
$$

The stability of such a complex ion couple in the solution is largely determined by its redox potential which itself depends on the nature of the chelating agent (ethylene diamine in the present case). Further, it has been observed that Co^{3+} state is strongly favoured to Co^{2+} state, in the case of phenonthraline or ethylene diamine tetra acetate couples [36]. Also, $[Co(en)_3]^{3+}$ is one of the most stable chelate of ethylene diamine. It is therefore believed that Co^{2-} may also oxidize to Co^{3+}

couple of ethylene diamine. Further, since the size difference between iron and cobalt ions is less than 15%, it is possible that some of the Fe^{3+} of $BaFe_{12}O_{19}$ molecule may get replaced by Co^{3+} ions. Moreover, the hexagonal ferrite phase is known to persist even with little deviation in stoichiometry [20], it is expected that the crystal structure of the compound will not change drastically even if some Co^{2+} ions replace Fe^{3+} ions. Keeping these factors in view, we have partially substituted iron with cobalt by adding different amounts of $Co(NO_3)_2 6H_2O$ to the metal-nitrate-citrate solution. This way, six samples of barium ferrite with cobalt replacing iron (x = 0.5, 1.0, 1.5, 2.0, 2.5 and 3.0) having composition $BaFe_{12-x}Co_xO_{19}$ are prepared.

The magnetization versus applied field curves for all the cobalt substituted barium ferrites are shown together in Figure 16 and individually in Figures 18-23. Their nature clearly reveals that with increase of cobalt content the coercivity decreases drastically and the squareness of the hysterisis loop improves. The coercivity is a measure of central tendency of material to reverse magnetization. Hence it must be determined by variance of field at which individual particles reverse their direction of magnetization. To understand this, the switching field distribution is obtained by plotting the slope of magnetization curve against the normalized half width (i.e.,$\Delta H/H_c$), as shown in Figure 1. Thus, the smaller value of $\Delta H/H_c$, relates to narrow distribution of fields at which individual particles reverse their magnetization. In the present case, the squareness of the magnetization curve is increasing with increasing cobalt substitution. This means that the cobalt substitution is decreasing the $\Delta H/H_c$ and perhaps can be attributed to emergence of nearly uniform size particles, an important requirement of recording media. The variation of coercivity with increasing amount of cobalt substitution is shown in Figure 17. As is
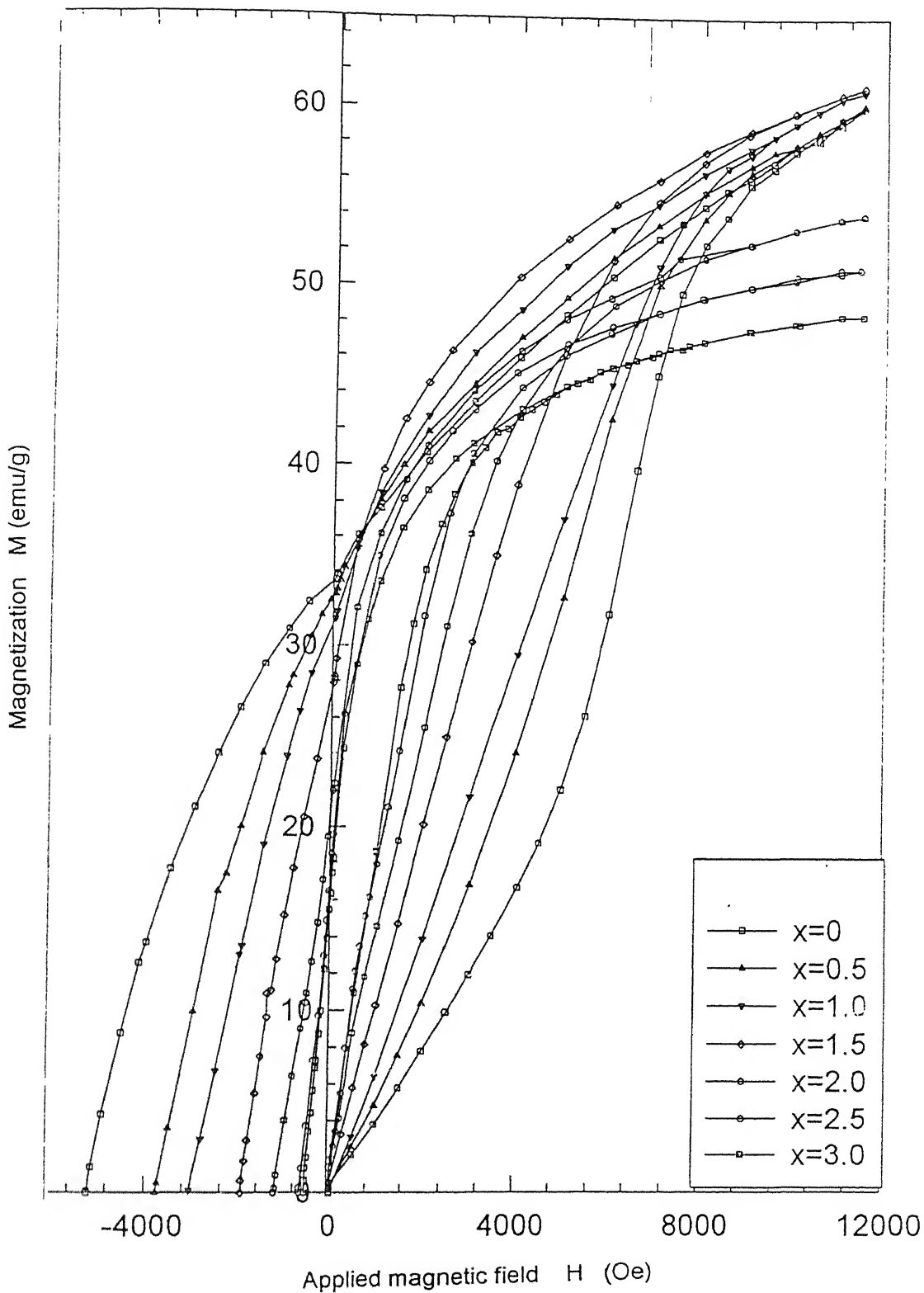
Figure 16: Magnetization versus applied field curves for cobalt substituted barium ferrites, BaFe$_{12-x}$Co$_x$O$_{19}$ (x = 0, 0.5, 1.0, 1.5, 2.0, 2.5, 3.0).
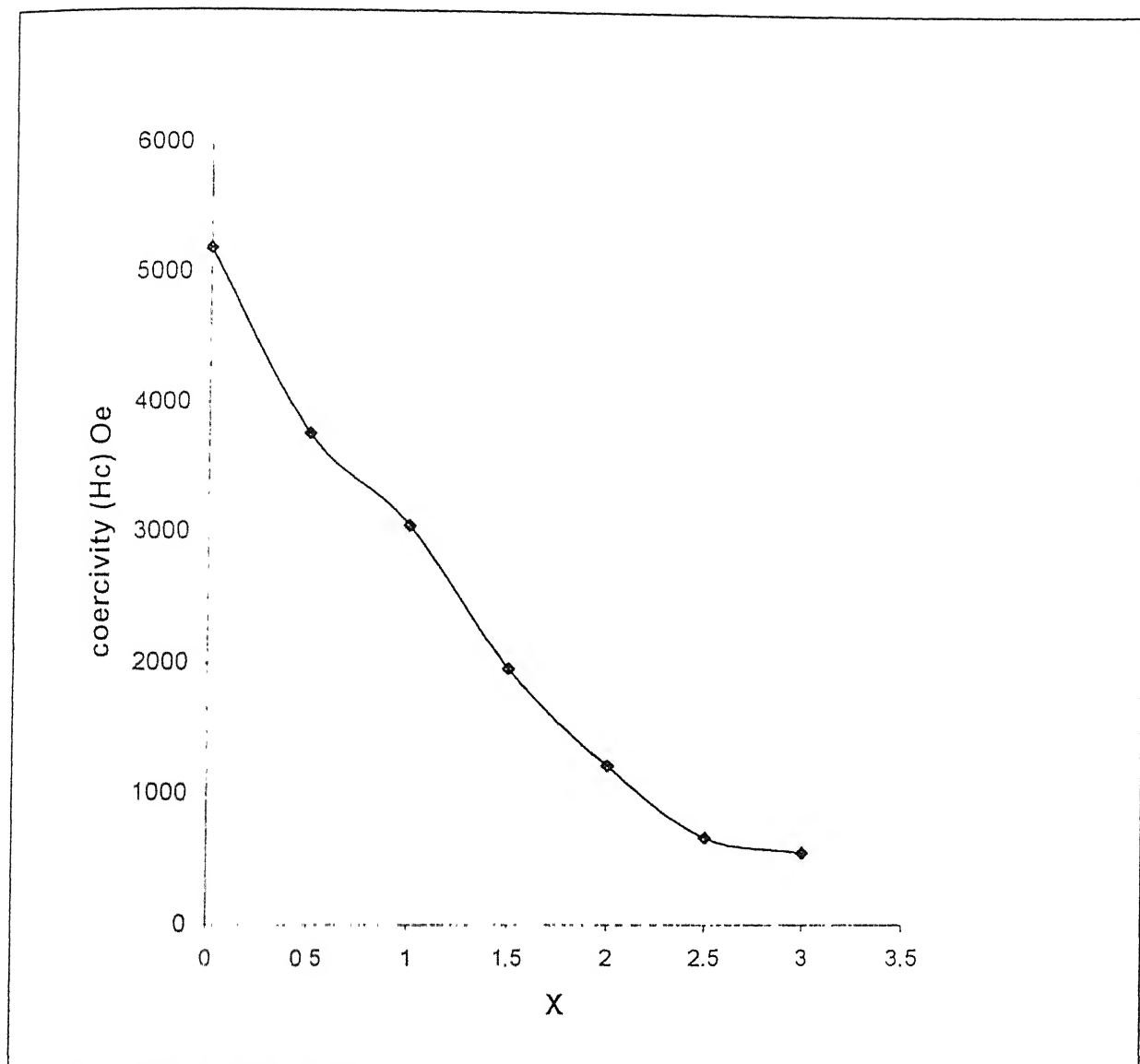
59

Figure 17: Variation of coercivity H_c (Oe) with cobalt content in $BaFe_{12-x}Co_xO_{19}$ (x = 0, 0.5, 1.0, 1.5, 2.0, 2.5, 3.0).
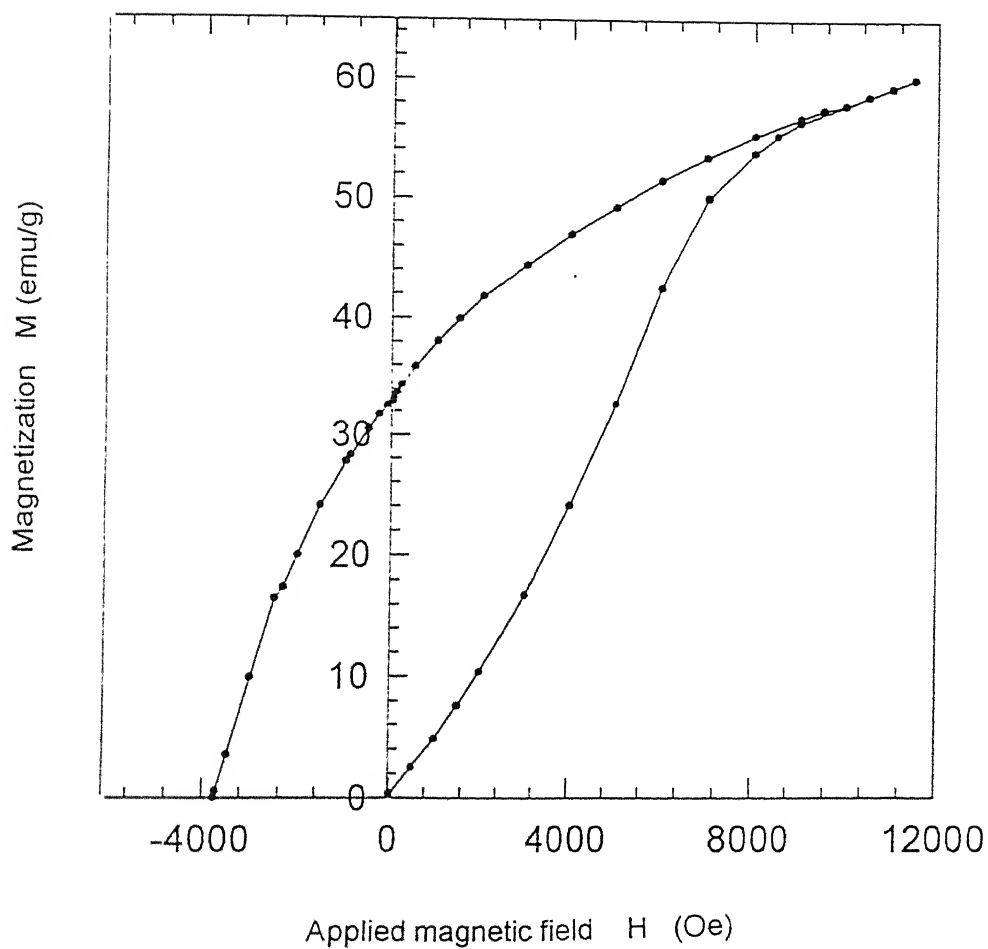
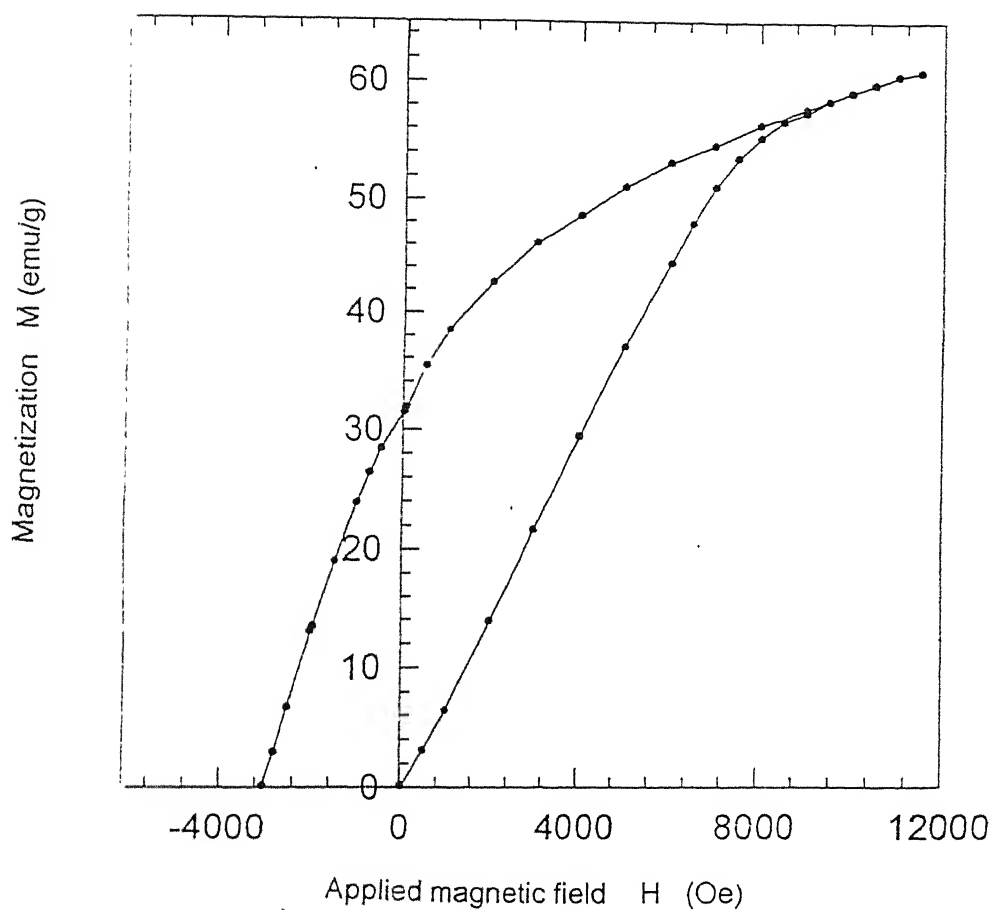Figure 18: Magnetization versus applied field curve for cobalt substituted barium ferrite, $BaFe_{12-x}Co_xO_{19}$ (x = 0.5).

Figure 19: Magnetization versus applied field curve for cobalt substituted barium ferrite, $BaFe_{12-x}Co_xO_{19}$ (x = 1.0).
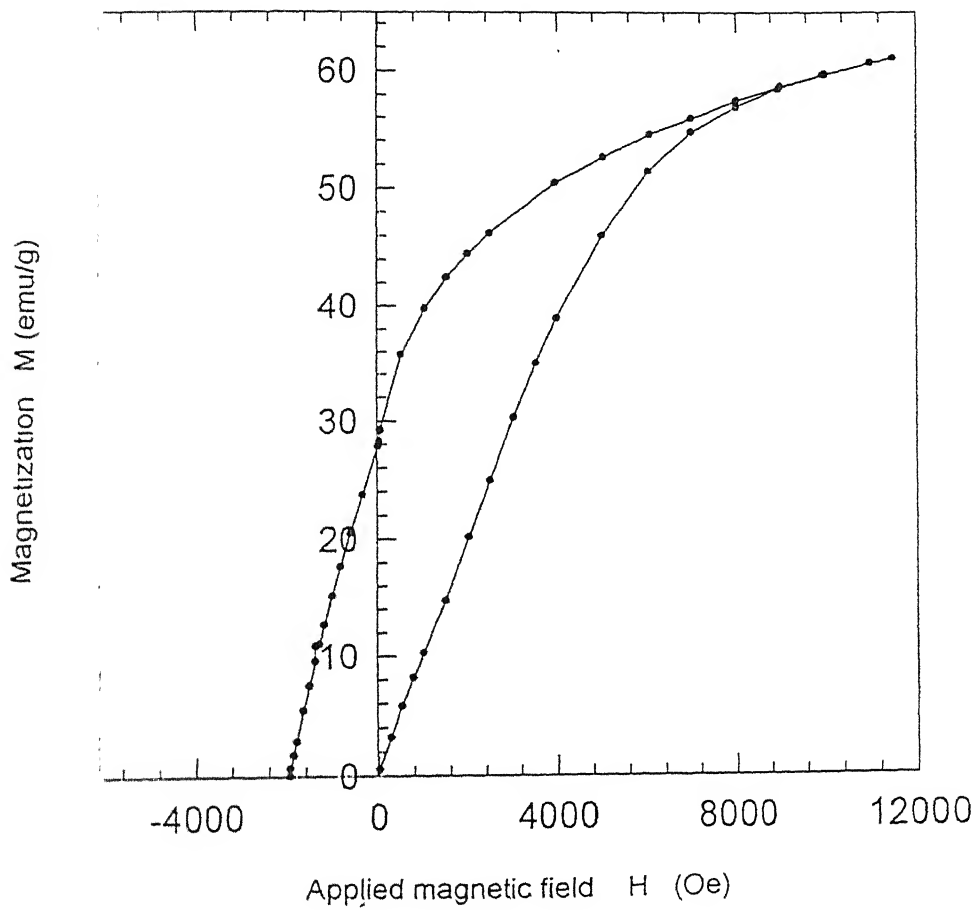
Figure 20.   Magnetization versus applied field curve for cobalt substituted barium ferrite. $BaFe_{12-x}Co_xO_{19}$ (x = 1.5).
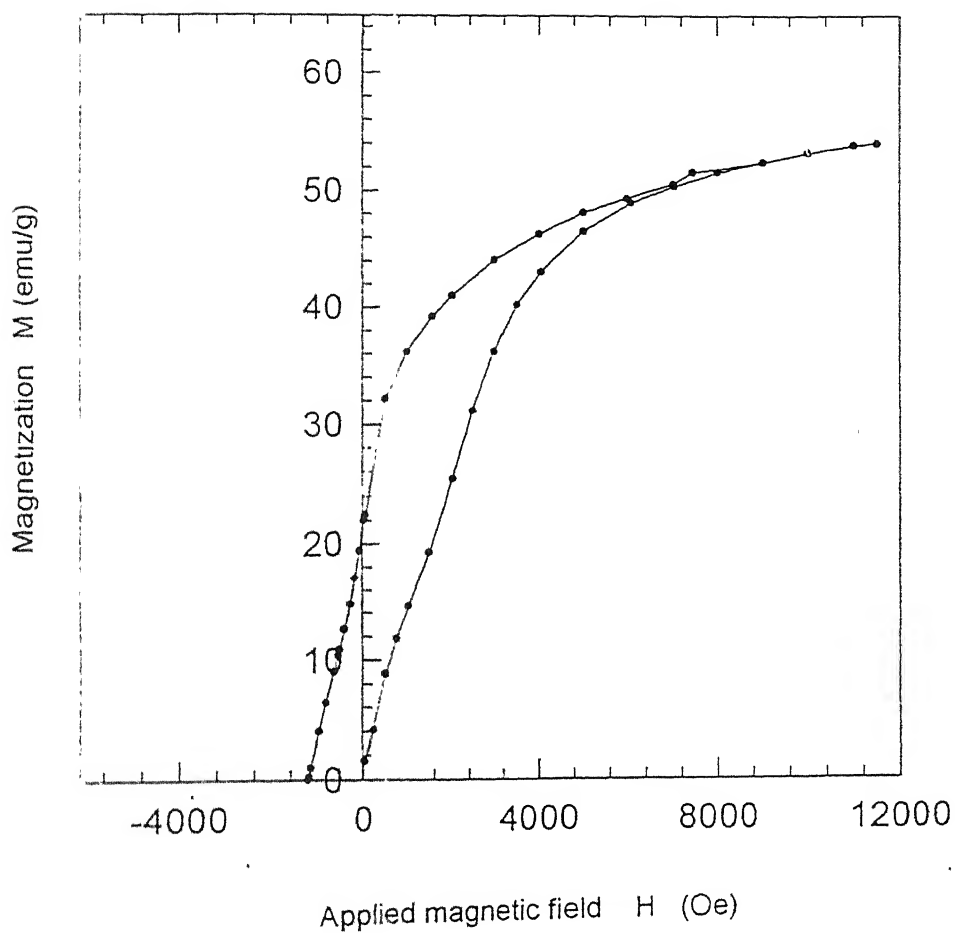
Figure 21: Magnetization versus applied field curve for cobalt substituted barium ferrite, $BaFe_{12-x}Co_xO_{19}$ (x = 2.0).

Figure 22: Magnetization versus applied field curve for cobalt substituted barium ferrite, $BaFe_{12-x}Co_xO_{19}$ (x = 2.5).

Figure 23: Magnetization versus applied field curve for cobalt substituted barium ferrite, $BaFe_{12-x}Co_xO_{19}$ (x = 3.0).

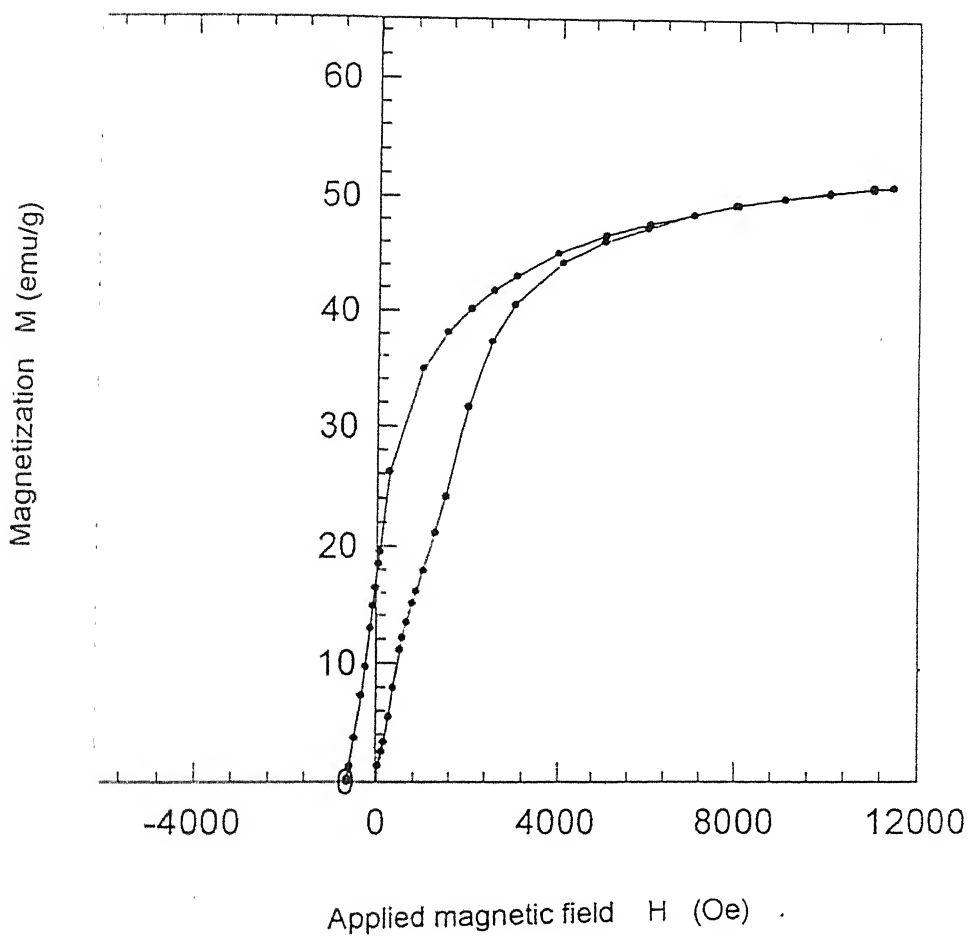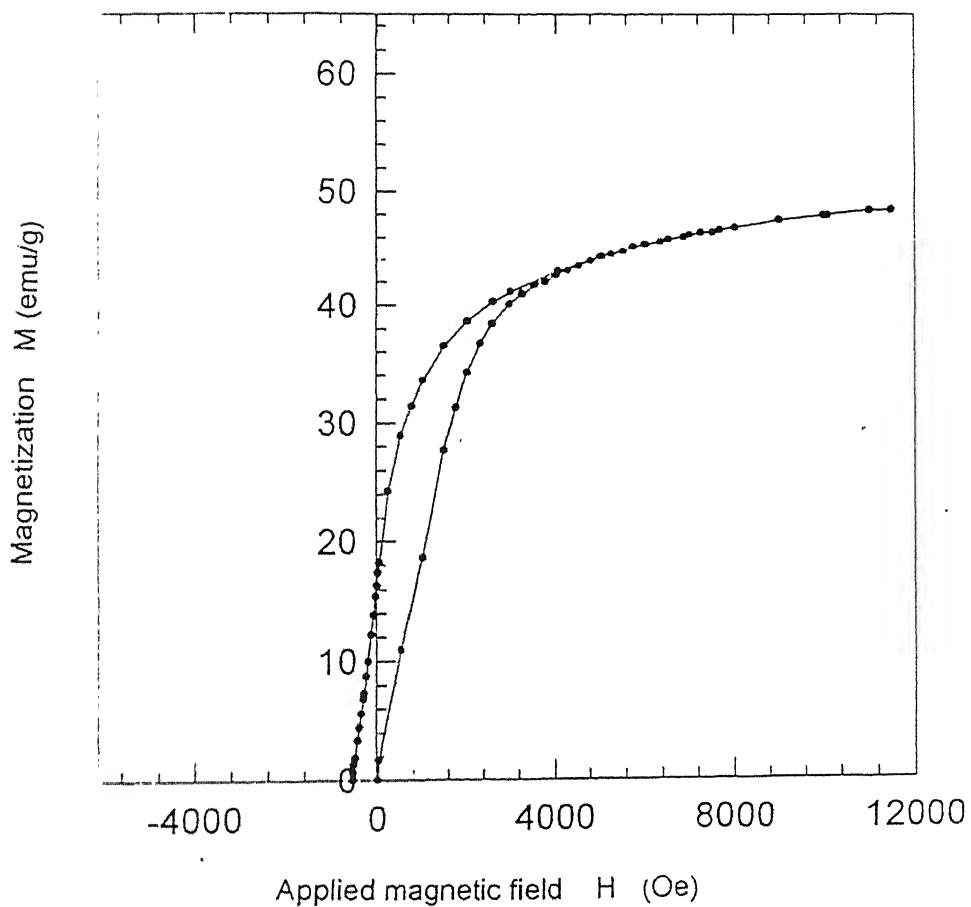evident, the value of coercivity decreases continuously with increase in amount of Fe^{3+} substitution by cobalt (x = zero to 3.0). It is worth noting that the coercivity values decreases to 1945 Oe at x =1.5. The product with this coercivity value is suitable for recording application, specially in magnetoresistive mode, and therefore the composition with x ~1.5 is important from application viewpoints. As the substitution amount increases further, the coercivity of the samples continues to decrease and attains a value as low as 548 Oe at x = 3.0. The effect of cobalt

substitution on magnetic saturation magnetization (M_S) is presented in Table 9.

Table 9 Saturation magnetization values of different cobalt substituted barium ferrites.:

Amount of substitution x	Saturation magnetization (M_s) emu/g
0.0	59.0
0.5	60.2
1.0	60.8
1.5	61.2
2.0	57.4
2.5	54.2
3.0	51.5

With increase in cobalt content, M_s increases initially, passes through maxima at about 61.2 emu/gm and then decreases again. The major shortcoming in use of barium ferrite in advanced applications lies in its low M_s value [25]. In contrast, it is reported that substitution by Co-Ti decreases the saturation magnetization of barium ferrite [38]. However, in the present work M_s is found to increase from 59 to 61.2 and this trend is of interest and great technical importance in recording applications. The sudden decrease of M_s in samples of $x \geq 2.0$, may be due to the formation of some extra phases. This conjecture derives support from Turulli [38] and Licci [39], who reported changes in the crystal structure of barium ferrite when on the average 1.8 Fe^{3+} ions per $BaFe_{12}O_{19}$ molecule are replaced by equal numbers of divalent and tetravalent ions. Magnetization versus temperature plots for cobalt substituted barium ferrite with x = 2, 2.5 and 3 are shown in Figures 24,25 and 26 respectively. The kinks observed in all the curves are indicative of the presence of more than one magnetic phase. Moreover, cobalt substitution increases the Curie temperature from 450°C (of a pure barium ferrite x = 0) to ~550°C for x = 2.0 and this may be due to the enhanced ferromagnetic interactions. The increase in cobalt, further decreases the T_c to lower values with changes in the nature of the plots characterizing the emergence of new magnetic phase(s), e.g., $CoFe_3O_4$ (Curie temperature ~520°C), etc.

The XRD patterns of all the six materials of composition $BaFe_{12-x}Co_{x-\delta}Co_{\delta}O_{19-2\delta}$ with x = 0.5, 1.0, 1.5, 2.0, 2.5 and 3.0 are shown in the Figures 27-32. The d-values and respective intensities of various diffracted peaks are given in Tables 10-15. The analysis reveal that barium hexaferrite maintains the crystal structure upto x = 1.5. At high x, $CoFe_2O_4$ (a soft ferrite) begins to
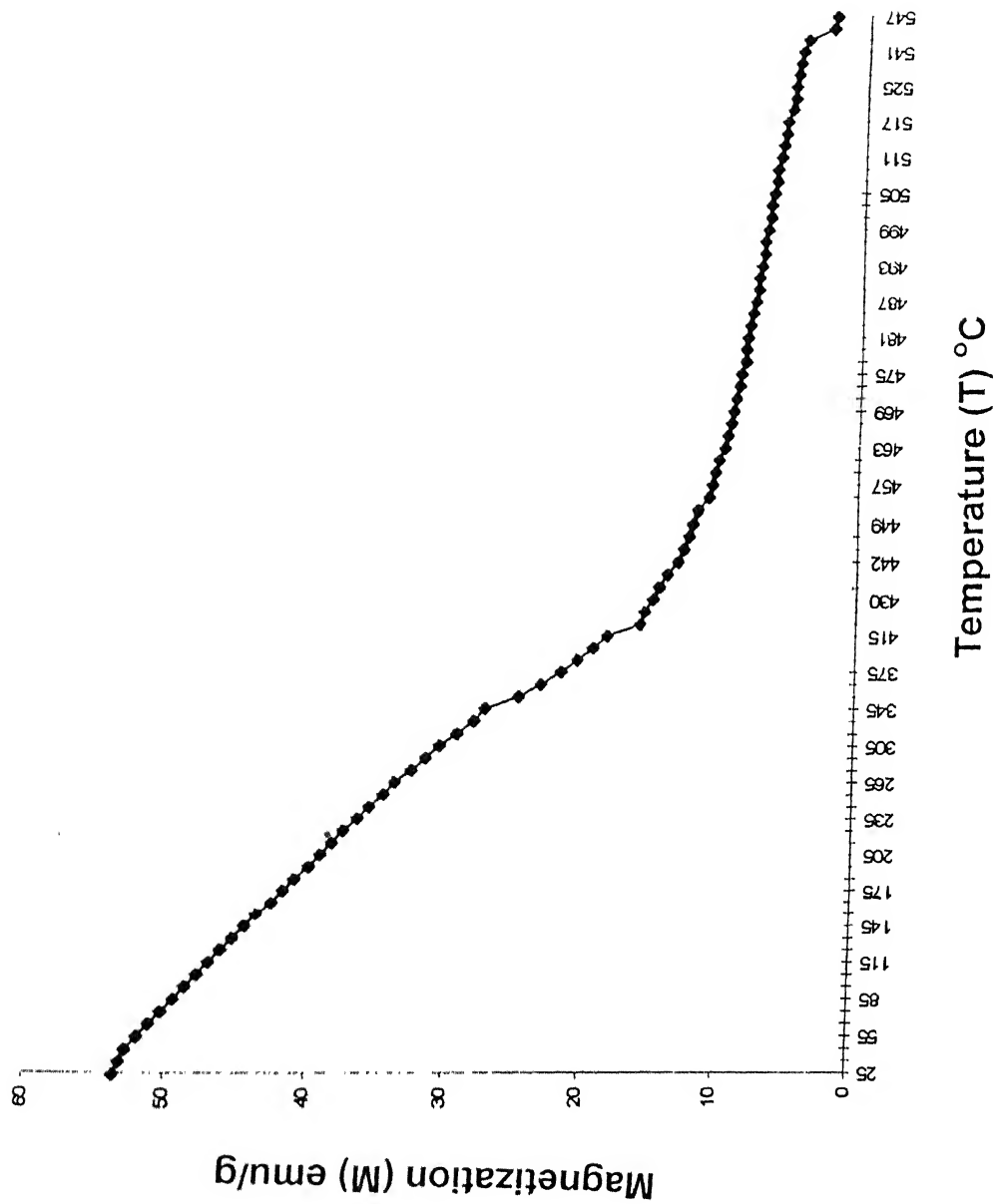
68
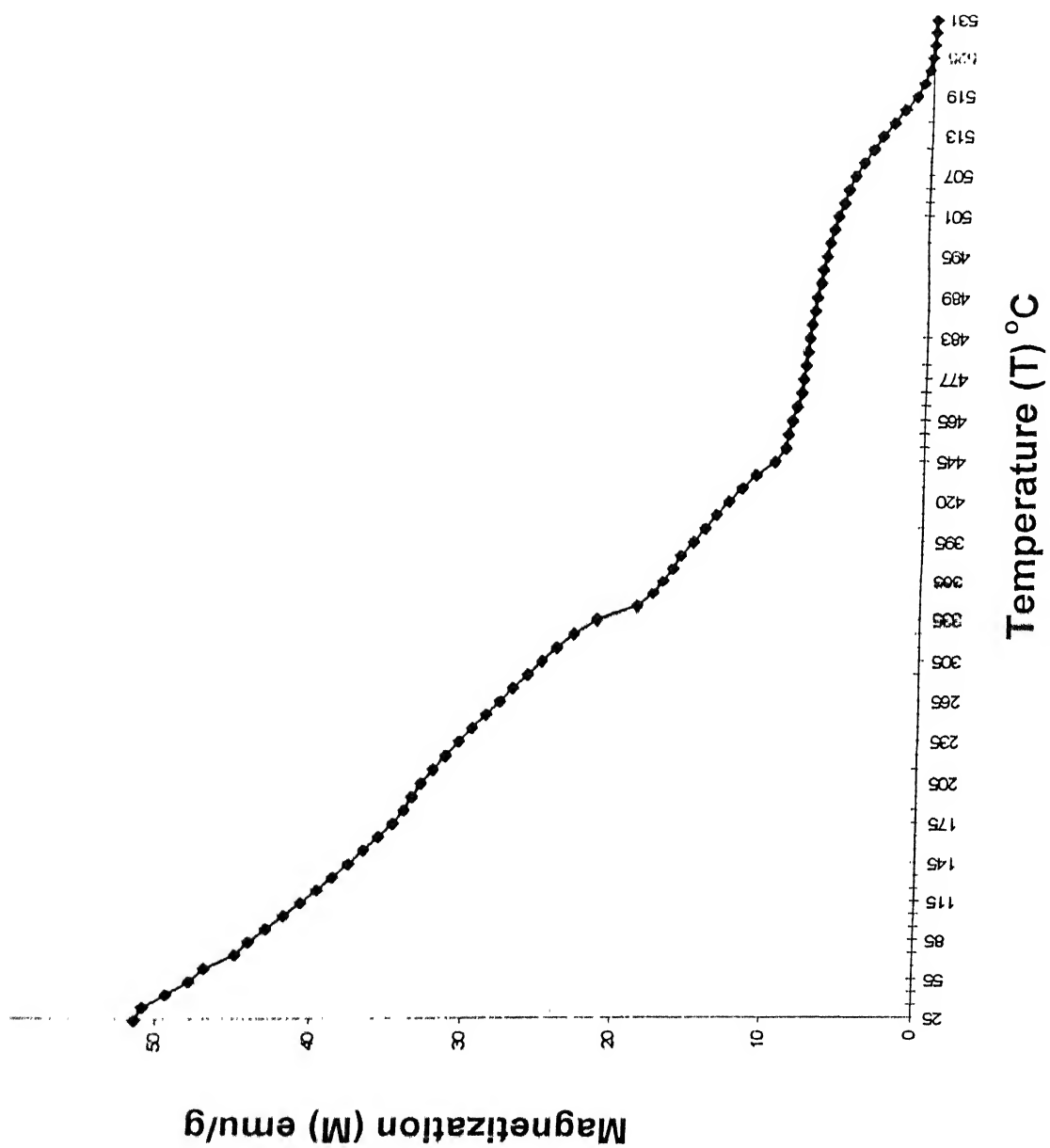
Figure 24: Magnetization versus temperature curve of cobalt substituted barium ferrite, $BaFe_{12-x}Co_xO_{19}$ ($x = 2.0$) at a fixed magnetic field of 10K Oe.

Figure 26: Magnetization versus temperature curve of cobalt substituted barium ferrite, $BaFe_{12-}$ ...

71

Figure 27: XRD pattern of cobalt substituted barium ferrite, $BaFe_{12-x}Co_xO_{19}$ ($x = 0.5$).

Figure 28: XRD pattern of cobalt substituted barium ferrite, $BaFe_{12-x}Co_xO_{19}$ (x = 1.0).

Figure 29: XRD pattern of cobalt substituted barium ferrite, $BaFe_{12-x}Co_xO_{19}$ ($x = 1.5$).

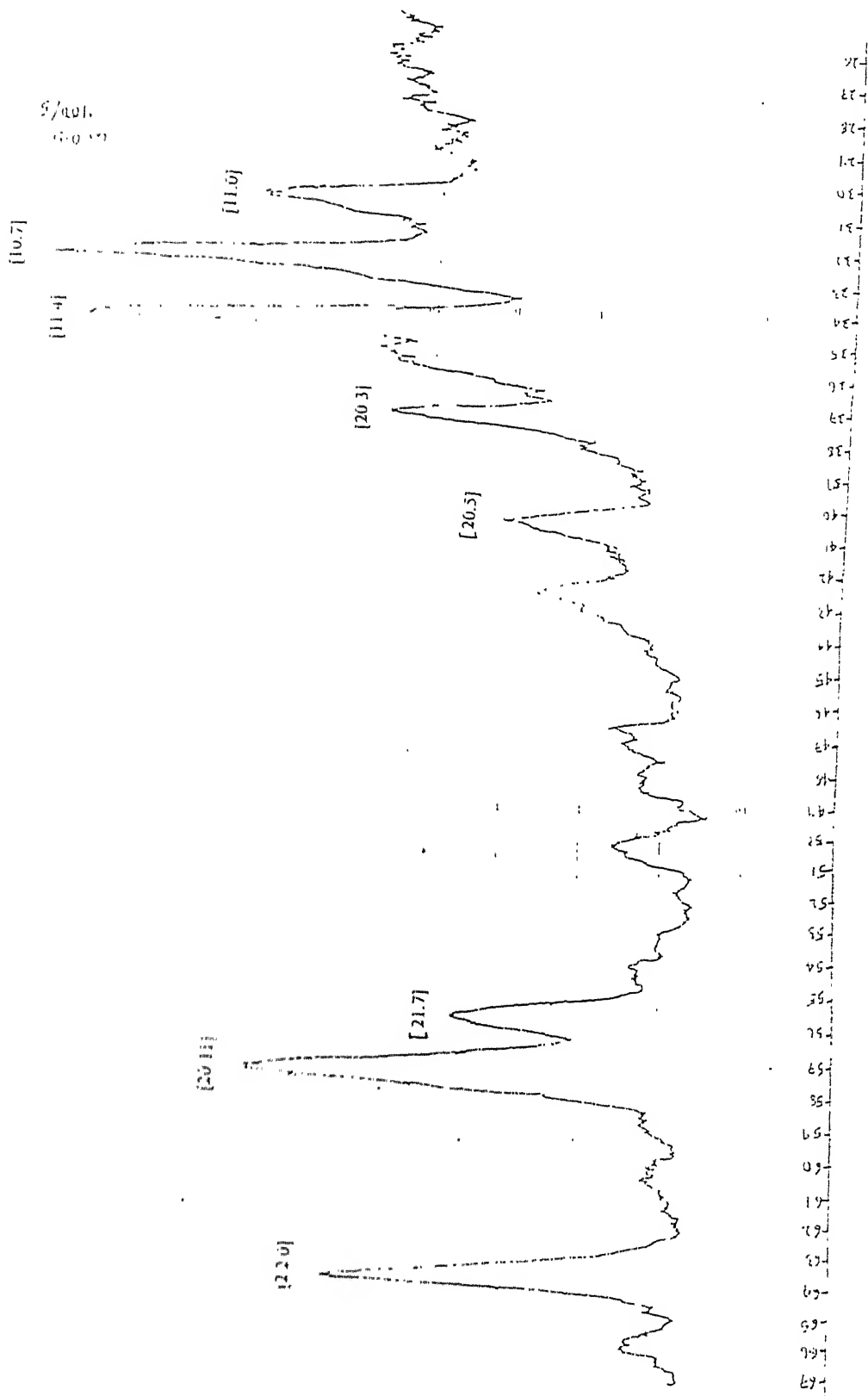Figure 30:   XRD pattern of cobalt substitued barium ferrite, $BaFe_{12-x}Co_xO_{19}$ (x = 2 0).
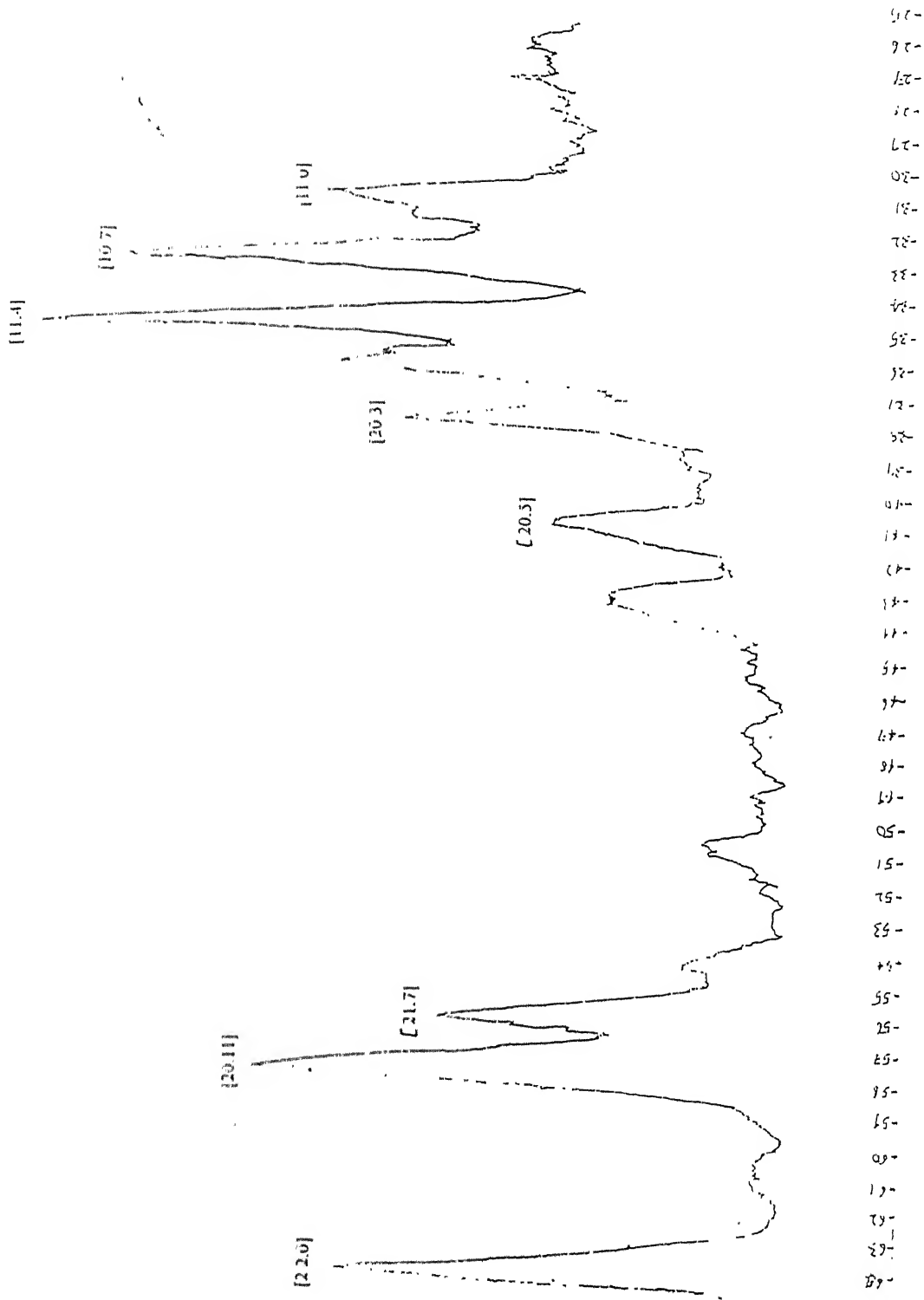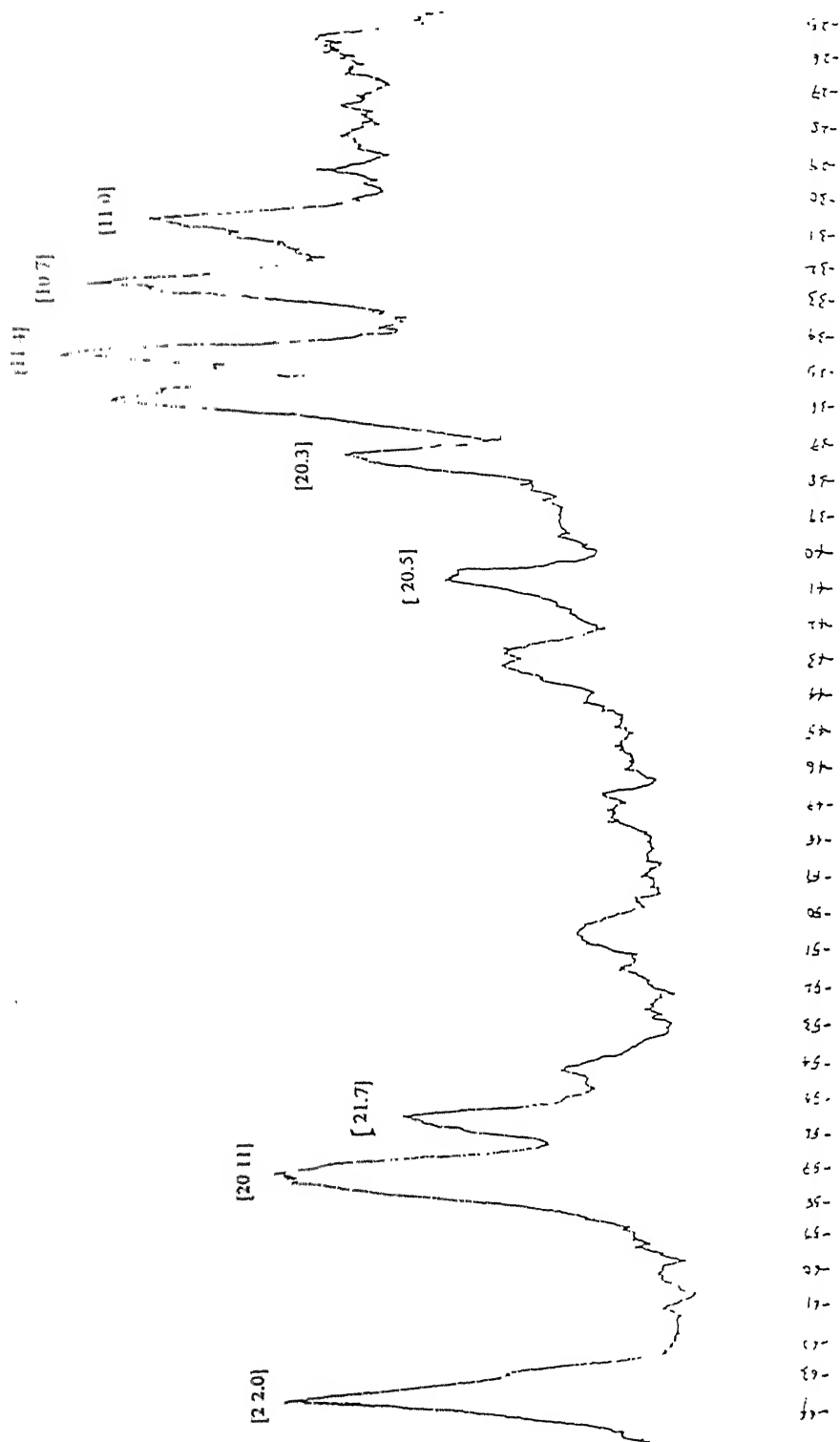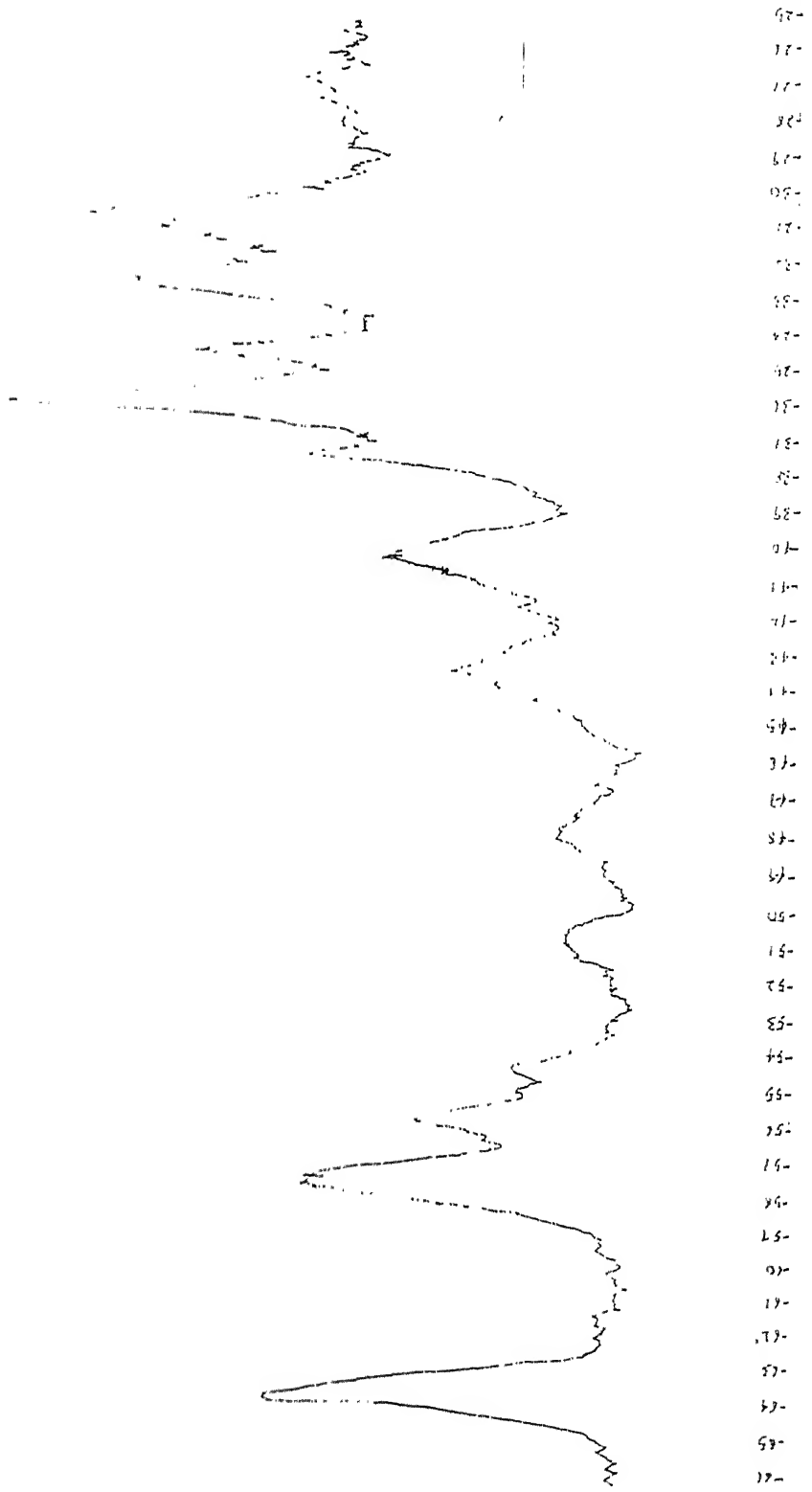
Figure 31: XRD pattern of cobalt substituted barium ferrite, $BaFe_{12-x}Co_xO_{19}$ (x = 2.5).

Figure 32: XRD pattern of cobalt substituted barium ferrite, $BaFe_{12-x}Co_xO_{19}$ (x = 3.0).

Table 10: Interplanar spacings and intensities of various peaks observed in XRD of cobalt substituted barium ferrite, $BaFe_{12-x}Co_xO_{19}$ (x = 0.5)

d-values for $BaFe_{12}O_{19}$ (A°)	Interplanar spacings observed for $BaFe_{12-x}Co_xO_{19}$ (x = 0.5) d(A°)	Intensities for $BaFe_{12}O_{19}$	Intensities observed for $BaFe_{12-x}Co_xO_{19}$ (x = 0.5)	hk.l indices
2.94	2.93	55	52	1 1. 0
2.78	2.77	100	100	1 0 .7
2.62	2.63	98	99.3	1 1 .4
2.55	2.56	11	45.1	2 0 .0
2.42	2.44	60	47.9	2 0 .3
2.23	2.24	29	31.2	2 0 .5
2.13	2.13	18	26.3	2 0 .6
1.81	1.82	10	14.5	2 0 .9
1.66	1.66	53	51	2 1 .7
1.63, 1.62, 1.61	1.62	30, 58, 10	97.2	2 0 .11
1.47	1.47	63	77.4	2 2 .0

The standard data for pure $BaFe_{12}O_{19}$ phase is given for the sake of comparison.

Table 11: Interplanar spacings and intensities of various peaks observed in XRD of cobalt substituted barium ferrite, $BaFe_{12-x}Co_xO_{19}$ (x = 1.0)

d-values for $BaFe_{12}O_{19}$ (A°)	Interplanar spacings observed for $BaFe_{12-x}Co_xO_{19}$ (x = 1.0) d(A°)	Intensities for $BaFe_{12}O_{19}$	Intensities observed for $BaFe_{12-x}Co_xO_{19}$ (x = 1.0)	hk.l indices
2.94	2.94	55	57	1 1 . 0
2.78	2.79	100	75.4	1 0 . 7
2.62	2.62	98	100	1 1 . 4
2.55	2.55	11	47.4	2 0 . 0
2.42	2.42	60	44.5	2 0 . 3
2.23	2.23	29	27.4	2 0 . 5
2.13	2.13	18	28	2 0 . 6
1.81	1.82	10	10.2	2 0 . 9
1.66	1.66	53	50.2	2 1 . 7
1.63, 1.62, 1.61	1.62	30, 58, 10	76	2 0 . 11
1.47	1.47	63	64	2 2 . 0

The standard data for pure $BaFe_{12}O_{19}$ phase is given for the sake of comparison.

Table 12: Interplanar spacings and intensities of various peaks observed in XRD of cobalt substituted barium ferrite, $BaFe_{12-x}Co_xO_{19}$ (x = 1.5)

d-values for $BaFe_{12}O_{19}$ (A^o)	Interplanar spacings observed for $BaFe_{12-x}Co_xO_{19}$ (x = 1.5) d(A^o)	Intensities for $BaFe_{12}O_{19}$	Intensities observed for $BaFe_{12-x}Co_xO_{19}$ (x = 1.5)	hk.l indices
2.94	2.94	55	69.6	1 1 . 0
2.78	2.77	100	83.7	1 0 . 7
2.62	2.61	98	100	1 1 . 4
2.55	2.54	11	65.2	2 0 . 0
2.42	2.42	60	47.9	2 0 . 3
2.23	2.24	29	49.6	2 0 . 5
2.13	2.13	18	27.4	2 0 . 6
1.81	1.81	10	13.3	2 0 . 9
1.66	1.66	53	58.5	2 1 . 7
1.63, 1.62, 1.61	1.63	30, 58, 10	88.8	2 0 . 11
1.47	1.47	63	88.1	2 2 . 0

The standard data for pure $BaFe_{12}O_{19}$ phase is given for the sake of comparison.

Table 13: Interplanar spacings and intensities of various peaks observed in XRD of cobalt substituted barium ferrite, $BaFe_{12-x}Co_xO_{19}$ (x = 2.0)

d-values for $BaFe_{12}O_{19}$ (A°)	Interplanar spacings observed for $BaFe_{12-x}Co_xO_{19}$ (x = 2.0) d(A°)	Intensities for $BaFe_{12}O_{19}$	Intensities observed for $BaFe_{12-x}Co_xO_{19}$ (x = 2.0)	h k.l indices
2.94	2.94	55	52	1 1 . 0
2.78	2.77	100	100	1 0 . 7
2.62	2.61	98	99.3	1 1 . 4
2.55	2.53	11	45.1	2 0 . 0
2.42	2.42	60	47.9	2 0 . 3
2.23	2.23	29	31.2	2 0 . 5
2.13	2.09	18	24.7	2 0 . 6
1.66	1.65	53	32.3	2 1 . 7
1.63, 1.62, 1.61	1.61,1.62	30, 58, 10	51.1,51.1	2 0 . 11
1.47	1.46	63	58.8	2 2 . 0

The standard data for pure $BaFe_{12}O_{19}$ phase is given for the sake of comparison.

81

Table 14: Interplanar spacings and intensities of various peaks observed in XRD of cobalt substituted barium ferrite, $BaFe_{12-x}Co_xO_{19}$ (x = 2.5)

d-values of $CoFe_2O_4$ and some prominent peaks of $Ba_3Co_2Fe_{24}O_{41}$ d(A°)	Interplanar spacings observed for $BaFe_{12-x}Co_xO_{19}$ (x = 2.5) d(A°)	Intensities of $CoFe_2O_4$ and $Ba_3Co_2Fe_{24}O_{41}$	Intensities observed for $BaFe_{12-x}Co_xO_{19}$ (x = 2.5)
2.97, 2.94 (80% peak of $Ba_3Co_2Fe_{24}O_{41}$)	2.94	20, 80	62.6
2.74 (100% peak of $Ba_3Co_2Fe_{24}O_{41}$)	2.75	100 (peak belonging to $Ba_3Co_2Fe_{24}O_{41}$)	38
2.53	2.53	100	100
2.41, 2.42 2.44 (the last two peaks belong to $Ba_3Co_2Fe_{24}O_{41}$)	2.42	6, 50,20 (the last two peaks belong to $Ba_3Co_2Fe_{24}O_{41}$)	32.3
2.08	2.09	20	34.5
1.70	1.65	16	23.2
1.61, 1.60 (the last peak belong to $Ba_3Co_2Fe_{24}O_{41}$)	1.60	40, 30 (the last peak belongs to $Ba_3Co_2Fe_{24}O_{41}$)	66.1
1.48	1.47	64	62.6

The standard data for $CoFe_2O_4$ and d-values of some prominent peaks for $Ba_3Co_2Fe_{24}O_{41}$ are given for comparison.

Table 15: Interplanar spacings and intensities of various peaks observed in XRD of cobalt substituted barium ferrite, $BaFe_{12-x}Co_xO_{19}$ (x = 3.0)

d-values for $CoFe_2O_4$ d(A°)	Interplanar spacings observed for $BaFe_{12-x}Co_xO_{19}$ (x = 3.0) d(A°)	Intensities of $CoFe_2O_4$	Intensities observed for $BaFe_{12-x}Co_xO_{19}$ (x = 3.0)
2.97	2.96	20	35.2
2.53	2.53	100	100
2.08	2.09	20	33.1
1.61	1.60	40	48.1
1.48	1.47	64	54.9

The standard data for $CoFe_2O_4$ is given for comparison.

precipitate out and its content increases continuously at the expense of barium ferrite. At $x = 3$, no diffraction peak for barium ferrite is observed. Above $x=2$, peaks corresponding to various phases such as, $Ba_3Fe_{32}O_{51}$, $Ba_3Co_2Fe_{24}O_{41}$, $Ba_3Fe_2O_6$ and $Ba_2Co_2Fe_{12}O_{22}$ etc. are also observed. It can therefore be concluded that material having compositions of $BaFe_{10.5}Co_{1.5}O_{19}$ can be considered to meet both the crystallographic and the magnetic requirements of a recording media in GMR mode of technology.

4.2.2 Bismuth substitutions:

As bismuth can stay in 3+ state in the solution, and as Fe^{3+} is itself responsible for high coercivity of $BaFe_{12}O_{19}$, we intended to replace the Fe^{3-} by Bi^{3+} to control the coercivity. For this, calculated amounts of $Bi(NO_3)_35H_2O$ were added to the metal-nitrate-citrate solutions to get ash by autoignition method. The ashes so obtained were calcined at $900°C$ for five hours. Three samples of bismuth substituted barium ferrite, with composition $BaFe_{12-x}Bi_xO_{19}$ ($x = 0.5$, 1.0 and 1.5) were synthesized. The XRD patterns of these samples are shown in Figures 33-35. The d-values and corresponding intensities of diffraction peaks are summarized in the Tables 16-18. In all cases, barium ferrite phase is retained. The variation in intensities is expected as bismuth which is replacing iron has high atomic number and so scatters much heavily. The magnetization versus applied field curves are shown in Figures 36-38. The saturation magnetization (M_s) and coercivity (H_c) values are given in Table 19.
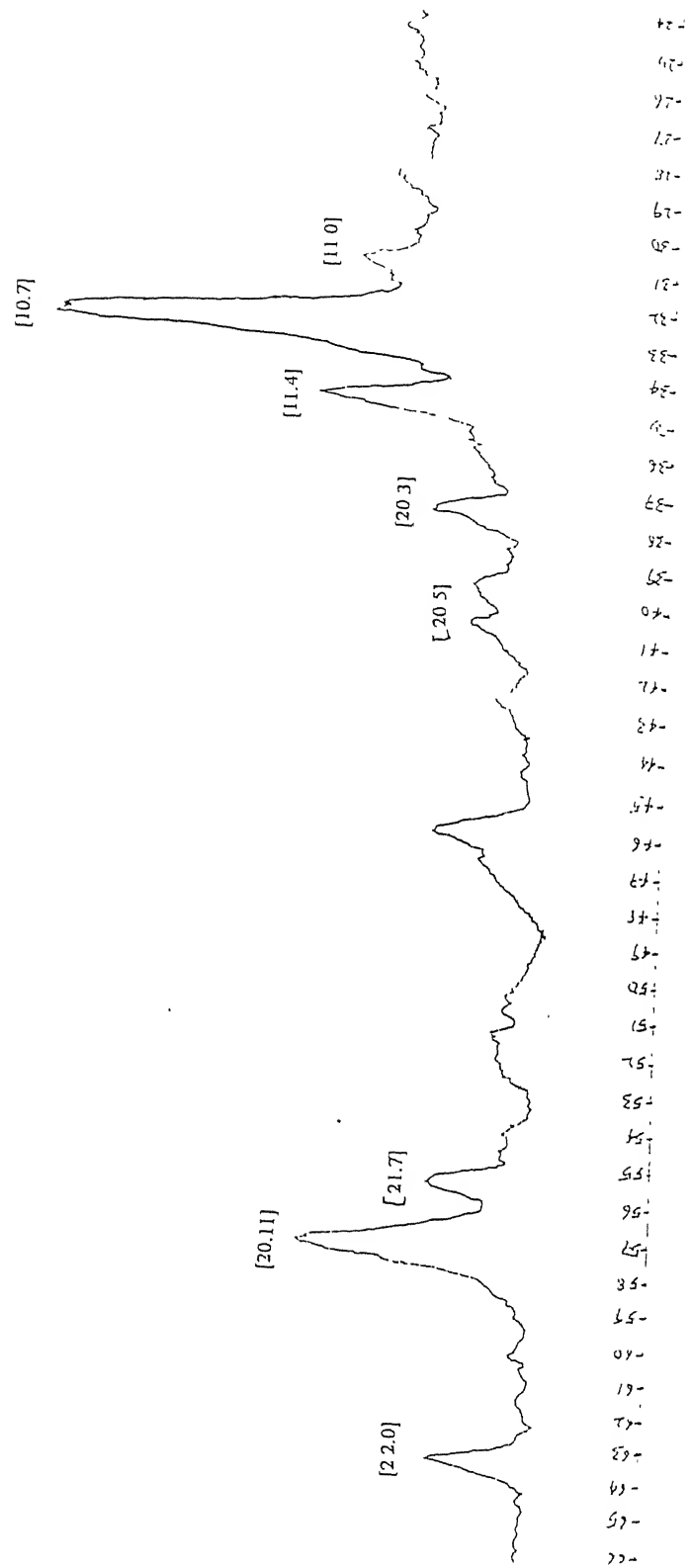
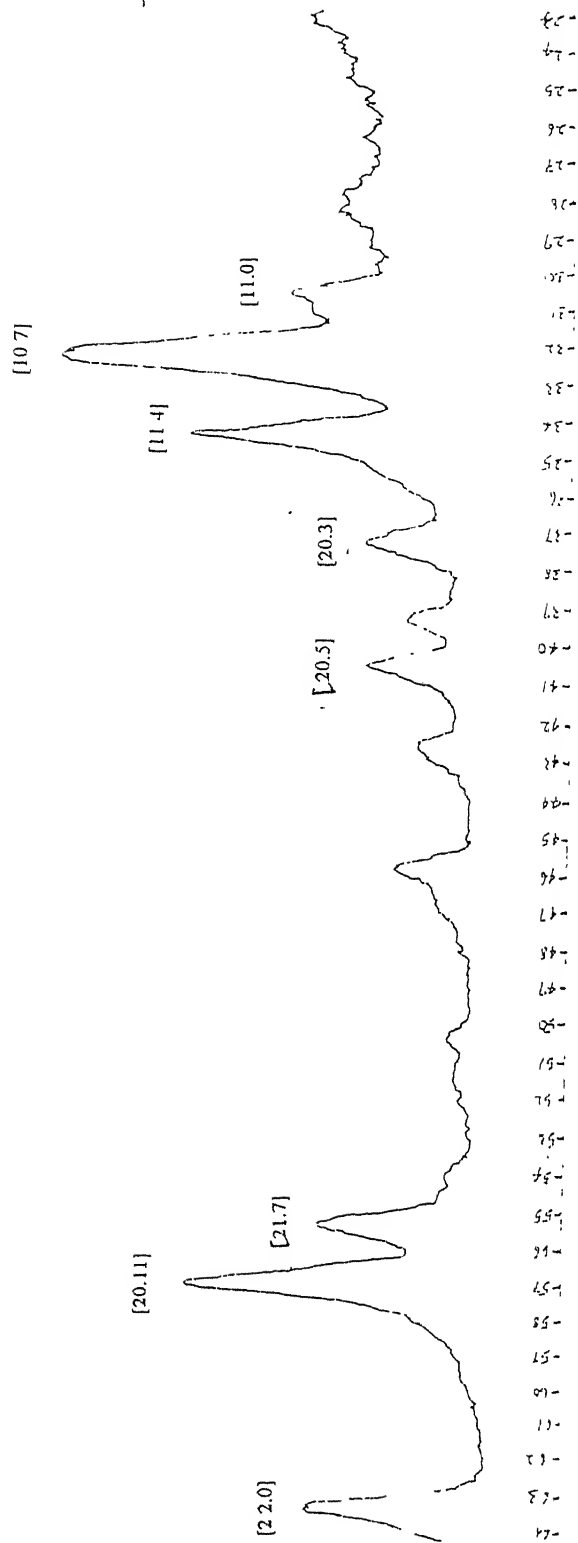Figure 33. XRD pattern of bismuth substituted barium ferrite, $BaFe_{12-x}Bi_xO_{19}$ (x = 0.5).

Figure 34: XRD pattern of bismuth substituted barium ferrite, $BaFe_{12-x}Bi_xO_{19}$ (x = 1 0).

Figure 35: XRD pattern of bismuth substituted barium ferrite, $BaFe_{12-x}Bi_xO_{19}$ (x = 1.5).

Table 16: Interplanar spacings and intensities of various peaks observed in XRD of bismuth substituted barium ferrite, $BaFe_{12-x}Bi_xO_{19}$ (x = 0.5)

d-values for $BaFe_{12}O_{19}$ (A°)	Interplanar spacings observed for $BaFe_{12-x}Bi_xO_{19}$ (x = 0.5) d(A°)	Intensities for $BaFe_{12}O_{19}$	Intensities observed for $BaFe_{12-x}Bi_xO_{19}$ (x = 0.5)	h k.l indices
2.94	2.95	55	23.8	1 1 .0
2.78	2.80	100	100	1 0 .7
2.62	2.63	98	38.9	1 1 .4
2.42	2.42	60	15.9	2 0 .3
2.23	2.25	29	9.7	2 0 .5
2.13	2.14	18	6.1	2 0 .6
1.66	1.66	53	23.0	2 1 .7
1.63, 1.62, 1.61	1.62	30, 58, 10	52.2	2 0 .11
1.47	1.47	63	23.8	2 2 .0

The standard data for pure $BaFe_{12}O_{19}$ phase is given for the sake of comparison.

Table 17: Interplanar spacings and intensities of various peaks observed in XRD of bismuth substituted barium ferrite, $BaFe_{12-x}Bi_xO_{19}$ (x = 1.0)

d-values for $BaFe_{12}O_{19}$ (A°)	Interplanar spacings observed for $BaFe_{12-x}Bi_xO_{19}$ (x = 1.0) d(A°)	Intensities for $BaFe_{12}O_{19}$	Intensities observed for $BaFe_{12-x}Bi_xO_{19}$ (x = 1.0)	h k.l indices
2.94	2.95	55	34.0	1 1 .0
2.78	2.79	100	100	1 0 .7
2.62	2.63	98	67	1 1 .4
2.42	2.42	60	26.3	2 0 .3
2.23	2.24	29	28.5	2 0 .5
2.13	2.13	18	13.1	2 0 .6
1.66	1.66	53	46.1	2 1 .7
1.63, 1.62, 1.61	1.63	30, 58. 10	86.8	2 0 .11
1.47	1.47	63	51.6	2 2 .0

The standard data for pure $BaFe_{12}O_{19}$ phase is given for the sake of comparison.

Table 18: Interplanar spacings and intensities of various peaks observed in XRD of bismuth substituted barium ferrite, $BaFe_{12-x}Bi_xO_{19}$ (x = 1.5)

d-values for $BaFe_{12}O_{19}$ (A°)	Interplanar spacings observed for $BaFe_{12-x}Bi_xO_{19}$ (x = 1.5) d(A°)	Intensities for $BaFe_{12}O_{19}$	Intensities observed for $BaFe_{12-x}Bi_xO_{19}$ (x = 1.5)	h k.l indices
2.94	2.94	55	21.6	1 1 .0
2.78	2.79	100	100	1 0 .7
2.62	2.63	98	43.3	1 1 .4
2.42	2.43	60	19.7	2 0 .3
2.23	2.25	29	19.1	2 0 .5
2.13	2.13	18	17.8	2 0 .6
1.66	1.67	53	23.5	2 1 .7
1.63, 1.62, 1.61	1.62	30, 58, 10	60.5	2 0 .11
1.47	1.47	63	21.6	2 2 .0

The standard data for pure $BaFe_{12}O_{19}$ phase is given for the sake of comparison.

Figure 36: Magnetization versus applied field curve bismuth substituted barium ferrite, $BaFe_{12-x}Bi_xO_{19}$ (x = 0.5).

Figure 37:   Magnetization versus applied field curve bismuth substituted barium ferrite, $BaFe_{12-x}Bi_xO_{19}$ (x = 1.0).
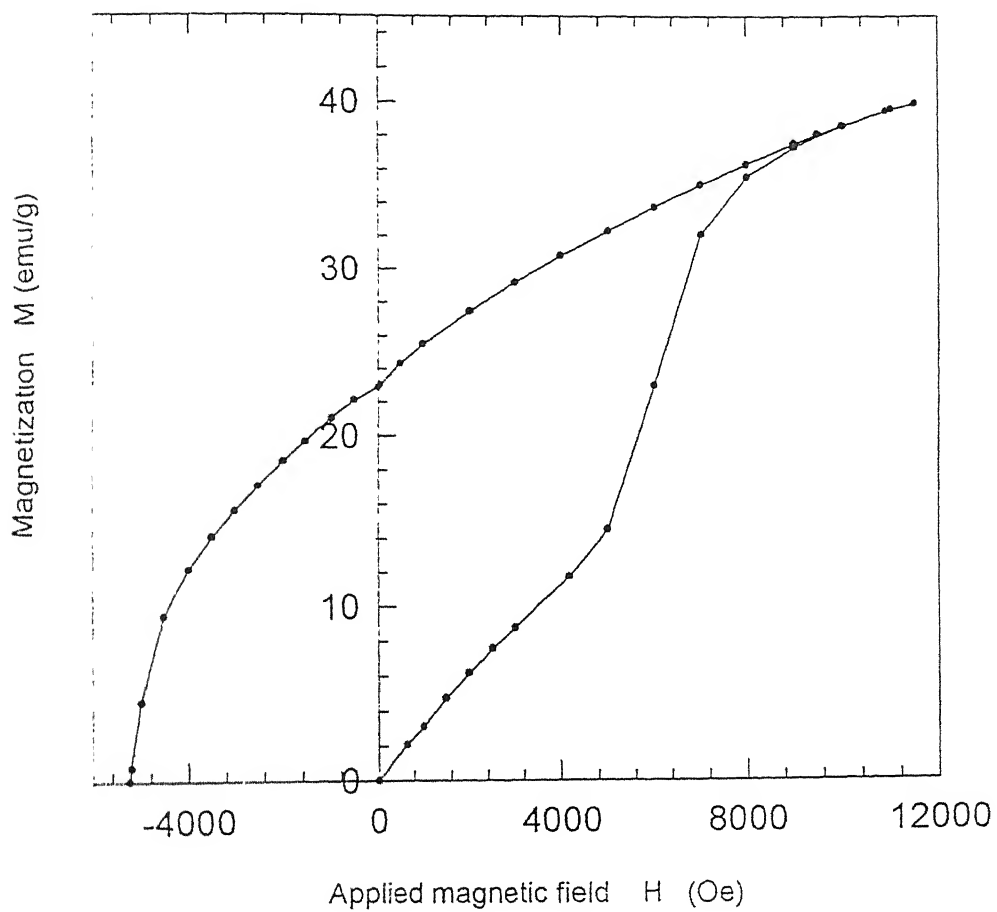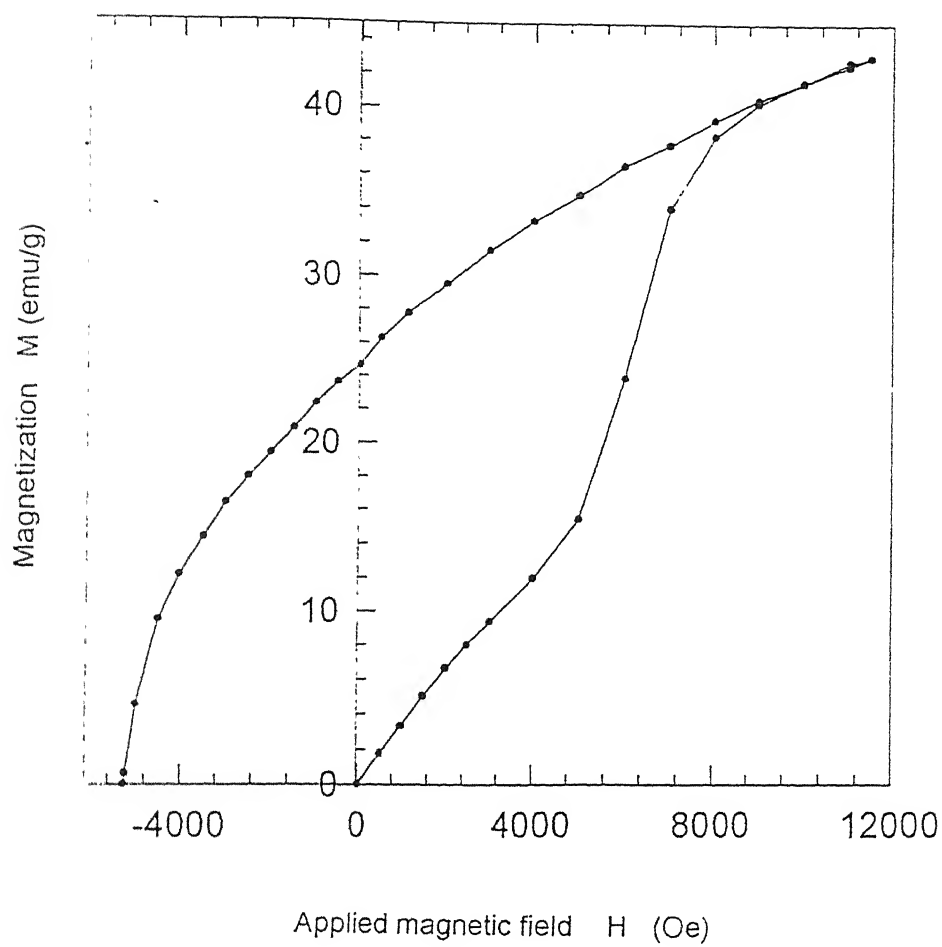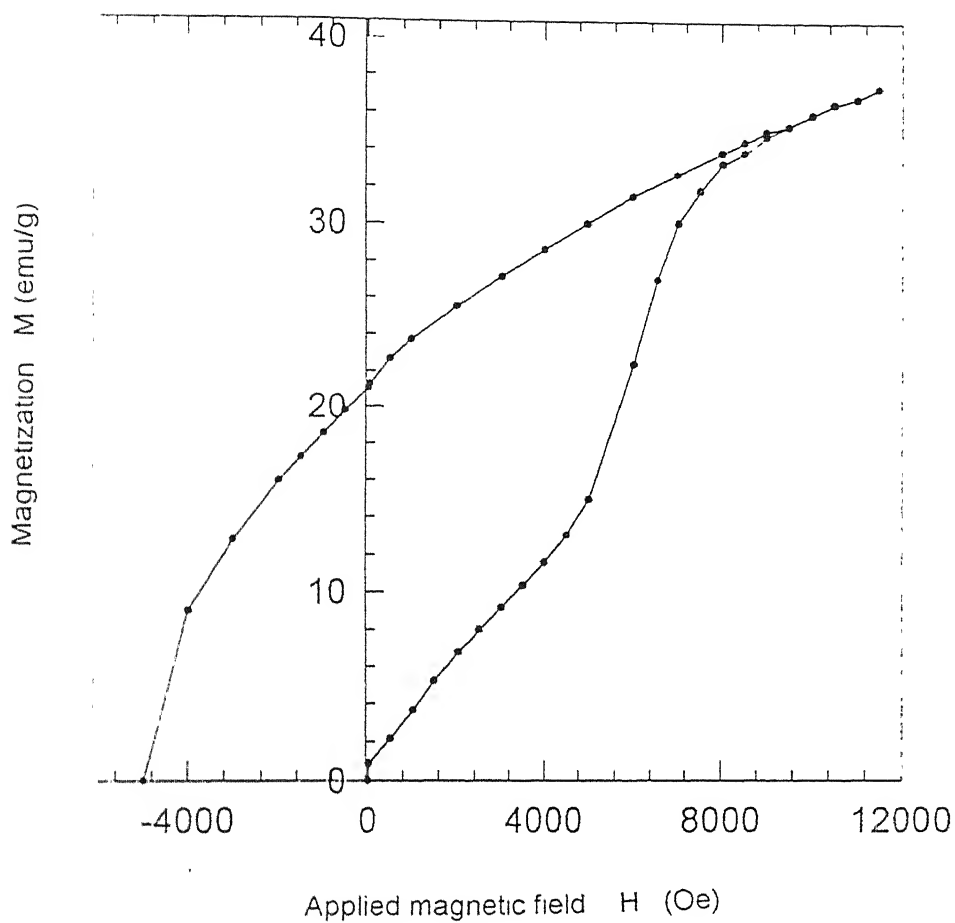
Figure 38 Magnetization versus applied field curve bismuth substituted barium ferrite, BaFe$_{12-x}$Bi$_x$O$_{19}$ (x = 1.5).

Table 19   Saturation magnetization and coercivity values of different bismuth substituted barium ferrites :

Composition	Saturation Magnetization M_s (emu/g)	Coercivity H_c (Oe)
$BaFe_{12-x}Bi_xO_{19}$ (x=0.5)	39.9	5249
$BaFe_{12-x}Bi_xO_{19}$ (x=1.0)	43	5251
$BaFe_{12-x}Bi_xO_{19}$ (x=1.5)	37.3	4985

It is clear that the coercivity values of bismuth substituted barium ferrite are not in the required range of 1000 - 2500 Oe and M_s values are very low. The reason for retention of the high coercivity may lie in Bi^{3-} ions not replacing the Fe^{3-} ions from the particular crystallographic sites (i.e., $4f_{vi}$ and 2b crystallographic sites) responsible for the enhancement of coercivity of barium ferrite [28]. As the coercivity value is not decreased by bismuth substitution, no further studies were undertaken for them.

4.2.3 Co-Ti Substitutions:

As been pointed out above, a possible way to decrease the coercivity of barium ferrite is to substitute two Fe^{3+} ions with a pair of Co^{2+} and Ti^{4+} ions to lead to an overall composition of $BaFe_{12-2x}Co_xTi_xO_{19}$ with x varying upto 0.9. If only Co^{2+} ions are added to replace Fe^{3+} ions, the

charge imbalance may occur or alternatively, some oxygen vacancies need to be created. In order to maintain the original oxygen intact and maintain charge neutrality, equal amount of Ti^{4+} is also added for charge compensation. Unfortunately, titanium ion does not, stay in 4+ state in aqueous solutions. The only way to incorporate titanium into barium ferrite is by solid state reaction. But TiO_2 is insoluble in water. Thus, addition of TiO_2 as such to the aqueous solution produces heterogeneous mixture. In order to achieve a near homogeneous ash, the coagulation precipitation of TiO_2 before ash formation should be avoided by ensuring its high dispersion in the solution prior to combustion. This requires that the pH of the solution be maintained at isoelectric point of the particular oxide (i.e., TiO_2) [40]. The isoelectric point of TiO_2 lies in the pH range of 4-6.

In the present study, partial substitution of Fe^{3+} in barium ferrite is made by both Co^{2+} and Ti^{4+} as well. For this, nitrates of cobalt, iron and barium were added to the citrate solution alongwith some amount of TiO_2 powder. To obtain maximum dispersion of TiO_2 particles, the pH was maintained at 4.0 by adding ethylene diamine to the solution. The ash formed autoignition combustion of gel was subjected to grinding and mixing in mortar pestle for an hour. Also, the calcination temperature was raised to $1100^{\circ}C$ and duration increased to 10 hours. The product with the composition ($BaFe_{12-x}Co_xTi_\delta O_{19-\gamma}$) with x = 0.5 and 0.75 and $xTiO_2$ addition were synthesized with the assumption that titanium incorporation would depend on the relative number of Co^{3+} and Co^{2+} ions present. The overall composition can be expressed as $BaFe_{12-x}Co^{3+}_{x-2\delta} Co^{2+}_\delta Ti_\delta O_{19}$ or $BaFe_{12-x-\delta} Co^{3+}_{x-\delta} Co^{2+}_\delta Ti_\delta O_{19}$ with x = 0.5 or 0.75. Since the exact number of Co^{2+} ions present could not be ascertained, addition was tentatively drawn from $xTiO_2$. The extra titanium along with cobalt or iron (as the case may be) was expected to precipitate out in some form or remain as impurities in

95

the ferrite phase. The XRD patterns are shown in Figures 39 and 40 and the d-values and relative intensities of various peaks are given in Tables 20 and 21. In both cases, hexagonal structure of barium ferrite is found to be clearly maintained. The magnetization behavior for both the samples are shown in Figures 41 and 42. The coercivities for the two compositions $BaFe_{12-x}Co^{3+}_{x-2\delta}Co^{2+}_{\delta}Ti_{\delta}O_{19}$ or $BaFe_{12-x-\delta}Co^{3+}_{x-\delta}Co^{2+}_{\delta}Ti_{\delta}O_{19}$ with x = 0.5 or 0.75 are 300 Oe and 89 Oe, respectively; saturation magnetization being 58.2 and 57.4 emu/g, respectively. Normal coercivity of pure barium ferrite is 5190 Oe. Notice the drastic lowering of coercivity values. So, it is felt that by properly adjusting substitution of Fe^{3+} with Co^{2+} and Ti^{4+}, one can easily attain coercivity in the desired range of interest (1000-2500 Oe). Also, as less amounts of iron (x < 0.5) is expected to be substituted for obtaining the desired coercivity, titanium content will be minimal leading to better stability of the final product.

Figure 39: XRD pattern of cobalt substituted barium ferrite, with addition of titanium dioxide, the composition being $BaFe_{12-x}Co^{3+}_{x-2b}Co^{2+}_{2b}Ti_bO_{19}$ or $BaFe_{12-x-b}Co^{3+}_{x}Co^{2+}_bTi_bO_{19}$ with x = 0.5 and b remaining unknown.
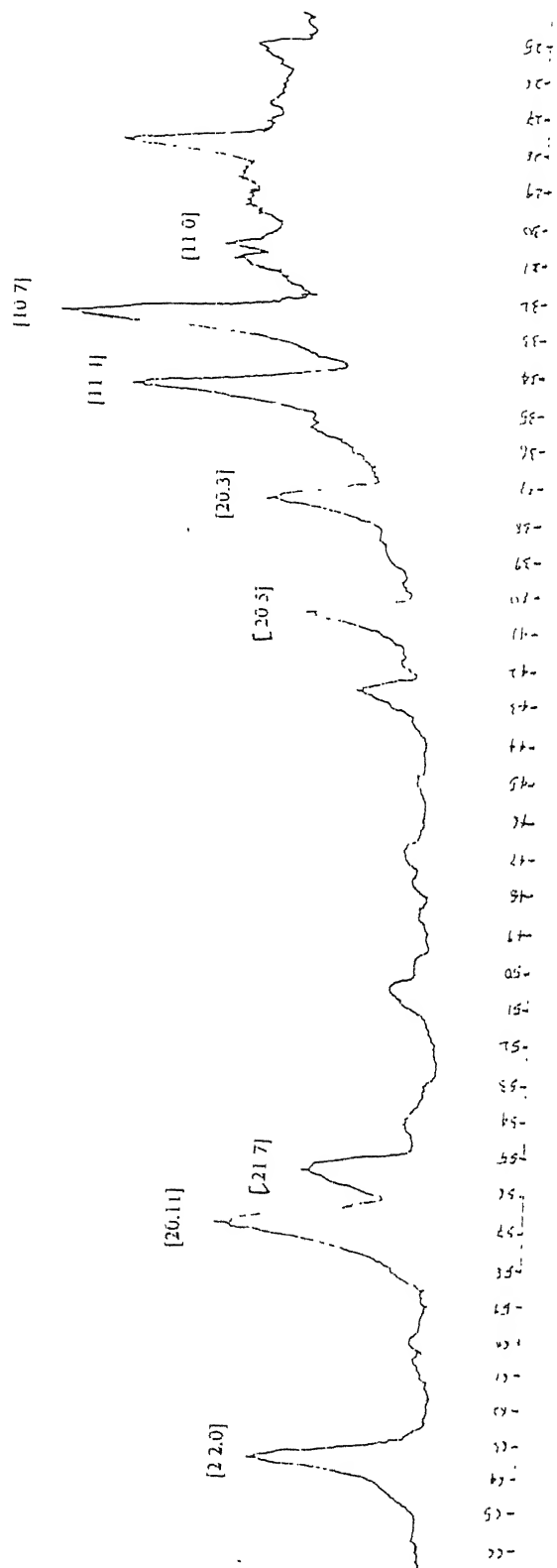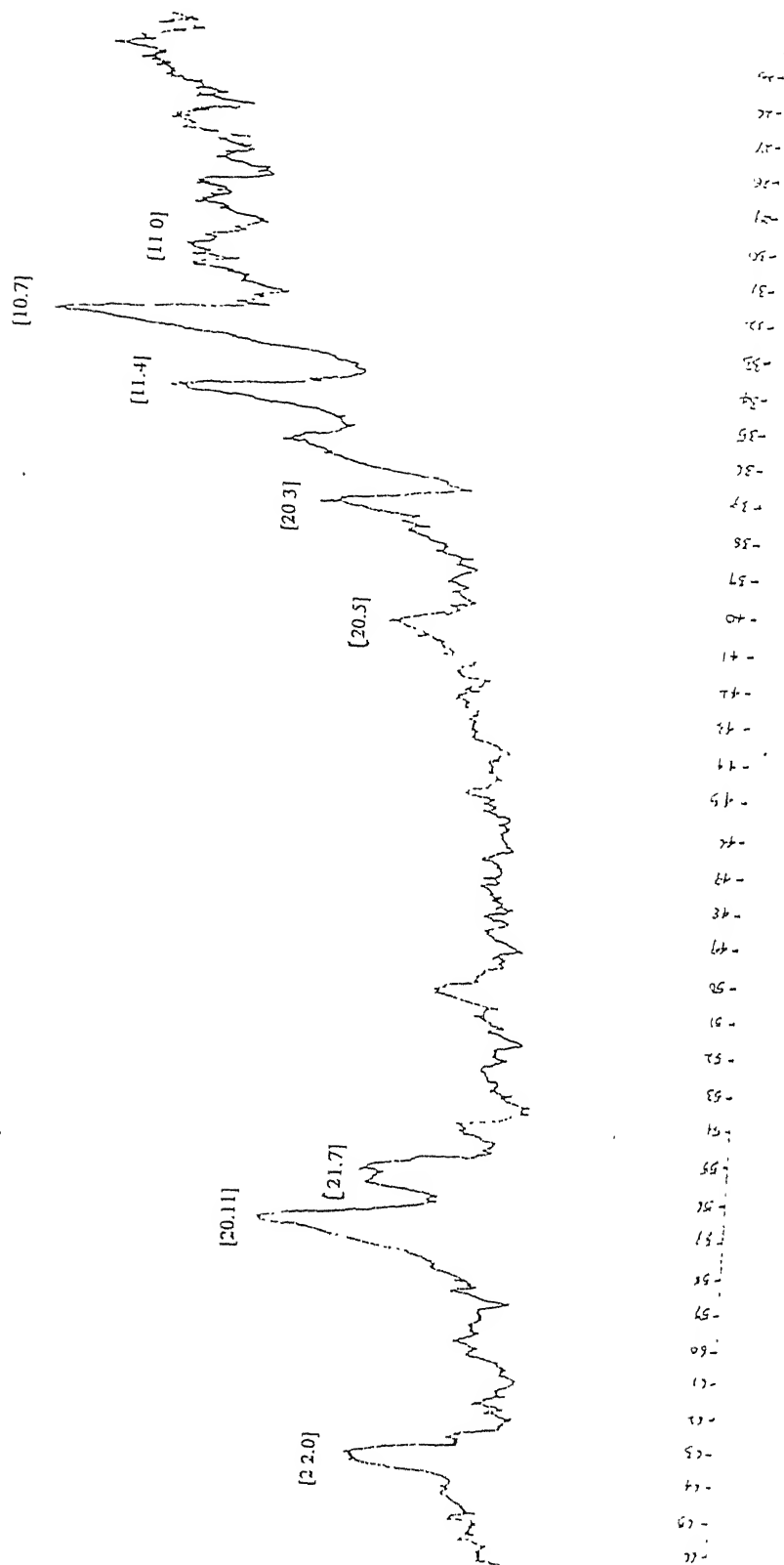
97

Figure 40: XRD pattern of cobalt substituted barium ferrite, with addition of titanium di oxide, the composition being $BaFe_{12-x}Co^{3+}_{x-2\delta}Co^{2+}_{2\delta}Ti_\delta O_{19}$ or $BaFe_{12-x-\delta}Co^{3+}_{x-\delta}Co^{2+}_{\delta}Ti_\delta O_{19}$ with x = 0.75 and δ remaining unknown.

Table 20: Interplanar spacings and intensities of various peaks observed in XRD of cobalt substituted barium ferrite, with addition of titanium di oxide, with the composition being $BaFe_{12-x}Co^{3+}_{x-2\delta}Co^{2+}_{2\delta}Ti_{\delta}O_{19}$ or $BaFe_{12-x-\delta}Co^{3+}_{x-\delta}Co^{2+}_{\delta}Ti_{\delta}O_{19}$ with x = 0.5 and δ value unknown.

d-values for $BaFe_{12}O_{19}$ (A°)	Interplanar spacings observed for * d(A°)	Intensities for $BaFe_{12}O_{19}$	Intensities observed for *	hk.l indices
2.94	2.94	55	31	1 1 .0
2.78	2.78	100	100	1 0 .7
2.62	2.62	98	80.3	1 1 .4
2.42	2.42	60	39.7	2 0 .3
2.23	2.23	29	18.9	2 0 .5
2.13	2.13	18	12	2 0 .6
1.66	1.66	53	35	2 1 .7
1.63, 1.62, 1.61	1.62	30, 58, 10	63.2	2 0 .11
1.47	1.47	63	56.9	2 2 .0

The standard data for pure $BaFe_{12}O_{19}$ phase is given for the sake of comparison.

* = $BaFe_{12-x}Co^{3+}_{x-2\delta}Co^{2+}_{2\delta}Ti_{\delta}O_{19}$ or $BaFe_{12-x-\delta}Co^{3+}_{x-\delta}Co^{2+}_{\delta}Ti_{\delta}O_{19}$ with x = 0.5

Table 21: Interplanar spacings and intensities of various peaks observed in XRD of cobalt substituted barium ferrite, with addition of titanium di oxide, with the composition being $BaFe_{12-x}Co^{3+}_{x-2\delta}Co^{2+}_{2\delta}Ti_\delta O_{19}$ or $BaFe_{12-x-\delta}Co^{3+}_{x-\delta}Co^{2+}_\delta Ti_\delta O_{19}$ with x = 0.75 and δ value unknown.

d-values for $BaFe_{12}O_{19}$ (A°)	Interplanar spacings observed for * $d(A^\circ)$	Intensities for $BaFe_{12}O_{19}$	Intensities observed for *	hk.l indices
2.78	2.77	100	100	1 0 .7
2.62	2.62	98	80.3	1 1 .4
2.55	2.53	11	12	2 0 .6
2.42	2.42	60	39.7	2 0 .3
2.23	2.23	29	18.9	2 0 .5
1.81	1.82	10	27.1	2 0 .9
1.66	1.66	53	35	2 1 .7
1.63, 1.62, 1.61	1.62	30, 58, 10	63.2	2 0 .11
1.47	1.47	63	56.9	2 2 .0

The standard data for pure $BaFe_{12}O_{19}$ phase is given for the sake of comparison.

* = $BaFe_{12-x}Co^{3+}_{x-2\delta}Co^{2-}_{2\delta}Ti_\delta O_{19}$ or $BaFe_{12-x-\delta}Co^{3+}_{x-\delta}Co^{2+}_\delta Ti_\delta O_{19}$ with x = 0.75

Figure 41: Magnetization versus applied field curve for cobalt substituted barium ferrite, with addition of titanium di oxide, the composition being $BaFe_{12-x}Co^{3+}_{x-2\delta}Co^{2+}_{2\delta}Ti_{\delta}O_{19}$ or $BaFe_{12-x-\delta}Co^{3+}_{x-\delta}Co^{2+}_{\delta}Ti_{\delta}O_{19}$ with x = 0.5 and δ remaining unknown.
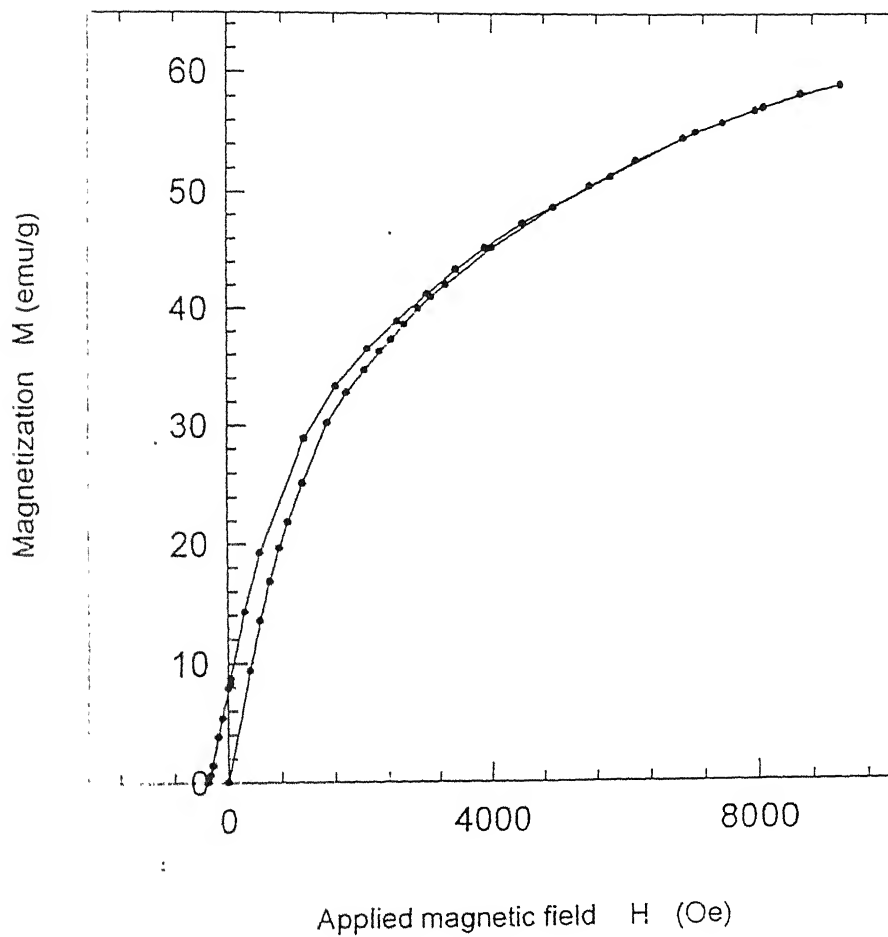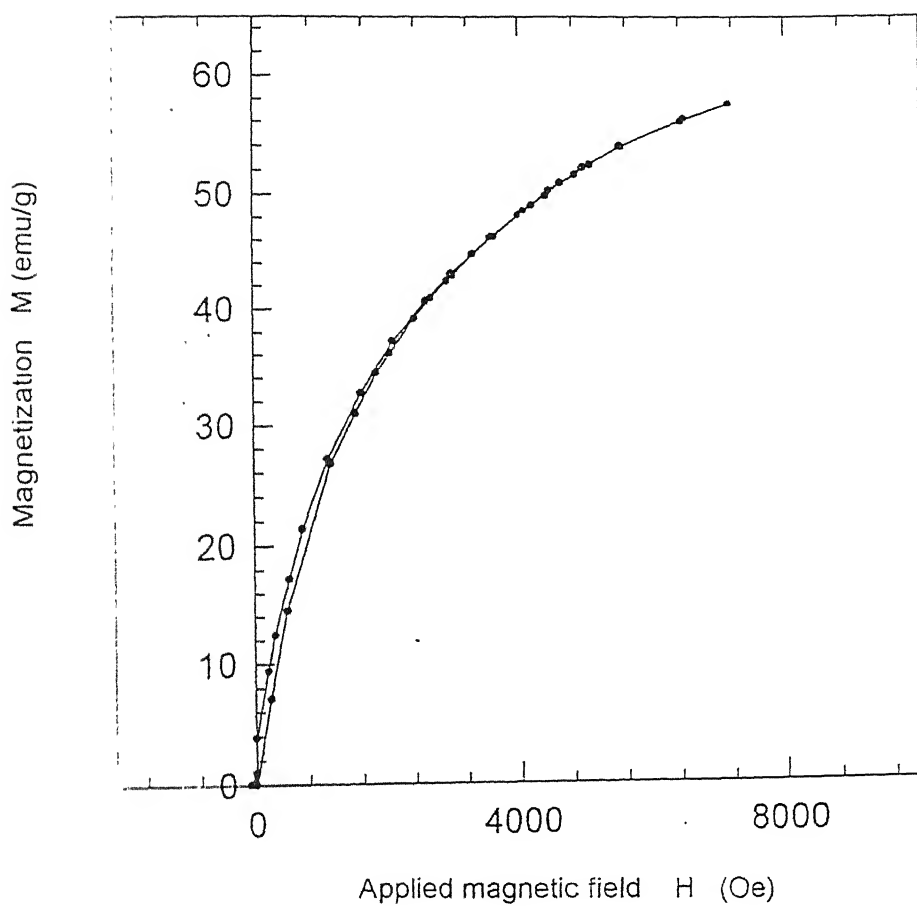
Figure 42: Magnetization versus applied field curve for cobalt substituted barium ferrite, with addition of titanium di oxide, the composition being $BaFe_{12-x}Co^{3+}_{x-2\delta}Co^{2+}_{2\delta}Ti_{\delta}O_{19}$ or $BaFe_{12-x-\delta}Co^{3+}_{x-\delta}Co^{2+}_{\delta}Ti_{\delta}O_{19}$ with $x = 0.75$ and δ remaining unknown.

CONCLUSIONS

1. Pure barium ferrite can be synthesized by (i) mixing barium and ferric nitrates with citric acid and adjusting the pH at 4.0 by adding ethylene diamine and securing gel formation, (ii) using autoignition combustion process to obtain ash from gel and (iii) subjecting calcination of ash at 900°C for five hours.

2. The utilization of autoignition combustion process for ash allows lowering of calcination temperature and reduction in synthesis time substantially.

3. Addition of ethylene diamine to metal nitrate citrate solution not only increases the pH but also ensures proper mixing of components and improves the stability of resulting complexes. Consequently, higher calcination temperature is required for the synthesis of barium ferrite.

4. Partial substitution of Fe^{3+} in $BaFe_{12}O_{19}$ with bismuth ions decreases saturation magnetization without affecting the coercivity. Such a substitution is therefore unsuitable for synthesis of barium ferrite for recording applications.

5. The coercivity of barium ferrite decreases significantly with increase in partial substitution of iron with cobalt. The resulting product maintains the hexagonal crystal structure upto a substitution of 1.5 Fe^{3+} ions per molecule. Further increase in substitution results in the formation of mixed phases comprising of $BaFe_{12}O_{19}$, $Ba_3Fe_{32}O_{51}$, $Ba_3Co_2Fe_{24}O_{41}$, $Ba_3Fe_2O_6$ and $Ba_2Co_2Fe_{12}O_{22}$.

6. The product corresponding to composition $BaCo_{1.5}Fe_{10.5}O_{19}$ is of great technical importance as it meets both crystallographic and magnetic characteristic requirements of a recording media in GMR mode of technology.

7. By adjusting partial substitution of iron in barium ferrite with cobalt and titanium together, it is possible to reduce the coercivity values to the desired range of 1000-2500 Oe and yet maintain the crystal structure.

104

SUGGESTIONS FOR FUTURE WORK

1. For ascertaining morphology and distribution of barium ferrite particles, transmission electron microscope studies may be undertaken for the synthesized products.

2. Partial substitution of Fe^{3+} ions by cobalt can be tried out by another method (e.g., co-precipitation method) where it is known to exist in 2+ oxidation state for comparing the results with those obtained here. This is essentially to check whether Co^{2+} indeed oxidizes to Co^{3+} on addition of ethylene diamine.

3. The partial substitution of Fe^{3+} ions by cobalt and titanium may be varied to study in depth the mechanism of remarkable decrease in coercivity values and to determine optimal composition for usage in high density recording applications.

REFERENCES

1. R.Wood, *"Magnetic megabits"*, IEEE Spectrum, 32-38, May 1990

2. M.P.Sharrock and L.W.Carlson, *"The application of barium ferrite particles in advanced recording media"*, IEEE Transactions on Magnetics, **31**, 2871-2876 (1995).

3. D.E.Speliotis, *"Performance of MP^{-+} and $BaFe^{++}$ tapes in high density recording applications"*, IEEE Transactions on Magnetics, **31**, 2877-2882 (1995).

4. J.C. Mallinson, *" The foundations of magnetic recording"*, Academic press, San Diego, CA (1987).

5. M.P.Sharrock, *"Particulate Magnetic Recording Media : A review"*, IEEE Transactions on Magnetics, **25**, 4374-4389 (1989).

6. G. Bate, *"Particulate recording Materials"*, Proceedings of the IEEE, **74**, 1513-1524 (1986).

7. D.F.Eagle and J.C.Mallinon, *"On coercivity of γ-Fe_2O_3 particles"*, J.Appl.phys, **38**, 995-997 (1967).

8. J.F.Knowles, *"Magnetic properties of individual acicular particles"*, IEEE Transactions on Magnetics, **MAG-17**, 3008-3013 (1981).

9. U.Kullman, E.Koster and B.Meyer, *"Magnetic anisotropy of Ir doped CrO_2"*, IEEE Transactions on Magnetics, **MAG-20**, 742-744 (1984).

10. A.E.Berkowitz, F.E.Parker, E.L.Hall and G.Podolsky, *"Towards a model for Co-surface treated Fe oxides"*, IEEE Transactions on Magnetics, **24**, 2871-2873 (1988).

11. S.Umeki, *"A new high coercivity magnetic particle for recording tape"*, IEEE Transactions on Magnetics, **MAG-10**, 655-656 (1974).

12. M.Kishimoto, *"On the coercivity of cobalt ferrite epitaxial iron oxides"*, IEEE Transactions on Magnetics, **MAG-17**, 3029-3031 (1989).

13. Hans Jurgen Pitcher and R.J.Veitch, *"Advances in magnetic tapes for high density information storage"*, IEEE Transactions on Magnetics, **31**, 2883-2888 (1995).

14. S.Barrom, A.Bray, S.Cheng, J.Elike, H.Fan, A.M.Lane and D.E.Nikles, *"Studies into the use of waterborne coating formulations for the preparation of magnetic tape"*, J.Appl.Phys, **75(10)**, 5578 (1994).

15. A.Morisako and M.Matsumuto, *"Sputtered hexagonal Ba-ferrite films for high density magnetic recording media"*, J.Appl.Phys, **79(8)**, 4881-4883 (1996).

16. S.Iwasaki and Y.Nakamura, *"An analysis for the magnetization mode for high density magnetic recording"*, IEEE Transactions on Magnetics, **MAG-13**,1272-1277 (1977).

17. S.Iwasaki, *"Perpendicular magnetic recording -Evolution and future"*, IEEE Transactions on Magnetics, **MAG-20**, 657-662 (1984).

18. T.Suzuki, *"Perpendicular magnetic recording-Its basics and potentials for the future"*, IEEE Transactions on Magnetics, **MAG-20**, 675-680 (1984).

19. J.R.Dessere, *" Crucial points in perpendicular recording"*, IEEE Transactions on Magnetics, **MAG-20**, 675-680 (1984).

20. R.Valenzuela, *" Magnetic Ceramics"*, 30-34, Cambridge University press (1994).

21. B.D.Cullity, " Introduction to magnetic materials" 198-200, Addison-Wesley publishing company (1972).

22. T.Fujiwara, *"Barium ferrite media for perpendicular recording"*, IEEE Transactions on Magnetics, **MAG-21**, 1480-1485 (1985).

23. D.E.Speliotis," *Media for high density magnetic recording"*, IEEE Transactions on

Magnetics, **MAG-20**, 669-674 (1984).

24. T.Fujiwara, *"Magnetic properties and recording characteristics of barium ferrite media"*, IEEE Transactions on Magnetics, **MAG-23**, 3125-3130 (1987).

25. D.E.Speliotis, *"Barium ferrite magnetic recording media"*, IEEE Transactions on Magnetics, **MAG-23**, 25-28 (1987).

26. T.Ido, O.Kubo and H.Yokoyama, *"Coercivity for Ba-ferrite superfine particle"*, IEEE Transactions on Magnetics, **MAG-22**, 675-680 (1986).

27. A.R.Corradi, D.E.Speliotis, A.H.Morrish, Q.A.Pankhurst, X.Z.Zhou, G.Bottoni, D.Candolfo, A.Cechetti, F.Masoli, *"Effect of the cation site occupancy on the magnetization reversal mechanism of hydrothermal barium ferrites"*, IEEE Transactions on Magnetics, **24**, 2862-2864 (1984).

28. X.Z.Zhou, A.H.Morrish and Z.W.Li, *"Site preference for Co^{2+} and Ti^{4+} in Co-Ti Substituted barium ferrite"*, IEEE Transactions on Magnetics, **27**, 4654-4656 (1991).

29. W.A.Kaczmarck and B.W.Ninham, *"Magnetic properties of Ba-ferrite powders prepared by surfactant assisted ball milling"*, IEEE Transactions on Magnetics, **30**, 717-719 (1994).

30. N.K.Ghosh, "Preparation characterization and magnetic property measurements of co-precipitated Barium hexaferrite powders" M.Tech thesis, (Unpublished), Dept of Metallurgy (1980).

31. I.J.McColm and N.J.Clark, *"Forming , shaping and working of high performance ceramics"*, 1-338, Blackie, Glasgow (1988).

32. P.Gornert, E.Sinn, W.Schuppel, H.Pfeiffer, M.Rosler, Th.Schubert, M.Jurish, R.Sellger, *"Structural and magnetic properties of $BaFe_{12-2x}Co_xTi_xO_{19}$ powders prepared by the Glass crystallization method"*, IEEE Transactions on Magnetics, **26**,12-14 (1990).

33. D.Rambabu, *"An efficient combustion process for synthesis of Yba$_2$Cu$_3$O$_7$"*, Jpn J Appl.phys, **29**, 507-508 (1990).

34. P.Sujatha Devi and H.S.Maiti, *"A novel autoignition combustion process for the synthesis of Bi-Pb-Sr-Ca-Cu-O super conductors with a T$_c$(0) of 125K"*, Journal of Solid State Chemistry, 35-42 (1994).

35. T.M.Chen and Y.H.Hu, *"Polymeric precursor for the preparation of Bi$_{1.5}$Pb$_{0.5}$Sr$_2$Ca$_2$Cu$_3$O$_x$"*, Journal of Solid State Chemistry, **97**,124-130 (1992).

36. F.P.Dwyer, *"Chelating agents and metal chelates"*, Academic press, New York and London (1964).

37. N.Sugita, M.Maekawa, Y.Ohta, K.Okinaka and N.Nagai, *"Advances in fine magnetic particles for high density recording"*, IEEE Transactions on Magnetics, **31**, 2854-2858 (1995).

38. G.Turilli, F.Licci, A.Paoluzi and T.Besagni, *"NiTi Substituted Hexaferrites for Magnetic Recording"*, IEEE Transactions on Magnetics, **24**, 2146-2149 (1988).

39. F.Licci, G.Turulli and T.Besagni, *"Phase analysis and single domain detection in hexaferrite powders for magnetic recording"*, IEEE Transactions on Magnetics, **24**,12-14 (1988).

40. James.S.Reed, *" Introduction to the principles of ceramic processing"*, John Wiley and Sons (1988).

109

MS- 1998- M - R₁₁₉ - 9TU